Linköping University
INSTITUTE OF TECHNOLOGY

Hydrostatic Transmission in Wind Turbines

Development of Test Platform

Joel Rapp
Jonatan Turesson

Division of Fluid and Mechatronic Systems

Master Thesis
Department of Management and Engineering
LIU-IEI-TEK-A- -15/02354- -SE

Hydrostatic Transmission in Wind Turbines

Development of Test Platform

Master Thesis in Fluid Power
Department of Management and Engineering
Division of Fluid and Mechatronic Systems
Linköping University
by

Joel Rapp
Jonatan Turesson

LIU-IEI-TEK-A- -15/02354- -SE

Supervisors: **Victor Juliano de Negri**
LASHIP, Universidade Federal de Santa Catarina
Petter Krus
IEI, Linköping University

Examiner: **Magnus Sethson**
IEI, Linköping University

Linköping, 31 August, 2015

Abstract

This master thesis project is a part of a larger project with the goal of developing a drivetrain, utilizing a hydrostatic transmission, for horizontal axis mid-size wind turbines. Some of the benefits from using a hydrostatic transmission are that a variable speed operation is possible without the use of a frequency converter, the generator may be placed on the ground and thus reduce weight in the nacelle and also using hydraulic components can increase lifetime and robustness of the system. The thesis work is a part of the second step towards this goal, which contains constructing a test platform of the concept.

The test platform is being built at the Laboratory of Hydraulic and Pneumatic Systems (LASHIP) in Florianópolis, Brazil, where also the master thesis project has been conducted. Two companies are involved in the construction of the platform, Parker Hannifin and Reivax. Parker Hannifin is a multinational diversified manufacturer of motion and control technologies and systems. Reivax develop technologies for control systems and automation applied in Hydroelectric, Thermoelectric and Nuclear power plants.

The project was performed during the period of February to August 2015 and governs dimensioning and selection of hydraulic components for the test platform, development of simulation model in AMESim, evaluation of control strategies and also a dynamic analysis of the system.

Dimensioning the platform resulted in a drivetrain with an output power of 28 kW. Standard hydraulic components with high efficiencies where selected from Parker's product portfolio. These components were then modeled in AMESim where simulations of the whole system could be performed. Control strategies were tested and results showed that the best performance is reached when using a regulator that is able to compensate for pressure changes in the system. Results also indicated that the hydrostatic transmission can perform very well as a replacement of frequency converters, in terms of stable frequency output of a variable wind turbine. The dynamic analysis showed that the parameter that sets the main characteristics of the system is the aerodynamic rotor with its large inertia.

Acknowledgments

The work presented in this thesis has been performed at the Laboratory of Hydraulic and Pneumatic Systems (LASHIP) placed at the Federal University of Santa Catarina, Florianópolis, Brazil. Our supervisor has been Professor Victor Juliano de Negri at LASHIP. Thank you for guidance, ideas and patience throughout the work and also for making the exchange possible.

We want to thank Henrique Raduenz and Adriano Martins, that also have been working with the test platform, for great teamwork, discussions and road trips.

Thank you Paulo Teixeira, Master student at LASHIP, for wise words, brilliant ideas and for always showing great patience with all our questions.

We also want to thank Björn Eriksson at Parker Hannifin, Sweden, for support and opening the connection to Parker in Porto Alegre, Brazil.

Thanks to Parker in Porto Alegre and Reivax in Florianópolis for supporting the project and making it possible.

And finally thank you everyone at LASHIP for showing superb hospitality!

Nós veremos quando nós voltarmos a Floripa! Until then, Helan går!
Linköping, August, 2015

Joel Rapp
Jonatan Turesson

Contents

List of Figures

List of Tables

List of Abbreviations

AC	-	Alternating Current
CFD	-	Computational Fluid Dynamics
CSI	-	Current Source Inverter
CVT	-	Continuously Variable Transmission
DC	-	Doubly Fed Induction Generator
DDT	-	Digital Displacement Transmission
DFIG	-	Doubly Fed Induction Generator
DTSRT	-	Direct Tip Speed Ratio Tracking
EMF	-	Electromotive Force
FC	-	Frequency Converter
FF	-	Feedforward
FFT	-	Fast Fourier Transform
Flumes	-	Division of Fluid and Mechatronic Systems
HST	-	Hydrostatic Transmission
LASHIP	-	Laboratory of Hydraulic and Pneumatic Systems
LEM	-	Lumped Element Method
LiU	-	Linköping University
MPC	-	Model Predictive Control
MPPT	-	Maximum Power Point Tracking
PLC	-	Programmable Logic Controller
PRV	-	Pressure Relief Valve
SFIG	-	Single Fed Induction Generator
TLM	-	Transmission Line Method
TSR	-	Tip Speed Ratio
UFSC	-	Federal University of Santa Catarina
VSI	-	Voltage Source Inverter

Chapter 1

Introduction

1.1 Background

Wind energy has been utilized by people as an energy source for centuries. At 5000 B.C the Egyptians propelled boats on the Nile river and around 1000 A.D the windmill technology spread to Europe where one of the first applications were to drain lakes [5]. During the last century and especially the last decades wind power has become a big topic in the global strive towards green energy production. Today wind energy is one of the fastest growing sources for energy production. Only in Brazil the amount of installed capacity increased by 133% from march 2014 until march 2015 resulting in a total capacity of 6,2 GW [6, 7] and the European Wind Energy Association, EWEA, expects the installed capacity in the EU to be 192 GW by 2020 [8]. This corresponds to a growth of 49% from the currently installed capacity of 128,8 GW in EU (February 2015) [9].

Although the technology in wind turbines have developed very rapidly over the last two decades there are still a lot that can be improved and new technologies emerge frequently. One area that is evolving rapidly at the moment is the offshore wind industry. The offshore wind resources blows more abundant, stronger and more consistently than land based wind resources [10]. However, installation and maintenance is complicated and wear from seawater and floating platforms gives design challenges. One example of a new technology in offshore wind is the MHI Vestas[1] hydraulic wind turbine powertrain [11, 12]. It utilizes a new type of hydraulic digital displacement technology developed by Artemis Intelligent Power Ltd[2]. The benefits of implementing the Digital Displacement Transmission (DDT) in a wind turbine are, among others, considered to be, no use of a mechanical gearbox, utilization of synchronous generators and no need for power converters.

Because of the rapidly growing wind energy market many companies are trying to find new, or adapt existing technology to be used in wind turbines. Reivax is an automation and control company that builds and develops technology for control of power systems in power plants such as, hydroelectric, thermal, nuclear and wind power plants. The company has its headquarters with production in Florianópolis, Santa Catarina, Brazil. Reivax have since 2009 been developing a power generation concept for a mid-size wind turbine with a capacity of 100 kW. So far their focus have been to develop a concept consisting of a multi-pole synchronous generator connected directly to the rotor shaft, a so called "direct drive system". The generator is then connected to the grid via a full-scale frequency converter that ensures the parameters of the outputted electricity will match the standards of the electric grid.

Lately Reivax have gained interest in another concept that make use of a Hydrostatic Transmission (HST) with similar benefits as the ones mentioned for the DDT. In 2012, the Laboratory of Hydraulic and Pneumatic Systems (LASHIP) at the Federal University of Santa Catarina (UFSC) did research on such a system [2]. This work featured modeling of the system in AMESim[3] and from these

[1] MHI-Vestas is a joint venture between Mitsubishi Heavy Industries Ltd and Vestas Wind Systems A/S that was formed in 2014 and is dedicated to offshore wind energy.

[2] Artemis Intelligent Power Ltd is since 2010 a group company of Mitsubishi Heavy industries that have developed a hydraulic digital displacement technology applied in hydraulic machines.

[3] LMS Imagine Lab Amesim is a simulation software for multi-domain systems.

simulations it was concluded that it would be feasible to use a HST in a 150 kW wind turbine. Reivax and LASHIP have a history of running projects together and it is from this relation the idea, of running this new common project to investigate the potential of the HST concept to become reality, emerged.

The reason that two master students from the laboratory of Fluid and Mechatronic Systems (Flumes) at Linköping University (LiU) in Sweden are involved in this project is that LiU and UFSC have a good relationship and an already existing exchange agreement. Through contact with Parker in Sweden the possibility of involving Parker in Porto Alegre, Brazil, appeared and later they agreed to supply the project with hydraulic components to build a test platform.

1.2 Purpose and problem formulation

The long term goal for the involved parties is to see if a mid-size wind turbine with a hydrostatic transmission is suitable for the commercial market. This project is a part of a second step towards this goal with the main purpose to constructing a test platform that can confirm that the drivetrain concept will work as concluded i.e. deliver stable energy to an electrical grid.

The main problem formulation is defined as follows,

Is a wind turbine, using a hydrostatic transmission and a synchronous generator, technically suitable for becoming a commercial product?

To answer the problem formulation it has been broken down into subqueries of which this project aims to answer the following ones,

- Will a hydrostatic transmission be able to control the speed of the generator, so that the generated electricity satisfies the electric grid standards during normal operational conditions, without the use of a power converter?
- Can the drivetrain be realized by using already existing standard components?
- Can the system have a good overall efficiency?
- What type of control strategy is best suited for regulating the system?
- Is it possible to place some of the powertrain components in the nacelle and some of the components close to the ground to reduce weight in the nacelle and enable easier maintenance of some components?

1.3 Delimitations

The focus of this project targets the parts of the drivetrain from the low speed rotor shaft to the connection with the electrical grid. Therefore only basic theory and working principles of the blades, rotor hub and wind extraction needed for

the project are studied. The blade model used by Flesch [2] will be used without changes to blade design parameters except length of the blades. The wind profiles used to evaluate the concept are made from existing wind data. No respect to the geographical origin of the wind data is considered.

The connection of a synchronous generator to an electrical grid and its dynamic behavior will only be studied briefly since an existing model of such a connection has been developed by Flesch [2]. This model is assumed to give an acceptable representation of the generator and grid dynamics.

Another delimitation is that only operation between cut-in speed and rated power of the drivetrain will be analyzed. This means that how to perform the startup and how to perform control when rated power is reached, will not be considered.

Furthermore the drawings and solid mechanics calculations of the structure for the test platform will not be presented in the report, hence mechanical construction is not the a part of this study. Designing the mechanical parts and designing the layout of the system will be performed by two other students at LASHIP, Henrique Raduenz and Adriano Martins. Their project will run a parallel to this.

The main components of the hydrostatic transmission are restricted to off the shelf components supplied by Parker Hannifin. Electrical motor, frequency converter and safety electronics are predetermined by existing components supplied by Reivax.

Type of hoses and tubes for the platform are not considered in this study, but selected by Henrique and Adriano. They will also continue working with the test platform after this project and perform the evaluation of the simulations.

1.4 Methodology

As previously mentioned, this project emerged from a previous thesis done at LASHIP which resulted in a AMESim model of a 150 kW wind turbine [2]. The primary directions for this project were to construct a test platform of approximately 20 kW to evaluate the model and the concept. Hence the first step was to get familiar with the existing model, downsize the components and verify that it worked satisfyingly. Theoretical studies were needed to understand the basics of wind turbines, hydrostatic transmissions and working principles of the different components in wind turbine drivetrains.

The idea was to only use commercial off the shelf components from Parker and therefore the model had to be iteratively adjusted and confirmed when selecting the different hydraulic components. The components were selected in association with engineers from Parker during a visit at Parker Hannifin facilities in Porto Alegre.

When hydraulic components had been selected the AMESim model was readjusted to represent the chosen products. Efficiency models were added to better estimate losses in the hydraulic machines.

Different control strategies were implemented and evaluated by simulations. To be able to compare the control strategies optimizations of controller parameters

were made using one commonly defined optimum.

Different hydraulic line models were evaluated to give a proposal on how the influence of wave propagation in the long hydraulic lines between nacelle and bottom of the wind turbine can be modeled.

Finally a mathematical model of the aerodynamic rotor was developed to better understand its dynamic behavior and influence on the system.

Chapter 2

Literature studies

This chapter covers the most important theory needed to fully understand the drivetrain concept and its pros and cons. The component studied were hydrostatic transmissions, accumulators, generators, frequency converters and wind turbines in general. The chapter explains the basic theory of these components and if the reader is familiar with the components he or she can proceed to Chapter 3.

2.1 Hydrostatic transmissions

A basic hydrostatic transmission (HST) consists of a hydraulic pump connected to a hydraulic motor. The pump is driven by a prime mover, usually an internal combustion engine, connected to the input shaft of the pump. The pump generates flow to drive a hydraulic motor that in turn controls a load connected to its output shaft. A HST usually regulates speed and torque, depending on the configuration it can also be able to control the rotational direction of the motor. If both pump and motor are of fixed displacement type the HST will have a fixed gear ratio. When the pump, motor or both of them are of variable displacement type the transmission becomes a Continuously Variable Transmission (CVT), meaning that it is possible to get an infinite variation in gear ratio within the gear ratio interval of the transmission. The gear ratio is set by the displacement setting of pump and motor. Figure 2.1 shows the main components of a simple hydraulic transmission with both pump and motor of variable displacement type.

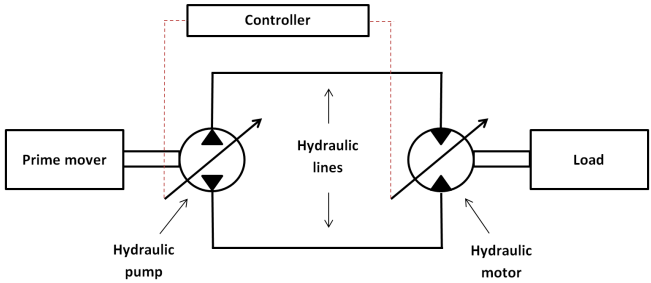

Figure 2.1: Simple illustration of a hydrostatic transmission with a controller that regulates the displacement of both pump and motor. The figure only presents the main components in a hydrostatic transmission, further components are required for the transmission to function properly.

In comparison with other types of power transmissions a HST, depending on configuration, offers the following advantages over other power transmissions [13]:

- Transmits high power in a compact size i.e. high power density.
- Efficient over a wide range of torque to speed ratios.
- Can maintain controlled speed regardless of load when within design limit.
- Can maintain a preset speed accurately against driving and braking loads.
- Able to transmit power from a single prime mover to multiple loads, even if position and orientation of the load differs.
- Under full load conditions it can remain stalled and undamaged with low power loss.

- Provides faster response than mechanical or electro mechanical transmissions of comparable rating.
- Can provide dynamic braking.

2.1.1 Hydraulic pumps and motors

The effective flow q_p and torque T_p from a hydraulic pump is calculated according to the following equations [14],

$$q_p = \varepsilon_p D_p n_p \eta_{volp} \tag{2.1}$$

$$T_p = \frac{\varepsilon_p D_p}{2\pi} \Delta p \frac{1}{\eta_{hmp}} \tag{2.2}$$

Similarly the equations for effective flow q_m and torque T_m for a hydraulic motor are [14],

$$q_m = \varepsilon_m D_m n_m \frac{1}{\eta_{volm}} \tag{2.3}$$

$$T_m = \frac{\varepsilon_m D_m}{2\pi} \Delta p \eta_{hmm} \tag{2.4}$$

where

$$\begin{aligned}
\varepsilon &= displacement\ setting\ [-] \\
D &= maximum\ displacement\ [m^3/rev] \\
n &= shaft\ speed\ [rev/s] \\
\Delta p &= pressure\ difference\ over\ pump/motor\ [Pa] \\
\eta_{vol} &= volumetric\ efficiency\ [-] \\
\eta_{hm} &= hydromechanical\ efficiency\ [-]
\end{aligned}$$

The displacement setting ε defines the actual displacement for a variable hydraulic machine according to, $D_{actual} = \varepsilon \cdot D$. For a variable displacement pump the displacement setting can vary between,

$$0 \leq \varepsilon_p \leq 1 \tag{2.5}$$

or for a variable displacement pump that can control the direction of flow,

$$-1 \leq \varepsilon_p \leq 1 \tag{2.6}$$

for a variable displacement motor the possible displacement setting is,

$$\varepsilon_{m,min} \leq \varepsilon_m \leq 1 \tag{2.7}$$

and for fixed displacement machines $\varepsilon = 1$ in Equation 2.1 to Equation 2.4. [15]

Figure 2.2 shows a common displacement control method used in mobile applications of a HST consisting of a variable displacement pump and a variable displacement motor.

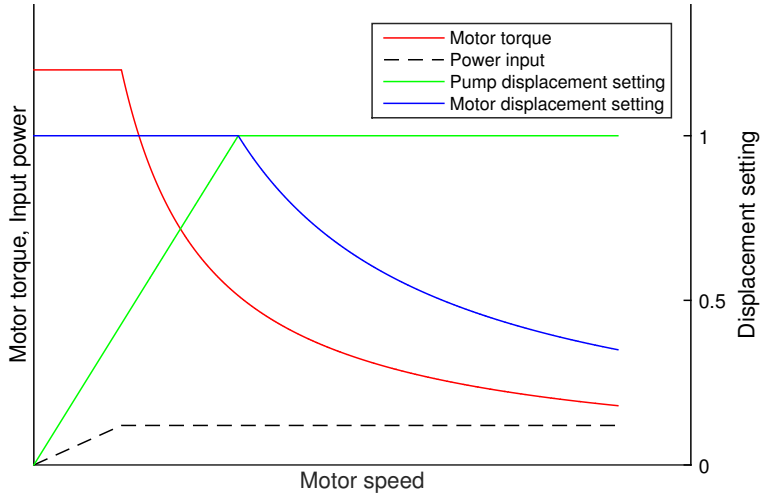

Figure 2.2: Displacement control method for increasing the speed of a hydrostatic transmission with variable pump and motor, with constant pump speed.

In Figure 2.2 the speed of the prime mover is constant and consequently the pump speed is constant. When at zero output speed the motor displacement setting is 1 and the pump displacement setting is 0. To increase the output speed the pump displacement setting is increased. As the displacement increase, the motor speed will increase and with it the input power from the prime mover also has to increase to keep the constant pump speed. When maximum input power from the prime mover is reached, at a nominal displacement of the pump, the motor torque starts to decrease due to decreasing pressure in the system. When maximum displacement of the pump is reached (displacement setting 1) the controller starts to decrease the motor displacement. Motor speed will increase until the minimum displacement setting is reached. Motor torque decrease together with the lowered motor displacement since the power input to the transmission remains constant.

2.1.2 Efficiency in hydrostatic transmissions

The efficiency η, see Equation 2.1 to Equation 2.4, of a hydraulic machine is dependent both on rotational speed n, pressure difference Δp and hydraulic fluid properties. For variable displacement machines the displacement setting also has a great influence on efficiency. The total efficiency of a hydraulic machine is divided into two types, the volumetric efficiency η_{vol} and hydromechanical efficiency η_{hm}. The volumetric efficiency represents flow losses and can in turn also be divided into two separate mechanisms. One is the slip, or internal leakage, that is the consequence of pressure gradients in small working clearances. The other

mechanism is due to that hydraulic fluid have a finite bulk modulus. This means that not all volume of fluid that is compressed/decompressed in a pump/motor will be delivered to the discharge line due to dead volumes. [15]

Torque losses in a hydraulic machine is represented by the hydro-mechanical losses η_{hm}. The torque losses are mainly dependent on the Coulomb friction, viscous friction and constant friction losses within the machine. These constant friction losses are dependent on the thin lubricant films between moving components in the machine. The viscous friction is associated with the velocity gradients within the fluid. These velocity gradients depend on both pressure differences within the fluid and on relative velocities between moving parts, normally the viscous friction is taken to be proportional to speed and viscosity but independent of pressure. The Coulomb friction is proportional to load pressure and the constant friction is represented by for example seal friction. [15, 16]

Another contribution to torque losses is the inertial forces that is needed to accelerate the fluid. In addition to these losses, both volumetric and hydromechanical efficiency is, as said, dependent on displacement setting. Running a machine at partial displacement is negative for the efficiency. [15]

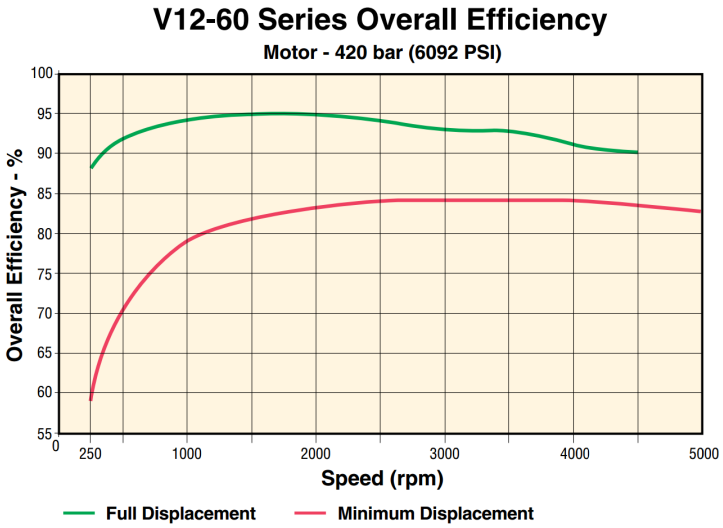

Figure 2.3: The figure shows the overall efficiency versus speed, at 420 bar pressure difference, for a model v12 variable bent-axis piston motor from Parker Hannifin. *Image courtesy of Parker Hannifin* [1]

As mentioned the efficiency of machines is also dependent on the fluid properties. Figure 2.4 shows how the efficiency of a hydraulic machine is affected by the fluid viscosity.

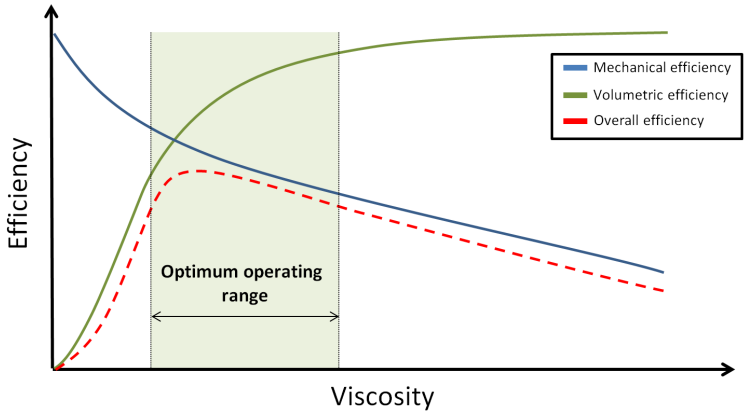

Figure 2.4: How the efficiency of hydraulic units are affected by fluid viscosity.

The viscosity is dependent on temperature and it is therefore important to keep the fluid at its optimum temperature to minimize losses. Friction losses in systems cause rise in fluid temperature and this is commonly handled by adding a heat exchanger to the hydraulic system. Losses in hydraulic transmission are not only caused by losses in machines, they occur in all components within the system such as lines, valves, heat exchangers and filters. Though in hydraulic transmission the biggest losses normally occurs in the machines.

2.1.3 Cavitation and air release

A phenomenon that is important to avoid for ensuring long lifetime and high efficiency of the components in a hydraulic system is cavitation. When the static fluid pressure in a system drops below the vaporization pressure the hydraulic fluid will vaporize. This creates gas bubbles in the fluid and as soon as the pressure increase above vaporization pressure the bubbles implode. As the bubbles implode they cause a local temperature rise that sometimes can be high enough to combust the fluid. This process, when vapor filled bubbles appears in the oil and implodes due to regained pressure, is known as cavitation and it can rapidly wear down both components and fluid. The efficiency of the system will drop due to changes in fluid properties and cavitation may also cause high noise in the system. [17, 18]

Air release is another phenomenon that also occurs at critical pressure drops. When the pressure in the fluid drops below its current saturation pressure, air bubbles are formed that, similar to cavitation, dissolves into the oil again when the pressure rise. Air release also affects the fluid properties, such as the bulk modulus, and thus cause lowered efficiency. [17]

Cavitation and air release are primarily something that occurs in valves but not seldom it also occurs in hydrostatic pumps [17]. In hydrostatic transmissions there is a risk for cavitation on the inlet side of the pump. If the supply pressure is not high enough it may cause pressure drops below vaporization or saturation pressure during certain operating conditions.

There are two main types of hydrostatic transmission circuits, open loop and closed loop circuits. The difference between the two are that in the open loop circuit all fluid pass through a reservoir whilst in a closed loop system the outlet of the motor is direct coupled to the inlet of the pump. To avoid cavitation in closed loop HST a charge pump system is often included. The charge pump ensures that no critical pressure drops occurs on the low pressure side of the transmission during normal operation.

2.2 Accumulators

A hydraulic accumulator is a reservoir that stores pressurized hydraulic fluid. The fluid is kept under pressure via an external source. Based on this external source there is two main type of accumulators, mechanical and hydro-pneumatic. The mechanical accumulators can be loaded either by a spring or via a weight, but both of them are rarely used these days. The two most common accumulator types used in industry today are the hydro-pneumatic piston type and hydro-pneumatic bladder type. Another common type is the hydro-pneumatic diaphragm type accumulator. [19, 20]

Accumulators are installed in hydraulic systems for numerous of different reasons. It can be to serve as an energy storage, to reduce pulsation, work as a shock cushioning, supplementing pump flow or maintaining pressure. The hydraulic fluid is quite incompressible, its volume reduces only about 1.7% with a pressure increase of 350 bar [19]. This enables a fast response to power demand but gives a poor dynamic power storage ability. A gas on the other hand can, at high pressures, be compressed into a small volume and store potential energy that later can be released on demand. This is the working principle of hydro-pneumatic accumulators.

If, as in many applications, the actuator in a hydraulic system suddenly stops, large pressure waves will be fed backwards through the system. The spike pressure of these waves can sometimes be several times greater than the normal working pressure. These shock spikes can be minimized by adding an accumulator to the system. When using an accumulator in a hydraulic system it is possible to store energy during idling periods and then release it when there is a peak in power demand. Hence the pump size can be reduced compared to a system without accumulators. This can reduce cost and power losses, since a pump driving at full load has a higher efficiency than one driven at partial load. Most hydraulic pumps delivers a pulsating flow which leads to pressure pulsations. These pulsations can wear the system and lead to noise. A correct installed accumulator can smoothen out these pulsations. [19]

If a system contains accumulators extra caution needs to be taken when disassembling or maintaining the system since it keeps a high pressure in the system even though the pump is turned off. If some part of the system is disassembled when the accumulator is charged it will release all pressurized fluid until the fluid reaches the precharge pressure of the accumulator. This can lead to severe personnel damages and therefore a manual or automatic blowdown valve should be

installed together with the accumulator. The blowdown valve can for example be composed of a ball valve and a variable orifice. [21]

2.2.1 Hydro-pneumatic accumulators

Hydraulic systems perform poorly if the hydraulic fluid is mixed with a gas so most hydro-pneumatic accumulators separates them. Hydro-pneumatic accumulators therefore consists of a dry side, with the compressed gas, and a wet side, with the hydraulic fluid. The gas is usually nitrogen and the dry side is filled with gas until it reaches wanted precharge pressure [20]. The precharge pressure of an accumulator should be chosen so that, regardless if the accumulator is of bladder, diaphragm or piston type, it will never fully discharge at minimum system pressure. Manufacturers gives recommendations about the precharge pressure and it is typically 80% of the minimum system pressure for bladder types and around 7 *bar* below minimum system pressure for piston types [19].

Bladder type accumulators use a balloon shaped synthetic rubber to contain the gas, see Figure 2.5. With increased system pressure hydraulic fluid enters the accumulator and contracts the bladder, as stated above the energy is then stored in the gas. When the system pressure goes below the pressure in the accumulator the bladder will expand and push the fluid back into the system. In the fluid port there is a poppet valve that prevents the bladder to extrude out into the tubes. It is preferable to mount a bladder accumulator with its fluid port downwards and its gas valve upwards hence this prevents uneven wear of the bladder. It also minimize risk of getting trapped fluid far away from the fluid port and have an early poppet valve closing. The size of bladder accumulators are typically between 1 *l* to 60 *l*. [20]

A diaphragm accumulator is using the same synthetic rubber as the bladder type, but instead of the balloon it is just a membrane that separates the gas and the fluid. They are available in sizes from 1 *dl* to around 4 *l* [20]. A quick check to see the state of an operative bladder or diaphragm accumulator is to check the body temperature. There should always be a significant temperature difference between the gas and the fluid. If that is not the case something has probably gone severely wrong with the bladder or the diaphragm [21].

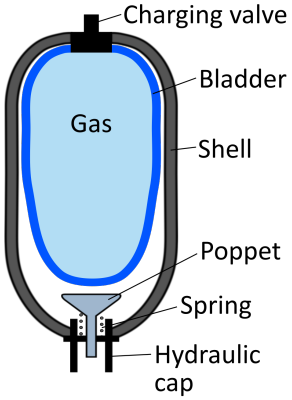

Figure 2.5: A schematic sketch of a hydro-pneumatic bladder accumulator.

Piston accumulators are designed quite similar to a rod-less hydraulic cylinder, see Figure 2.6. They have as the name implies a piston that divide the fluid and the gas. It is desirable, as for bladder accumulators, to mount piston accumulators with its fluid port downwards and gas valve upwards. Piston accumulators are currently supplied to up to 750 l in one vessel.

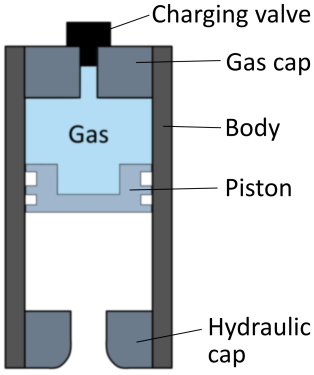

Figure 2.6: A schematic sketch of a hydro-pneumatic piston accumulator.

Bladder and diaphragm accumulators have a faster response than piston accumulators because of their low inertia, which make them suitable as shock absorbers. Advantages with piston accumulators on the other hand is that they can withstand higher temperatures and that they start leaking when failing instead of sudden rapture. [22]

2.3 Generators

A generator is a device that converts mechanical energy to electric energy. There are two types of generators, one that produce Alternating Current (AC) and one that produce Direct Current (DC). The working principle of a generator is based on Faraday's law of electromagnetic induction, i.e. an electromotive force, EMF, will be induced across a coil that is exposed to a varying magnetic field. Hence a generator has two essential parts, one part that creates a varying magnetic field, called Field, and another part where the EMF is induced, called Armature. Either the Field or the Armature is on the stationary part of the generator, called stator, and the other is on the rotating part, called rotor. The most common for AC-generators is that the Armature is on the stator and the Field is on the rotor meanwhile the opposite is most common for DC-generators. See Figure 2.7 showing a simplified model of a generator. [23, 24]

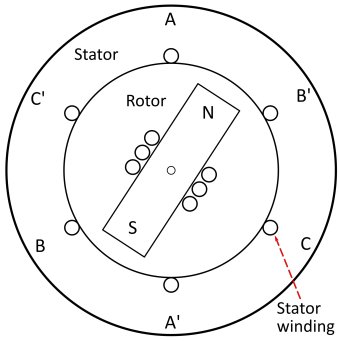

Figure 2.7: A simplified illustration of the main parts in a generator.

The stator and the rotor is usually made by electric steel[1] because it increase magnetic energy density and allows the machine designer to shape and distribute the magnetic fields in a more favorable way. The time varying magnetic flux that is present in the stator produces currents in the steel called eddy currents. This is a undesirable phenomenon which may be a significant source of losses. To reduce the eddy currents the stator is often built up by isolated laminates of electric steel. [24]

AC-generators, also called alternators, comprises two main types of generators, one that is called synchronous generators and one called induction (or asynchronous) generators. The synchronous generators works at a fixed speed called synchronous speed and a induction generator works in speeds above the synchronous speed. The process of generating a magnetic field by means of an electric current is called excitation and in a synchronous generator the Field excitation is made either by DC electromagnets or by permanent magnets. On the other hand, in an induction generator the Field is created by AC excitation.

[1] Electric steel is a special steel that is tailored to produce certain magnetic properties.

The frequency and voltage delivered from an induction generator depends on the rotational speed and the frequency of the excitation current. In a synchronous generator both the frequency and voltage are proportional to the rotational speed. [25]

To connect a generator directly with a grid, its frequency, voltage and phase shift must match the standards of the grid. First the frequency and voltage level are matched by bringing the generator to its rated speed with the right rotor field current. The phase shift is then matched by leading or lagging the delivered voltage compared to the grid voltage until the phase shift is zero and power can be delivered to the grid. [26]

2.3.1 Synchronous generators

A schematic figure of a three phase synchronous generator is presented in Figure 2.7. It has one rotor winding which creates a magnet with two poles. It also has three stator windings distributed 120 degrees apart. When the rotor rotates with a constant speed these stator windings will feel a periodically varying magnetic field and, as described above, EMF's will be induced in the windings. The EMF's will be AC for this configuration and have a frequency corresponding to the rotational speed of the rotor. So to reach 60 Hz with this generator the rotational speed has to be 3600 rpm. The frequency is also depending on the number of pole pairs, see Equation 2.8. Usually the number of poles used in a generator are based on the preferred rotational speed of its prime mover. For example steam turbines use a generator with 2 or 4 poles because of the turbines high rotational speed while in hydro turbines with their low rotational speed, typically from 60 to 750 rpm, generators with 8 to 80 poles are used. The rotor structure looks a bit different for the high and low speed generators. Low speed generators use a silent pole structure because they are more simple, thus cheaper to manufacture. High speed generators use the more robust cylindrical pole structure due to the large centrifugal forces, see Figure 2.8. [23, 27]

$$f^G = \frac{n^G}{60} \cdot \frac{p^G}{2} \tag{2.8}$$

where

$$f^G = frequency\ [Hz]$$
$$n^G = rotational\ speed\ [rpm]$$
$$p^G = number\ of\ poles$$

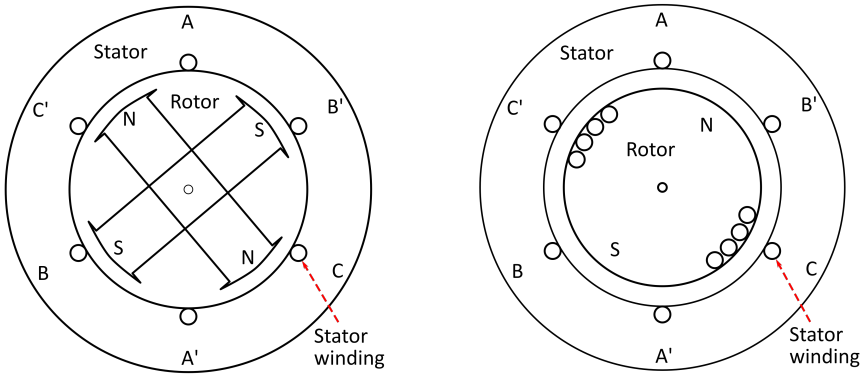

Figure 2.8: Cross section of a simple synchronous generator. To the left a generator with salient pole rotor structure and to the right a generator with cylindrical rotor structure.

In a synchronous machine there is no slip, relative movement, between the rotor speed and the rotational speed of the stator field. but there is a time lag between the rotor field and the stator field and this lag corresponds to an angle. This angle is called torque angle λ. The rotor field flux ϕ_f and the stator field flux ϕ_s also can be added to one resultant field flux ϕ_r and the angle between this flux and the rotor flux is called load angle δ_{rf}. The load angle is a measure of loading level, the higher the load the larger load angle and during idle it is zero. When operating as a generator the load angle is positive and can work in the range 0 to 180°. It reaches the highest torque, pull out torque, at 90° and usually the nominal working point should be at 30°. The torque delivered from a generator in steady-state is calculated according to see Equation 2.9. [24, 26, 27]

$$T = \frac{\pi}{2}\left(\frac{p^G}{2}\right)^2 \phi_r F_f \delta_{rf} \tag{2.9}$$

where

$$F_f = magneto - motive\ force,\ mmf,\ from\ the\ DC\ in\ the\ rotor\ [A]$$

A simplified single-phase equivalent circuit representation of a three phase synchronous generator connected to a power supply is displayed in Figure 2.9. It represents the characteristics of the generator under steady-state conditions.

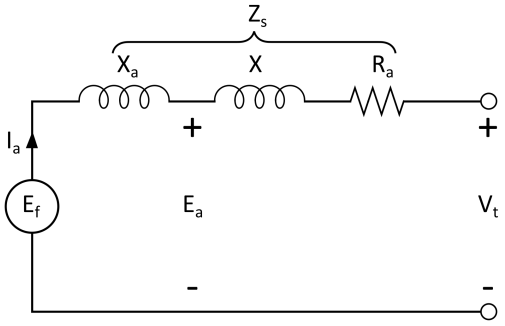

Figure 2.9: A single-phase equivalent circuit representation of a three phase synchronous generator.

The induced EMF across a winding, for example AA' in Figure 2.8, and the delivered voltage can be described by Equation 2.10 and 2.11 together with Figure 2.9. Each winding have a resistance R_a and a reactance X_a. The reactance X_a represents the magnetizing/demagnetizing effect on the rotor from the stator windings. There is also a stator leakage reactance, X. Together these form the total reactance of the machine called synchronous reactance X_s. The resistance R_s together with the synchronous reactance X_s forms the synchronous impedance Z_s. [23, 25, 26]

$$E_f = E_a - X_a I_a \tag{2.10}$$

$$V_t = E_a - I_a(R_a + X_s) = /X_s = X_a + X/ = E_a - I_a Z_s \tag{2.11}$$

where

$$\begin{aligned} E_f &= generated\ voltage\ [V] \\ E_a &= air - gap\ voltage\ [V] \\ I_a &= current\ [A] \\ R_a &= stator\ resistance\ [\Omega] \\ V_t &= terminal\ voltage\ [V] \\ X_a &= stator\ reactance\ on\ the\ rotor\ [\Omega] \\ X_s = X_a + X &= synchronous\ reactance\ [\Omega] \\ X &= stator\ leakage\ reactance\ [\Omega] \\ Z_s &= synchronous\ impedance\ [\Omega] \end{aligned}$$

Considering the Figure 2.9 the corresponding phasor diagram of voltages E_a, V_t and current I_a is presented in Figure 2.10. The two voltages E_a, V_t have an angle between them δ and this is known as the power angle and when working

as a generator this angle is positive. Also the current I_a and voltage V_t have an angle between them ϕ. Usually in electronics this angle is also called power angle and the cosine of this angle is known as the power factor pf. To avoid confusion between δ and ϕ the later will be called power factor hereinafter. [25, 26]

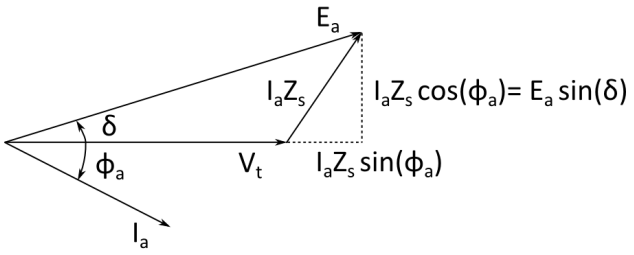

Figure 2.10: A phasor diagram of a synchronous generator.

The active power delivered by a three phase generator is given by:

$$P = 3V_a I_a cos(\phi_a)\ [W] \tag{2.12}$$

The reactive power it delivers is given by:

$$Q = 3V_a I_a sin(\phi_a)\ [var] \tag{2.13}$$

Together the reactive power and the active power gives the apparent power:

$$S = 3V_a I_a\ [VA] \tag{2.14}$$

Figure 2.10 gives that:

$$E_a sin(\delta) = I_a Z_s cos(\phi_a) \tag{2.15}$$

In most cases the winding resistance $R << Z_s$ so that $Z_s \approx X_s$. This gives with Equation 2.12, 2.13 and 2.15 the following expressions for the active and reactive power:

$$P = 3\frac{V_a E_a}{X_s} sin(\delta) \tag{2.16}$$

$$Q = 3\frac{V_a}{X_s}\big(E_a cos(\delta) - V\big) \tag{2.17}$$

Adjustment and control of E_a will control the reactive power that is produced. This can, if electromagnets are used, be made by changing the DC current in the rotor. When connected to an infinity bus, for example the grid, the terminal voltage V_t and rotational speed of a synchronous generator are held constant by this infinity bus. A bus that compared to the generator is infinitely strong meaning

that it can apply a high enough torque to force the generator to its right rotational speed but doing so with some dynamics. If the voltage E_a is smaller than V_t the generator will have a current leading the voltage V_t and this is called unexcited generator. But the most common is that a generator is driven in a overexcited state, i.e. the E_a is larger than V_t and the voltage V_t is leading the current, see Figure 2.10. [25]

2.3.2 Induction generators

Induction machines, or asynchronous machines, are totally dominant in the field of electric motors but it is rarely used as a generator. However for wind turbines they are quite widely used because of their ability of working at variable speeds. In an induction machine both the rotor and the stator have a cylindrical structure. In this type of machines AC flows in the rotor windings in contrast with a synchronous generator where DC flows, but in both of them AC flows in the stator windings. The stator and rotor are linked magnetically but not electrically. In an induction machine AC is applied on the stator windings and rotor currents are then produced by induction, transformer action. The stator is designed in a similar way as for the synchronous machine while the rotor have a bit different construction. There is two main designs of the rotor, one is called squirrel-cage rotor and the other is called slip-ring rotor. In a squirrel-cage rotor conducting bars are embedded in the rotor that are short-circuited and without external connections. This is why generators with a squirrel-cage rotor also are referred to as Single Fed Induction Generator (SFIG). A squirrel-cage machine has a simple rotor construction and no other rotational parts then the rotor bearing. This makes is cheap to manufacture and robust, hence its widely use as a motor. In the slip-ring rotor design the rotor winding have external connections and its electrical characteristics can be controlled externally, therefore a generator with slip-ring rotor is also called Doubly Fed Induction Generator (DFIG). [23, 24, 25, 27]

To generate electricity there have to be a slip between the rotor speed n_r and the rotational speed of the stator field n_s. The n_r needs to be larger than the n_s. The stator field will actually rotate with the synchronous speed calculated with Equation 2.8. Slip and slip speed is calculated by the following equations:

$$s = \frac{n_s - n_r}{n_s} \tag{2.18}$$

$$Slipspeed = n_s - n_r = n_s s \tag{2.19}$$

Hence, when working as a generator the slip is negative. Slip is the most important variable in an induction generator, hence the torque delivered is proportional to the slip speed. When the slip speed is zero the generator doesn't deliver any torque. Even if the rotor speed is higher than the stator field speed the rotor fields rotational speed is the same as for the stator field. This means that the rotor field rotates backwards relative to the rotor in an induction generator. The efficiency of an induction generator is a function of the nominal slip, a large nominal slip yields

a low efficiency. Therefore large induction generator, in the MW range, have a quite small nominal slip, below 1%, which give them a peak efficiency around 0.96. Smaller generators in the kW range usually have a larger nominal slip, hence also a lower efficiency. [25, 27]

As for a synchronous generator there is an angle between the delivered voltage and current from a induction generator. The difference is that for the induction generator the current lead the voltage. So it delivers a leading reactive power which can be absorbed by other components on the grid it is connected to. From another point of view it absorbs lagging reactive power from the grid. An induction generator has a quite large angle between the current and the voltage meaning that it delivers a lot of leading reactive power. A way of absorbing this power instead of delivering it to the grid is to use capacitors. [23, 25]

2.4 Frequency converters

A Frequency Converter (FC) is a device with the main purpose of converting Alternating Current (AC) of one frequency to into another frequency. Traditionally FCs were electro-mechanical and consisted of an electrical motor and a generator. Nowadays, with the solid state electronics, it is possible to build completely electronic FCs with no moving parts. Since the electro-mechanical types have moving parts they are often referred to as dynamic FCs and accordingly the solid state types are called static FCs. [28]

To perform the frequency conversion there exists two different approaches, direct conversion and intermediate conversion. FCs that use direct conversion are generally used in high power applications above one megawatt [28]. This is outside the power range of wind turbines that this work regards and will therefore not be further explained.

The more common conversion type is the intermediate circuit conversion. The intermediate circuit is also called ”Direct Current bus” (DC bus) and within this category of converters there are two subtypes, converters with constant intermediate circuit and converters with variable intermediate circuit. FCs with intermediate circuit consists of four main components, rectifier, intermediate circuit, inverter and control circuit, see figure 2.11. [28]

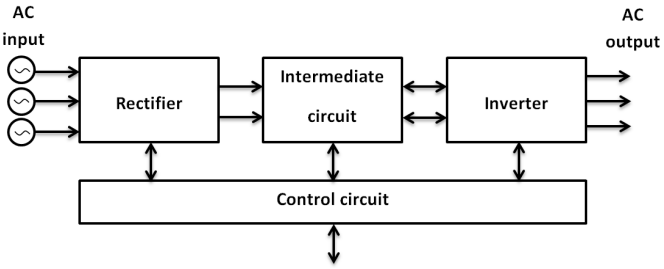

Figure 2.11: Block scheme of the main components in a frequency converter with intermediate circuit.

2.4.1 Rectifier

The rectifier is a AC to DC conversion unit, meaning that the input to the rectifier is an AC source and the output is DC. Rectifiers can be divided in two types of rectifiers, uncontrolled and controlled rectifiers [23]. Uncontrolled rectifiers are converters that does not have any control signal that operate the primary switching elements, the diodes. Controlled rectifiers are thus the opposite, they need a control signal to operate. Uncontrolled rectifiers consists of diodes and are, as the name indicates, unable to control the rectifier output. This means that a certain AC input will give a certain DC output.Figure 2.12 shows how an uncontrolled three phase rectifier converts a three phase AC input.

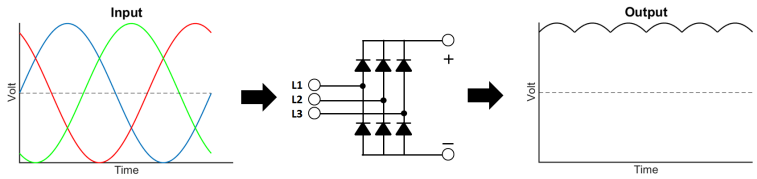

Figure 2.12: The figure shows a sinusoidal input of a three phase AC to the uncontrolled three phase rectifier (in the middle), which outputs a DC signal.

Further on the controlled rectifiers can be divided in semi-controlled rectifiers and fully-controlled rectifiers. The semi-controlled rectifiers consists of both diodes and thyristors. By controlling the firing times of the thyristors it is possible to limit the inrush currents of the units. This enables to perform soft-charging[2] of the capacitors. The output voltage of the semi-controlled rectifiers is identical to the output voltage of an uncontrolled rectifier. Fully-controlled rectifiers consists of thyristors and they are able to control the amplitude of the voltage output. Fully-controlled rectifiers result in major losses and disturbances in the supply network. This is due to high reactive current that they draw when the thyristors conduct. For this reason the thyristors are mainly used only in the inverter circuit. [28]

[2]Soft-charging limits the inrush currents to a capacitor during charge up, this eases stress on the capacitors which increase their lifetime. [29]

2.4.2 Intermediate circuit

The intermediate circuit have different functions depending on design. The functions of the circuit is to act as an energy buffer to allow the motor/generator to draw energy from/return energy to the grid via the inverter. Another function is to decouple the rectifier from the inverter and a third function is to reduce interference with the electric grid. Intermediate circuits are based on four different circuits and the type used in the FC depends on the combination of rectifier and inverter, see Figure 2.13. Depending on combination of rectifier and intermediate circuit, it delivers three different types of electricity to the inverter, variable DC, variable DC voltage or constant DC voltage. [28]

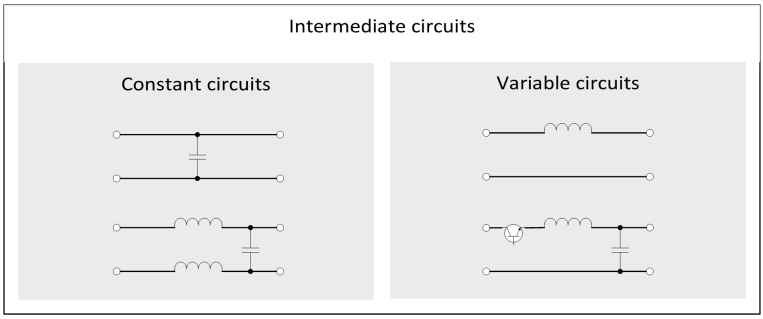

Figure 2.13: Four different types of intermediate circuits. To the left is two types used in constant DC circuits and to the right two used in variable circuits.

2.4.3 Inverter

The inverter is the final stage in the FC which generates the desired output voltage and frequency by converting the DC from the rectifier back into an AC. Depending on if the input is constant or variable the control method of the inverter varies. When the inverter is designed for a constant DC voltage the inverter is called a Voltage Source Inverter (VSI) and when designed for a constant DC current it is called a Current Source Inverter (CSI). Square-wave or Pulse Width Modulation (PWM) are the two control methods mainly used to control a VSI. If square-wave control is used only the frequency of the output can be controlled, the amplitude varies with the DC voltage input to the inverter (variable DC voltage intermediate circuit). When PWM control is used both amplitude and frequency can be varied. [23]

CSI drives can be operated either by square-wave control or by PWM control. The difference between CSI and VSI is that the CSI is fed with a constant current and that the output voltage amplitude varies with the load impedance, whilst the current amplitude is constant. Conversely the output voltage amplitude of a VSI is independent of the load. [30, 31]

The basic design of inverters are the same for all different types. Controlled semiconductors are the main components that are arranged in pairs, one pair for each output phase, see Figure 2.14.

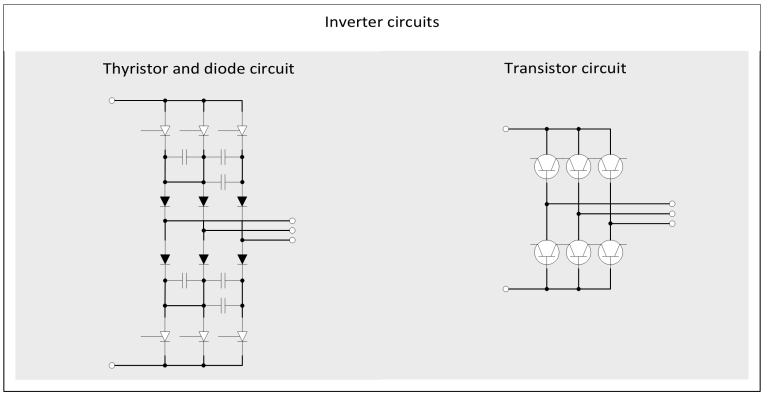

Figure 2.14: Two types of inverter circuits, one with thyristors and diodes and one with transistors.

2.4.4 Control circuit

The fourth main components in the FC is the control circuit and it has four tasks. The first one is to control the semiconductors (thyristors and transistors) in the FC. The second task is to exchange data with surrounding equipment such as Programmable Logic Controllers (PLCs) or encoders. The third task is to act as a monitoring system by measuring, detecting faults and showing warnings. And the last main task is to perform protective functions for the FC. [28]

The two main applications of the FC is to convert power from one distribution standard into another and to control the speed and torque of alternating current (AC) motors.

Control of electrical motors

The general basic functions of a FC controlling an electrical motor is to:

- Control rotation or position of the rotor.
- Control speed of AC motors.
- Control torque of AC motors.
- Monitor the operation of the motor.

To perform this type of control several different control methods exists. All control method are primarily handled by software and the more dynamic the motor control need to be, the more complex control algorithm is needed. Speed control of a motor is performed by increasing the output frequency of the FC. If the motor torque is higher than the load torque the motor speed will increase according to the raised frequency. Torque control is accomplished by controlling the current to the motor. The relationship between torque and current is not direct, it depends on slip, $\cos(\phi)$ and temperature, see Section 2.3. [28]

2.5 Wind turbines

2.5.1 Wind as energy resource

The amount of available energy in the wind is proportional to the cube of wind speed. Therefore it is of great importance to understand the characteristics of the wind as an energy resource. This is essential through the whole design process from blade design to choosing a suitable site for the turbine to be installed.

The most important characteristic of the wind resource is its variability. Wind speed varies both on a global scale and on local scale. On the global scale the wind varies with climate regions in the world, they have different amount of insolation. Within these climate regions the wind varies with geography such as distribution between land and sea. More locally the topography have a great influence on the wind, where high wind speeds are experienced on top of hills and mountains whilst in sheltered valleys, the wind speed is lower. On an even smaller scale the wind speed is affected by obstacles such as trees and buildings. On top of this the wind speed at a specific location varies over time. Gusts that vary with a time scale of seconds to minutes are called turbulent winds. These fluctuations in wind speed cause power fluctuations in the wind turbine and depending on system configuration, the impact on the quality of produced electricity will vary. [32, 33]

To extract the power from the wind the main concept for wind turbines is to use aerodynamic lift. They use blades that interact with the wind which result in a lift force perpendicular to the direction of the air flow intersected by the blades. The turbines can be divided into two main groups depending on their axis of rotation, vertical axis wind turbine and horizontal axis wind turbine. The most common type today and the only one further addressed in these studies are the horizontal axis wind turbines. The horizontal turbine can have different number of blades depending on their purpose. For electric energy production they generally have two or three blades. The benefits of having two blades instead of three is that the tower weight is lower and thereby the structure does not need to be made that strong which can give a lower cost. On the other hand the benefits of having three blades are that it gives less noise and they are also considered to be more restful to look on. These two attributes are extra important if the turbines are installed close to well populated areas. [32, 33]

2.5.2 Energy extraction in horizontal axis wind turbines

A wind turbine produce electric energy by extracting kinetic energy from the wind that powers an electrical generator. The available power in the wind is dependent on the cube of the wind speed v, the swept area A of the blades and the air density ρ according to Equation 2.20.

$$P_{air} = \frac{1}{2}\rho A U_{\infty}^{3} \tag{2.20}$$

where

$$\begin{aligned} \rho = &\ \textit{air density } [kg\ m^{-3}] \\ A = &\ \textit{swept area of blades } [m^2] \\ U_\infty = &\ \textit{upstream free wind speed } [m\ s^{-1}] \end{aligned}$$

Air density ρ is a function of air pressure, air temperature and the height above sea level. The air density at a height z above the sea level is given by [33],

$$\rho(z) = \frac{P_0}{RT} exp\left(\frac{-gz}{RT}\right) \tag{2.21}$$

where

$$\begin{aligned} P_0 = &\ \textit{standard sea level atmospheric density } (1.225\ [kg\ m^{-3}]) \\ R = &\ \textit{specific gas constant for air } (287.05\ [J\ kg^{-1}\ K^{-1}]) \\ g = &\ \textit{gravity constant } (9.81\ [m\ s^{-2}]) \\ T = &\ \textit{temperature } [K] \\ z = &\ \textit{height above sea level } [m] \end{aligned}$$

All available energy in the wind can not be extracted. A simple model used for calculating the power output of an ideal turbine rotor is called the actuator disc model [34], presented in Section 2.5.2. Rotor disc is the name of the circular swept area that the blades make when rotating. As kinetic energy is extracted from the wind, it consequently slows down. Only the speed of air that passes through the rotor disc is affected. If it is assumed that the affected air remains separated from air that does not pass through the rotor disc, the affected air can be represented by a stream tube with circular cross section. The stream tube can be extracted upstream and downstream from the rotor disc. As the upstream air within the stream tube approaches the rotor disc it slows down but is not compressed, consequently the cross section of the stream tube must expand to compensate for the bigger volume of air due to the constant mass flow, see Figure 2.15. [32, 34]

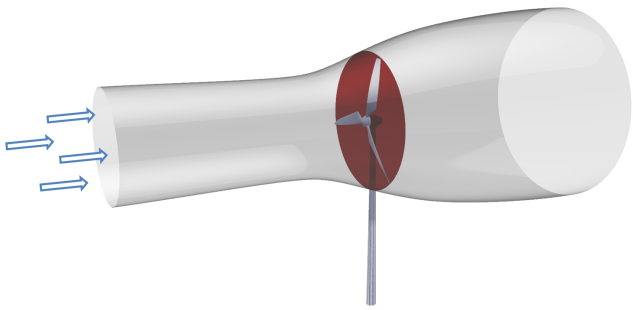

Figure 2.15: Illustration of the stream tube (grey) consisting of the affected air passing through the rotor disc (red).

When the air reach the rotor no work has yet been done on or by the air, but the kinetic energy has decreased so the static pressure must have increased. The design of the turbine blades is made to cause a static pressure drop below atmospheric pressure in the air. Hence, the air leaving the blades have a reduced speed and pressure. When the air continues to flow downstream the pressure rise to atmospheric pressure again and as consequence the speed is further reduced. This means that the air far upstream and far downstream from the rotor disc have the same static pressure but a difference in kinetic energy. The region behind the rotor disc where the air have a reduced static pressure and speed is called the wake. [32]

Actuator disc model

The actuator disc model is a simple model used to do an aerodynamic analysis of a wind turbine without any specific turbine design, it only consider the energy extraction process. In this model the turbine rotor is replaced by a circular disc through which the air flows. The model can not be used to design the rotor blades but is useful when investigating energy extraction and overall efficiency of a wind turbine. Far upstream the actuator disc in a region called $free\ stream\ region$ the air flows with the velocity U_∞ and at this point the stream-tube has a smaller area than the actuator disc. Far downstream in a region called $far\ wake\ region$ the air flows with the velocity U_w and here the area of the stream-tube is larger than the actuator disc. The expansion of the disc comes from the fact that the mass flow rate must be the same everywhere. Except these two regions you usually consider the one region just before the actuator disc and one just after it, here called *upstream region* and *downstream region* respectively. In actuator disc model there is an assumption that the speed is constant across the disc meaning that the speed in the regions around the disc is the same, here called U_{disc}. Another assumption is incompressibility of the fluid which gives that the air density remains the same everywhere in the stream-tube, simply called ρ. See Figure 2.16 for a better overview of the actuator disc model. [32, 34]

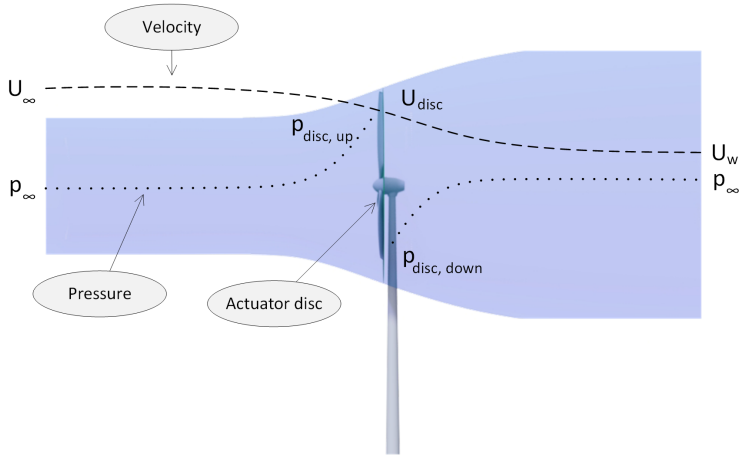

Figure 2.16: How the wind speed and pressure changes from the *free stream region* to the *far wake region* inside the stream tube (blue).

The continuity equation in the stream tube can be written as Equation 2.22.

$$\rho A_\infty U_\infty = \rho A_{disc} U_{disc} = \rho A_w U_w \tag{2.22}$$

where

$$\begin{aligned} \rho &= \ air\ density\ [kg\ m^{-3}] \\ A &= \ stream\ tube\ area [m^2] \\ U &= \ air\ flow\ velocity\ [m\ s^{-1}] \end{aligned}$$

At steady state flow the mass flow rate is described by Equation 2.23

$$\dot{m} = \rho A_{disc} U_{disc} \tag{2.23}$$

where

$$\dot{m} = \ mass\ flow\ rate\ [kg\ s^{-1}]$$

The air that passes through the actuator disc will reduce its velocity from U_∞ to U_w and the change of momentum is the speed difference time the mass flow, see Equation 2.24

$$T = \dot{m}(U_\infty - U_w) \tag{2.24}$$

where

$$T = \ rate\ of\ change\ of\ momentum\ [kg\ s^{-2}]\ (= [N])$$

Since the stream-tube is surrounded by air with atmospheric pressure, which gives no net force, the thrust that causes this change of momentum can only come from the pressure difference over the disc. This gives Equation 2.25

$$T = A_{disc}(p_{disc,up} - p_{disc,down}) \tag{2.25}$$

where

$$p_{disc,up} = \textit{ upstream pressure at the actuator disc } [Pa]$$
$$p_{disc,down} = \textit{ downstream pressure at the actuator disc } [Pa]$$

Bernoulli's equation can be used on each side of the actuator disc to obtain this pressure difference. There has to be separate equations for each side because the total energy is different on the upstream side compare to the downstream side. Assuming that the flow is horizontal will give Equation 2.26 and Equation 2.27 from the Bernoulli's equation.

$$p_{disc,up} + \frac{1}{2}\rho U_{disc}^2 = p_0 + \frac{1}{2}\rho U_\infty^2 \tag{2.26}$$

$$p_{disc,down} + \frac{1}{2}\rho U_{disc}^2 = p_0 + \frac{1}{2}\rho U_w^2 \tag{2.27}$$

where

$$p_0 = \textit{ atmospheric pressure } [Pa]$$

The pressure difference is then given in Equation 2.28 by combining Equation 2.26 and Equation 2.27.

$$(p_{disc,up} - p_{disc,down}) = \frac{1}{2}\rho(U_\infty^2 - U_w^2) \tag{2.28}$$

Combining Equation 2.28 with Equation 2.23, Equation 2.24 and Equation 2.25 gives the velocity at the disc, see Equation 2.29.

$$U_{disc} = \frac{(U_\infty + U_w)}{2} \tag{2.29}$$

If introducing the axial flow induction factor a, see Equation 2.30, the velocity at the disc can also be expressed by Equation 2.31 which gives Equation 2.32 for the velocity in the $farwakeregion$.

$$a = \frac{(U_\infty - U_{disc})}{U_\infty} \tag{2.30}$$

$$U_{disc} = U_\infty(1 - a) \tag{2.31}$$

$$U_w = U_\infty(1 - 2a) \tag{2.32}$$

This means that half of the speed loss occurs upstream from the disc and half downstream from the disc.[32, 34]

Power coefficient

The power output from the rotor can be given by Equation 2.33

$$P = TU_{disc} \tag{2.33}$$

Which together with Equation 2.25, Equation 2.28, Equation 2.31 and Equation 2.32 gives Equation 2.34 for the power extraction.

$$P = 2\rho A_{disc} U_{\infty}^3 (1-a)^2 \tag{2.34}$$

where

$$P = \ extracted\ power\ [W]$$

A power factor commonly used as a performance parameter for wind turbines called C_p is defined in Equation 2.35

$$C_p = \frac{P}{\frac{1}{2}\rho A_{disc} U_{\infty}^3} \tag{2.35}$$

where the denominator represents the power available in the wind [32]. Consequently the power extracted from the wind can be expressed as,

$$P = \frac{1}{2}\rho A_{disc} C_p U_{\infty}^3 \tag{2.36}$$

The C_p can then also be expressed as in Equation 2.37

$$C_p = 4a(1-a)^2 \tag{2.37}$$

Lanchester-Betz limit

Maximum C_p is reached when

$$\frac{dC_p}{da} = 4(1-a)(1-3a) = 0 \tag{2.38}$$

which occur when $a = \frac{1}{3}$. This gives,

$$C_{P,max} = \frac{16}{27} = 0.593 \tag{2.39}$$

This maximum achievable power coefficient is called Lanchester-Betz limit after a British and a German aerodynamicist. This limit is not caused by any design of the rotor but from the fact that stream-tube has to expand upstream of the actuator disc. Thereby is the area of the tube in the $free-stream\ region$ smaller than the area of the actuator disc. [32]

Rotor blade theory

When considering a real wind turbine rotor with a finite number of blades, not a disc, and also with a thickness some more parameters has to been taken into account. Since the blades in not uniform spanwise it is also common to split the blades spanwise into small elements, see Figure 2.17.

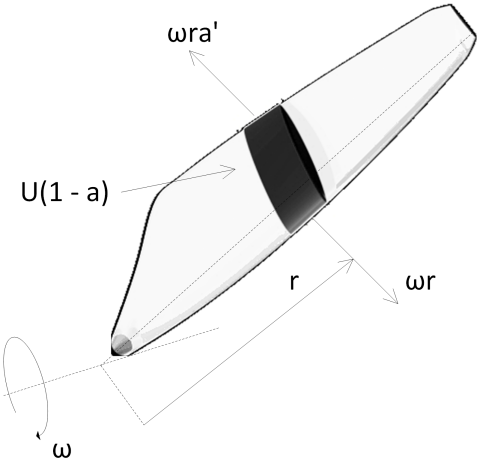

Figure 2.17: A blade element, as a small spanwise section of a blade.

There are a number of forces and velocities acting on the blades and they are presented in Figure 2.18.

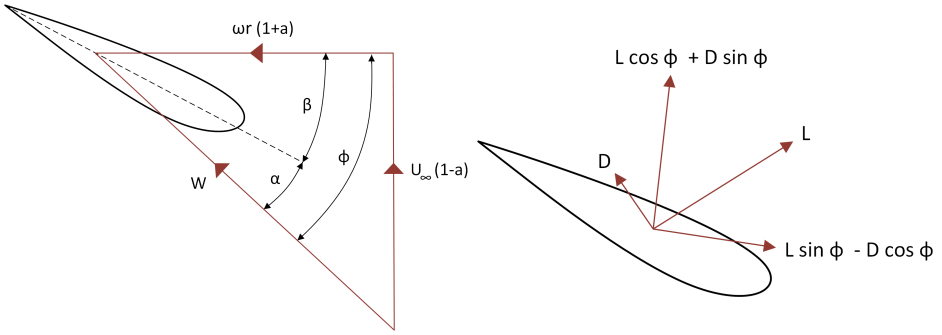

Figure 2.18: The velocities and forces acting on a blade element. To the left is the velocities and to the right is the forces.

W is the resultant relative velocity at the blades and it can be expresses as

$$W = \sqrt{U_\infty^2(1-a)^2 + r^2\omega^2(1+a')^2} \tag{2.40}$$

where

$$a' = \ tangential\ flow\ induction\ factor\ [-]$$

This velocity acts on the wing with an angle ϕ from the rotational plane of the rotor. The attack angle α is also shown in Figure 2.18 which gives that it is

$$\alpha = \phi - \beta \tag{2.41}$$

where

$$\beta = \ pitch\ angle\ of\ the\ blade\ [rad]$$

Using these equations above with a theory called Blade Element Momentum theory, which is thoroughly described by Burton [32] and Kulunk [34], the expression for the total torque from the rotor, given in Equation 2.42, can be derrived.

$$\tau_r = \frac{1}{2}\rho U_\infty^2 \pi R^3 \lambda \int_0^R \mu^2 \Big(8a'(1-a)\mu - \frac{WcB}{U_\infty R\pi} C_d(1+a')\Big) d\mu \tag{2.42}$$

where

$$\begin{aligned} R &= \ rotor\ radius\ [m] \\ \lambda &= \ tip\ speed\ ratio\ [-] \\ \mu &= r/R\ [-] \\ c &= \ chord\ length\ [m] \\ B &= \ number\ of\ blades\ [-] \\ C_d &= \ drag\ coefficient\ of\ airfoil\ [-] \end{aligned}$$

The tip speed ratio λ is defined as

$$\lambda = \frac{\omega R}{U_\infty} \tag{2.43}$$

The flow induction factors, a and a', can for a blade be described as

$$a = \frac{1}{1 + \frac{2\pi r}{Bc}\frac{4sin^2\phi}{C_l cos\phi + C_d sin\phi}} \tag{2.44}$$

$$a' = \frac{1}{\frac{2\pi r}{Bc}\frac{4sin\phi cos\phi}{C_l sin\phi - C_d cos\phi} - 1} \tag{2.45}$$

where

$$C_l = \ lift\ coefficient\ of\ airfoil\ [-]$$

The coefficients of the airfoil C_l and C_d is dependent on the shape of the airfoil and the attack angle, α. Their values can be taken from wind tunnel data of the specific airfoil.

The power extracted by the rotor can be expressed as

$$P = \tau_r \omega \tag{2.46}$$

The power coefficient, C_p, is still expressed as in Equation 2.35 but the equation for P is now substituted to Equation 2.46. Which together with Equation 2.42 gives

$$C_p = \lambda^2 \int_0^R \mu^2 \Big(8a'(1-a)\mu - \frac{WcB}{U_\infty R\pi} C_d (1+a') \Big) d\mu \tag{2.47}$$

Consequently the rotor torque extracted from the wind can be expressed as,

$$\tau_r = \frac{1}{2} \rho \pi R^3 \frac{C_p}{\lambda} U_\infty^2 \tag{2.48}$$

Performance curves

The Equation 2.47 shows that the power factor, C_p, is strongly dependent on the tip speed ratio, λ, especially since λ also affects the angle ϕ, see Figure 2.18. The C_p value is also dependent of the pitch angle, β, because of its correlation with ϕ and α. Since C_p, as stated above, is one of the most common performance factor for the rotor on a wind turbine the performance is usually presented with a $C_p - \lambda$ curve. The maximum C_p, hereinafter called $C_{p,ideal}$, will be achieved when the axial flow induction factor, a, is close to $\frac{1}{3}$. For lower tip speed ratios the axial flow induction factor gets smaller and the attack angle of the airfoil increases which then lead the blades towards stalling. At high tip speed ratios the attack angle gets smaller which makes the drag force dominant over the lift force. Meaning that when the tip speed ratio either is higher or lower than the optimum the extracted power will be reduced. An example of a $C_p - \lambda$ curve for a wind turbine with three blades is given in Figure 2.19. Three blades give a good characteristics of the curve. For a lower number of blades the curve gets flatter, meaning that changes in λ gives smaller changes of C_p, but it then reaches a lower maximum value, $C_{p,ideal}$. For more blades than three the curve gets more narrow at the top but without any increase of $C_{p,ideal}$. So from this point of view three blades is the best choice. [32]

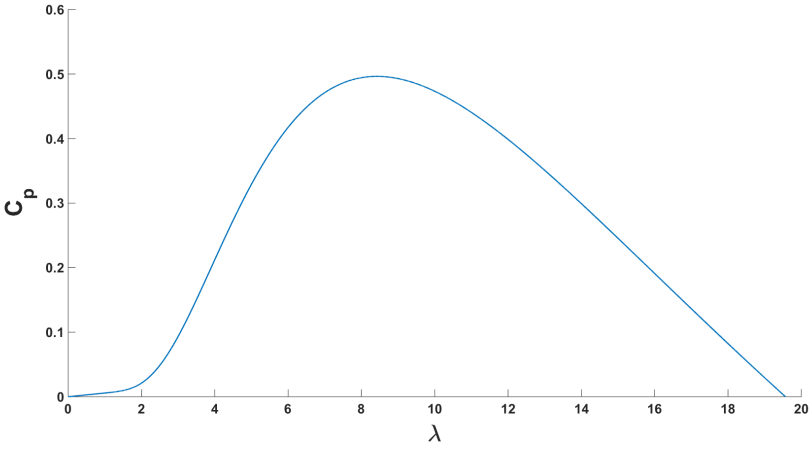

Figure 2.19: A $C_p - \lambda$ curve for a typical three blade wind turbine.

Other common performance curves to look at is the $C_Q - \lambda$ curve and the $C_T - \lambda$ curve. Where the first one is basically the C_p divided by λ, which means that it does not give any new information about the performance of the wind turbine but it is used for torque assessment purposes. The $C_T - \lambda$ curve represents the thrust force on the rotor and since this directly affects the tower this curve is used during the structural design of the tower.

2.5.3 Fixed-speed wind turbines

According to rotational speed there are two main types of wind turbine systems. One type that uses one, or two, fixed rotor speeds and the other with variable speed of the turbine's rotor. The majority of the older, smaller wind turbines uses a fixed rotor speed meanwhile the new, big turbines mainly are of variable type. [27, 33]

For a fixed-speed wind turbine, also called constant speed wind turbine, its speed is decided by the generator type, number of poles in the generator, gear ratio and the grid frequency. When the wind speed change the rotor speed will be kept constant meanwhile the electromagnetic torque will change, hence also the electrical output power will change. [35]

Control

There is two main ways to achieve this. One is to control the pitch angle of the turbine blades and varying it as the wind change, called pitch control. Either the whole blades or just the tip of them can be rotated, most common is to rotate the whole blades. The other way is to have a fixed pitch angle and a blade design that introduce stall in high wind speeds, called stall control. An advantage of the later is that it doesn't need any pitch angle actuators and control system. But a drawback with the stall control is that is has to work closer to stall than a

turbine with pitch control and this gives it lower aerodynamic efficiency. [32, 35] The benefits with fixed-speed wind turbines are that they are cheap and have a high reliability. The biggest down side is easily understood looking at Figure 2.19. Since for a fix rotational speed the tip speed ratio will vary with the wind and the $C_{p,ideal}$ can then only be reached at one specific wind speed. Which will give a low power extraction.

Concepts

In fixed speed wind turbines it is most common to use a squirrel cage induction generator directly coupled to the grid. Normally a capacitor bank, to reduce the reactive power demand, and a soft-starter, to reduce the inrush current when connecting to the grid, is also used in these systems. For an overview of this concept see Figure 2.20 . [33]

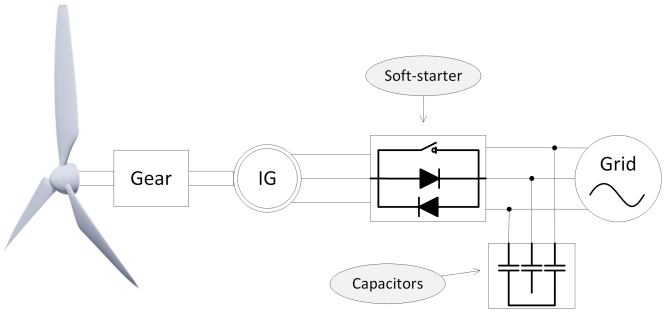

Figure 2.20: An induction generator directly coupled to the grid used for fixed-speed wind turbines.

There is also some fixed-speed wind turbines that don't use one but two fixed-speeds. This makes the deviation from the optimal C_p smaller, hence gives a higher power extraction. They usually then have two induction generators, one small generator used at low wind speeds and one larger used for high wind speeds. Thier biggest disadvantage apart from a higher cost from an extra generator is a more complex gearing and control. [27]

2.5.4 Variable speed wind turbines

As described in Section 2.5.3 one of the biggest disadvantages with a Fixed-speed wind turbine is the low power extraction due to a tip speed ratio that gives a low C_p. This is the issue the Variable speed wind turbine concepts tries to address by having a variable speed, they can then adjust the speed in some range to here get an optimal tip speed ratio that gives $C_p = C_{p,ideal}$ hence get the best power extraction. That a Variable speed wind turbine can extract more energy than a Fixed-speed wind turbine is its biggest advantage. It also have lower noise emissions which is good for wind turbines installed close to populated areas. The disadvantage of a variable speed wind turbine is a more complex control and the

need of extra equipment, that always comes with a cost, to decouple the rotor speed and the delivered frequency. This decoupling is needed since the frequency delivered by a generator is dependent on its rotational speed. So either the speed of the generator has to be kept constant by decoupling its speed from the rotor speed or the delivered frequency has to be adjusted by a frequency converter. It can either be a synchronous or induction generator together with a full scale frequency converter that, as the name implies, has to take in and convert all the produced power. The other solution is to use a Doubly Fed Induction Generator, DFIG, with a partial power frequency converter. [27, 32]

Control

For a variable speed wind turbine you usually talk about three or four control regions, see Figure 2.21. The first region is between zero wind speed to cut-in speed[3] and in this part when the wind are getting close to the cut-in speed the startup of wind turbine start. Meaning get the rotor from standstill towards its minimum operation speed and connect the system to the grid.

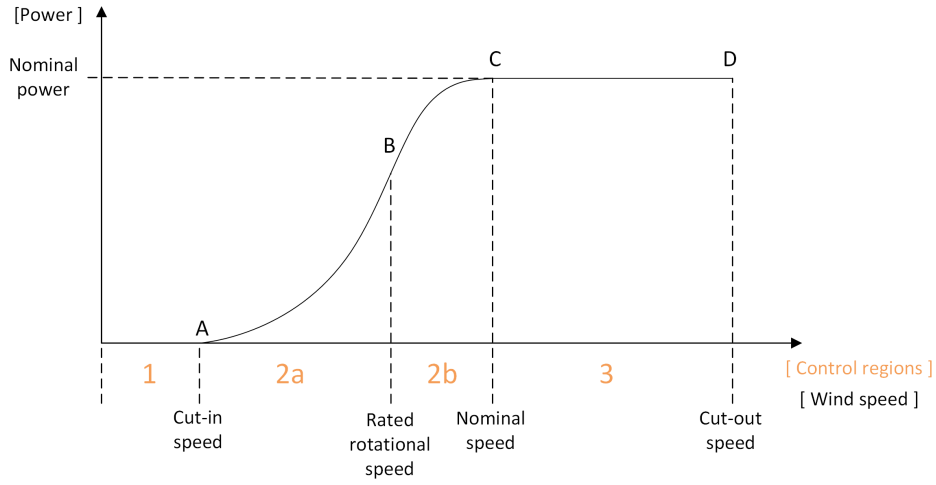

Figure 2.21: Illustration of the four different control regions from stand still to cut-out speed.

The second region, *Region* 2, is usually split into two regions, hereinafter called *Region* 2*a* and *Region* 2*b*. Where *Region* 2*a* is from cut-in speed to rated rotational speed[4] and it is in this region a variable speed wind turbine can by adjusting the rotational speed follow the optimal tip speed ratio. *Region* 2*b* is from rated rotational speed to nominal speed, the wind speed where the wind turbine reaches its nominal power, see Figure 2.22. In this region the rotational speed of the rotor has to be kept constant at its rated speed to not risk damage on

[3]The minimum wind speed where the wind turbine generates useful power.
[4]The maximum rotor speed allowed to not damage the blades, rotor or structure.

the wind turbine and this is done by increasing the opposing torque on the rotor. Depending on the design, used concept and construction of the wind turbine the *Region* 2*b* can differ in size and if the design is made to not reach the rated rotational speed until the nominal power *Region* 2*b* will not exist or at least be very small. [32, 35]

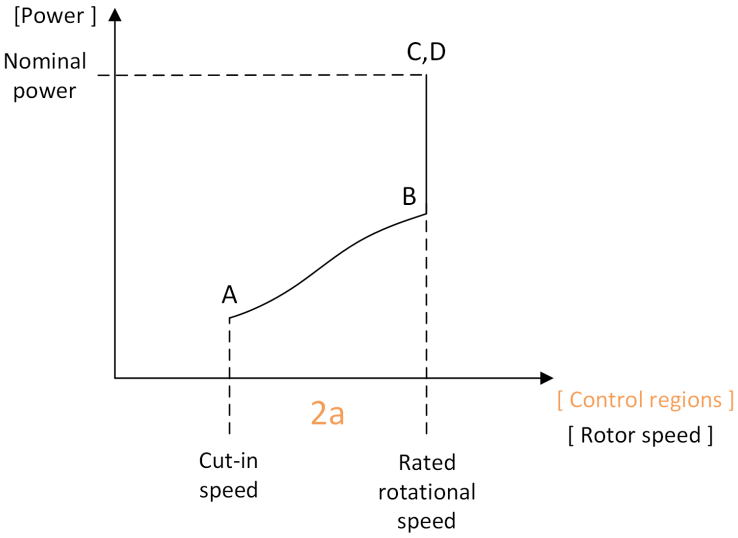

Figure 2.22: How the rotor speed changes in the different control regions.

In the last region, *Region* 3, which is from nominal wind speed to cut-out speed[5] the power input is kept constant at nominal power. This is done by using pitch control[6] to reduce the C_p, hence reduce the percentage of power extraction from the total wind power available, when the wind speed increases and the available power in the wind with it. When reaching the cut-out speed the wind speed is of that magnitude that it can damage the wind turbine and the wind turbine is therefore shut off and the rotor is turned away from the wind. [35]

$K\omega^2$ control

To extract as much energy as possible in the control region Region 2*a* the tip speed ratio needs to be kept constant at its value that gives $C_{P,ideal}$. To achieve this some kind of Maximum Power Point Tracking, also called Tip Speed Ratio Tracking, control strategy has to be implemented. One of the most widely used strategies is the one called $K\omega^2$ [36]. It sets a torque in the system called control torque, or reference torque. This torque is given by

$$\tau_c = K\omega_r^2 \tag{2.49}$$

[5]The maximum operational wind speed.
[6]Rotating the blades along their own axis to change their attack angle.

where

$$K = \ gain\ factor\ [kgm^2]$$

K is given by

$$K = \frac{1}{2}\rho A R^3 \frac{C_{p,ideal}}{\lambda_*^3} \tag{2.50}$$

where

$$\lambda_* = \ optimal\ tip\ speed\ ratio\ where\ C_{p,ideal}\ occurs\ [-]$$

The correlation between control torque and generator torque when a gearbox is used is

$$\tau_c = \ (gear\ ratio) \cdot \tau_g \tag{2.51}$$

With the assumption that the rotor is rigid the rotor acceleration will be

$$\dot{\omega}_r = \frac{1}{J}(\tau_r - \tau_c) \tag{2.52}$$

where

$J = \ combined\ rotational\ inertia\ of\ rotor,\ gearbox,\ generator\ and\ shafts\ [kgm^2]$

Combinding Equation 2.48, Equation 2.49, Equation 2.50 and Equation 2.52 gives the following expression for the rotor acceleration

$$\dot{\omega}_r = \frac{1}{2}\frac{1}{J}\rho A R^3 \omega_r^2 \left(\frac{C_p(\lambda, \beta)}{\lambda^3} - \frac{C_{p,ideal}}{\lambda_*^3} \right) \tag{2.53}$$

Since all the parameters outside the large brackets are positive the sign of the difference inside the brackets will decide if the rotor will accelerate or decelerate.

If $\lambda < \lambda_*$ and

$$C_p > \frac{C_{p,ideal}}{\lambda_*^3}\lambda^3 \ \left(= F(\lambda) \right) \tag{2.54}$$

the aerodynamic torque acting on the rotor will be bigger than the control torque set in the system by the control method, hence the rotor will accelerate and it will accelerate until $\lambda = \lambda_*$.

Meanwhile when $\lambda > \lambda_*$ the control torque will be bigger than the aerodynamic torque which will make the rotor decelerate instead. Also this time it will go towards $\lambda = \lambda_*$. For a better understanding of this see Figure 2.23 where the left hand side and right hand side from Equation 2.54 is presented as a function of λ. So when the blue curve is above the red curve in Figure 2.23 the rotor will accelerate and when the red curve is above the blue curve the rotor will decelerate

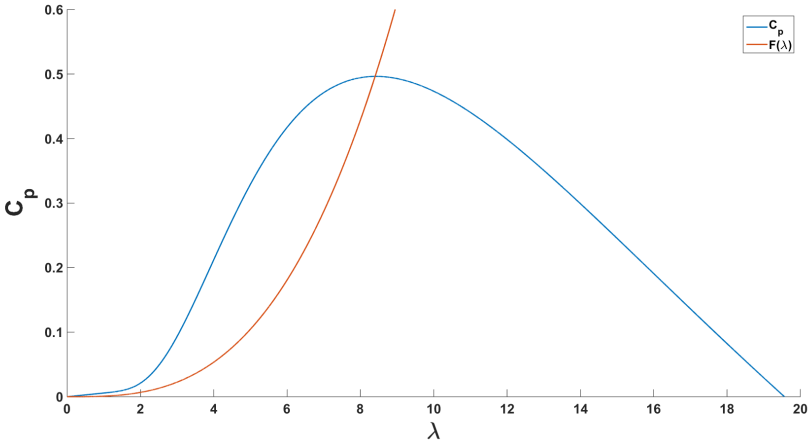

Figure 2.23: Working principle of the $K\omega^2$ control strategy.

However when $\lambda << \lambda_*$ the inequality, Equation 2.54, is not fulfilled and the control torque set by the $K\omega^2$ control method will be bigger than the aerodynamic torque acting on the rotor, hence this will drive the rotor speed towards zero. Usually wind turbines have some separate control mechanism that prevents the rotor speed from going to zero when the wind speed is above the cut-in speed, this then has to take over the control until the tip speed ratio, *lambda*, reaches a value to again fulfill the inequality, Equation 2.54. [37]

The $K\omega^2$ strategy is seen as a robust and simple control strategy but it also got some critics for being too slow which can result in a low energy extraction from the wind [36]. One other downside with this control strategy if using PID or other simple controllers is that since the control region 2 is split into two parts also two separate controllers are needed. Where the $K\omega^2$ PID-controller can be used only for the first part when the rotational speed is lower than the rated rotational speed. Then another PID-controller have to take over to make sure that the rotational speed doesn't exceeds the rated rotational speed. This add some complexity to the control system and it also add the need for a smooth transition between the controllers.

Concepts

As mention in the beginning of this subsection there is two common concepts for variable speed wind turbines. Where one is to use a synchronous or induction generator together with a full power frequency converter, the concept is presented in Figure 2.24. This concept can either be without or with a gearbox. If no gearbox is used the generator need to have many poles because of the low rotational speed, it is between 20 - 40 rpm for large MW wind turbines [27]. This will increase the size, hence also the price, of the generator. The advantage with this solution is that one of the most common components to break, the gearbox, is removed [27].

The more common solution is to use a gearbox to be able to increase the rotational speed of the generator so a smaller generator with less poles can be used.

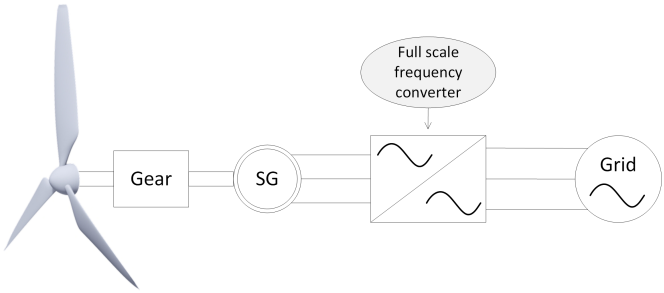

Figure 2.24: A synchronous generator with a full scale frequency converter used for variable speed wind turbines.

The other common concept with a DFIG directly coupled to the grid and a partial scale frequency converter is presented in Figure 2.25. The reason only a partial power frequency converter is needed in this concept is because the output frequency of a DFIG can be controlled by controlling the frequency fed to the generator rotor winding. So by feeding the rotor winding in the generator with the right frequency a desired output frequency can be reached. The frequency converter used usually has a power around 30% of nominal power [33]. The percentage of total power the frequency converter needs is decided by the desired speed range. A need for a larger span of achievable speeds yields for a higher rated power of the frequency converter [32]. This solution has become widely used since a smaller frequency converter is much cheaper than a big one, but also because when not all generated power has to be converted the total efficiency can get higher [33].

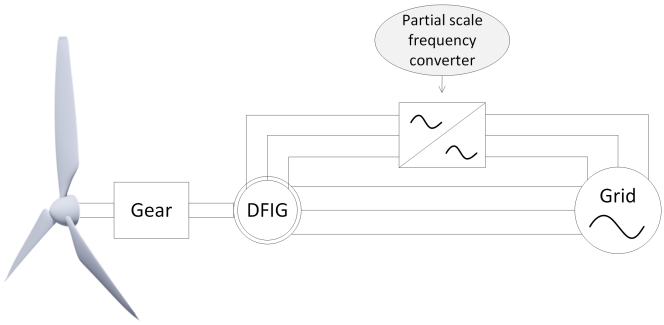

Figure 2.25: A doubly fed induction generator directly coupled to the grid with a partial scale frequency converter used for variable speed wind turbines.

Other concepts that not yet have become a commercial success is for example using a mechanical continuously variable transmission or a continuously variable hydrostatic transmission similar to those used in vehicles [32]. These concepts are

able to disconnect the rotor speed from the generator speed which gives that the delivered frequency can be kept constant without any need of a complex frequency converter.

2.5.5 Hydrostatic transmissions in wind turbines

To use a hydrostatic transmission, HST, in wind turbines has at this moment not yet become a commercial product. Some research has been done in the area and apart from at Federal University of Santa Catarina, the work that this study is based on [2], also at for example Aachen University, University of Minnesota, and by Mitsubishi. Mitsubishi has with its Sea Angel project been closest to release a big wind turbine with a HST implemented as a commercial product. Whereas the studies at the universities are more far from being a commercial product, some was purely theoretical and some reached a bit further with a test bench to evaluate their concepts. All of them use very simplified the same basic concept, see Figure 2.26, with a big "fixed" displacement pump with low rotational speed, directly coupled to the wind turbine rotor without any gearbox and a variable displacement motor coupled to the generator. The generator is then supposed to be directly coupled to the grid without any frequency converter.

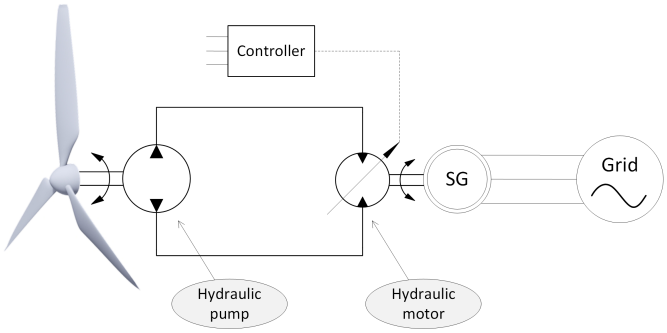

Figure 2.26: A HST with a synchronous generator directly coupled to the grid used for variable speed wind turbines.

In Aachen University they started with several different concept, then they chose the most promising one and built a test bench of it. The concept contains of multiple hydraulic pumps with fixed displacement and multiple hydraulic motors with variable displacement. The idea with this was to make the drivetrain modular to fit a various sizes of wind turbines and to increase the efficiency. The built test bench is for a power of 1 MW where the drivetrain consists of two pumps and 4 motors. Apart from this they for the test bench additionally used two electric motors, two hydraulic pumps with variable displacement and two hydraulic motors with fixed displacement to simulate the load of a generator and the power input from a wind turbine rotor. They concluded that using a HST in a wind turbine can be a good option, since it gave good characteristics in controlling the rotor speed while keeping the generator speed constant. The later should make

the frequency converter redundant. They also showed that a HST have excellent damping characteristics of torque impulses from the wind. The overall efficiency was above 85% for a wide power range. The only downside they saw was that there is yet no any available hydraulic pumps large enough for multi-MW wind turbines. [38]

The work done at University of Minnesota focused on mid-sized wind turbines with a nominal power from 100 kW to 1 MW. In this power range the most common is to use the fixed speed concept described in Section 2.5.3 so their first goal was to investigate if a HST in a wind turbine could produce more energy than that concept. At the University of Minnesota they built a test bench with a rated power of 50 kW to conduct their studies on. The drivetrain for the test bench consisted of a fixed displacement pump and a variable displacement motor. Also for this test bench the generator and the rotor was simulated in the same was as in Aachen University, here by using two hydraulic machines and one electric motor. They considered the damping to reduce shock loads and flexible system configurations as advantages with using a HST in mid-sized wind turbines. They also saw it as a concept with low cost and high reliability that potentially could replace the gearbox and power electronics used in many variable speed concepts. Their biggest concern was the efficiency of the drivetrain components. But since it foremost was compared to fixed speed wind turbines, tracking the optimal C_p will still give it a higher output power for their concept. [36, 39]

In further studies they have by simulation evaluated two control strategies for *Region*2*b*. Where they compared the $K\omega^2$ control law with a Model Predictive Control, MPC. They concluded that their MPC controller was faster for small wind changes than the $K\omega^2$ but had a large overshoot and for a large step down in wind speed it totally lost the control. So more studies is needed to optimize their MPC parameters before more conclusions can be drawn from that study. [36]

Mitsubishi have installed one 7 MW turbine with a HST as drivetrain in Scotland and as this is written they are installing one more on a floating platform outside the coast of Fukushima. This is supposed to be up and running before the end of this year, 2015 [40]. At first the whole wind turbine was supposed to be released as a commercial product but after the joint venture between Mitsubishi and Vestas, forming the company MHI Vestas that will produce large offshore wind turbines, the idea now is instead to commercialise only the hydrostatic drivetrain. Then put this HST in the MHI Vestas V164 8 MW turbine [41]. The drivetrain is made by the Mitsubishi owned company Artemis that has developed a new type of hydraulic machines called digital displacement hydraulic machines. These machines have a peak efficiency of approximately 97% at full displacement and 96% at 20% displacement. But what differentiate them the most from the conventional hydraulic machines is that they keep a very high efficiency for a wide operational range [42]. Since the efficiency is seen as one of the greatest disadvantages for using a HST in wind turbines [39], the use of a HST with digital displacement hydraulic machines seems to be a promising concept.

Chapter 3

Concept description

This chapter aims to give the reader an overview of the drivetrain concept using a hydrostatic tranmission. How it will be implemented in a wind turbine and also how the test platform will be designed. In the project a simulation model is used, developed by Eduardo Augusto Flesch [2]. This model together with other project prerequisites are also briefly explained in this chapter.

3.1 Wind turbine concept

The wind turbine concept that this project is based on is a variable wind turbine utilizing a hydrostatic transmission and a synchronous generator. The generator is coupled directly to the electrical grid which entails that it will have to run at a constant speed to produce electricity with a certain frequency. The hydrostatic transmission disconnects the generator speed from the aerodynamic rotor speed and by doing so, it allows the generator to run at a fixed speed whilst the rotor speed may vary. The main hydraulic pump in the transmission is directly coupled to the aerodynamic rotor and placed in the nacelle, in the top of the wind turbine. From the pump, hydraulic lines, runs to the bottom of the wind turbine tower where they are connected to the hydraulic motor. The hydraulic motor is, in turn, coupled to the synchronous generator that delivers electricity to the grid. Figure 3.1 visualizes the concept and the main drivetrain components.

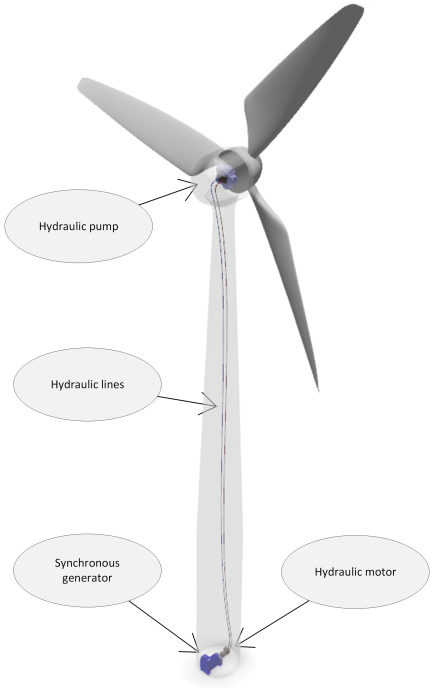

Figure 3.1: Illustration of the concept with the main components of the drivetrain.

The generator will, as mentioned, be coupled directly to the grid but this must be done under controlled conditions. These conditions are monitored by safety electronics that disconnects the system from the grid if not fulfilled. Figure 3.2 shows a schematic sketch of the wind turbine concept. Power is extracted from the wind by the aerodynamic rotor, the mechanical power of the rotor shaft is transferred to the hydraulic pump that generates hydraulic power, flow and pressure.

The hydraulic power is then converted back to mechanical power by the hydraulic motor which, in turn, drives the generator that generates electricity. If the parameters (frequency, phase and voltage) is within the allowed conditions determined by the safety electronics, the generator is connected to the grid and the produced electricity is delivered.

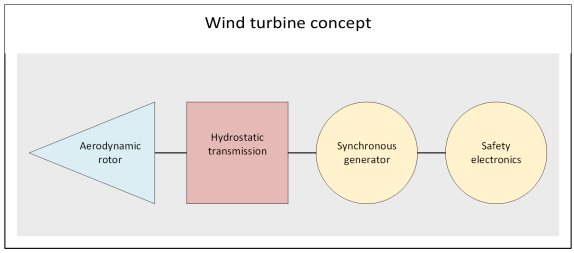

Figure 3.2: Schematic sketch of the wind turbine concept.

3.2 Test platform concept

The long term goal is to design a test platform that enables evaluation of the wind turbine concept. Some practical aspects determine how the test platform will take shape. Instead of using a real aerodynamic rotor to drive the pump, the torque from the rotor on the pump will be simulated by using an electric motor. The motor is controlled by a frequency converter and coupled to a speed reducer. This enables simulation of almost any desired wind profile, since both measured wind speed and designed wind profiles can be evaluated. It also makes it possible to build and run the test platform inside the laboratory since the test platform location is independent of site specific wind characteristics. Figure 3.3 illustrates how the aerodynamic rotor torque will be simulated using a frequency converter and a electric motor.

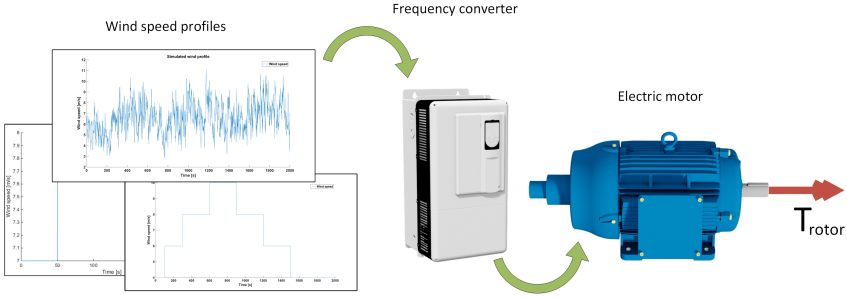

Figure 3.3: How the aerodynamic rotor will be simulated in the test platform.

Comparing the wind turbine concept with the test platform concept they are identical from the hydrostatic transmission to the electrical grid, seen from rotor to grid. Meaning that the same type of components, except the aerodynamic

rotor, as earlier explained, may be used in both systems, compare Figure 3.2 with Figure 3.4.

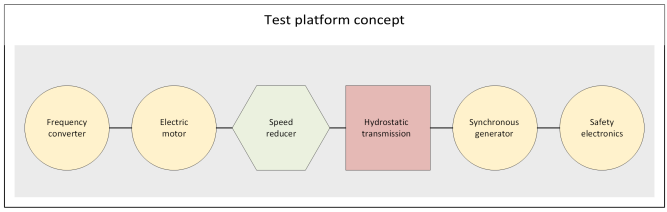

Figure 3.4: Schematic sketch of the test platform concept.

To get even more similarity to how the transmission would be implemented in a wind turbine, the hydraulic pump will be mounted with a height difference of roughly 8 meters above the hydraulic motor. Figure 3.5 shows how the test platform will be constructed in the laboratory. The height difference is achieved by installing the hydraulic pump and the components that represents the aerodynamic rotor on a steel platform located on the roof of the laboratory meanwhile the other components are placed at the bottom floor of the building.

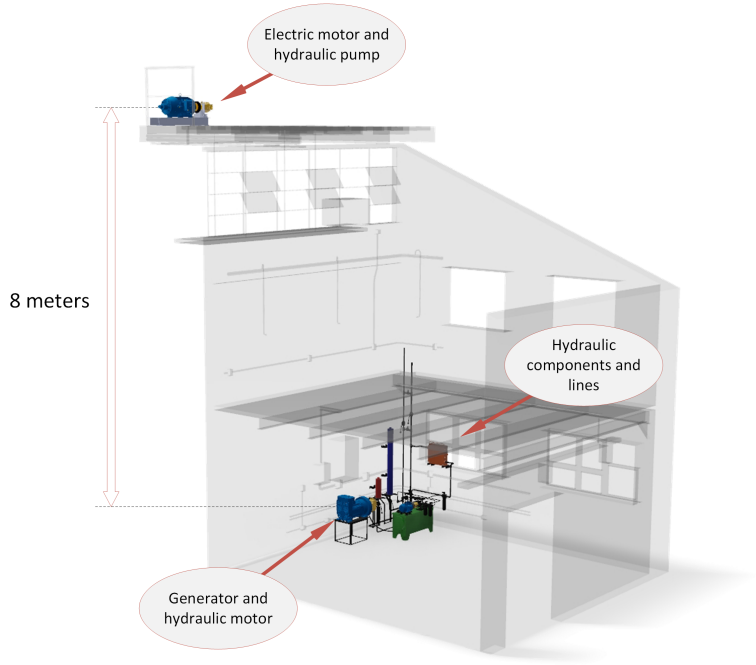

Figure 3.5: CAD model that illustrates how a height difference is achieved when constructing the test platform in the laboratory of LASHIP.

3.3 Starting point of the project

This section aims to give the reader an idea of the project prerequisites. Which includes a brief explanation of the AMESim model and the components that will be used in the test platform to simulate the torque from the aerodynamic rotor.

One predetermined parameter was the maximum aerodynamic rotor speed. It had been scaled from the 150 kW wind turbine of 80 rpm to suit the 20 kW test platform and was given as maximum rotor speed of 120 rpm.

The original model consists of four main parts, see Figure 3.6, where the first part models the aerodynamic rotor i.e. how power is extracted from the wind. It uses wind speed and rotor speed as input signals and output a torque to the pump shaft. The second part models the hydrostatic transmission and all its components. It has torque from the rotor as input and it output torque via the hydraulic motor to the shaft of the electrical generator. The system is regulated by the controller in part three. The controller use pressure and rotor speed feedback from the transmission and wind speed measurement to control the displacement of the hydraulic motor. The fourth part models the generator and how it interact with the electrical grid. It has the torque from the transmission as input and as output it has power delivered to the electrical grid.

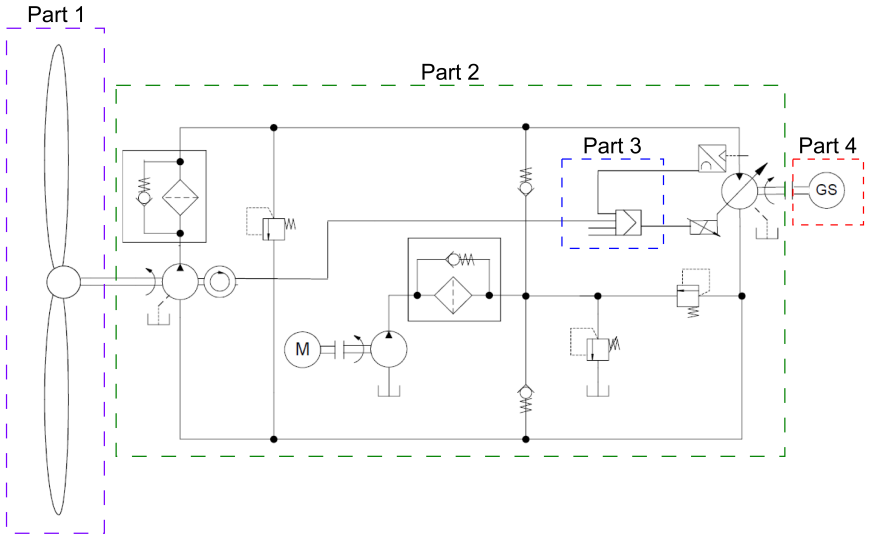

Figure 3.6: Illustration of the four main parts of the original model, based on a picture from Flesch [2].

In the following sections a brief description of the four parts will be given. For a profounder description see the report from Flesch [2].

3.3.1 Model of aerodynamic rotor and wind extraction

In this section the model of the aerodynamic rotor and its interaction with the wind is described. Figure 3.7 illustrate how the model is composed.

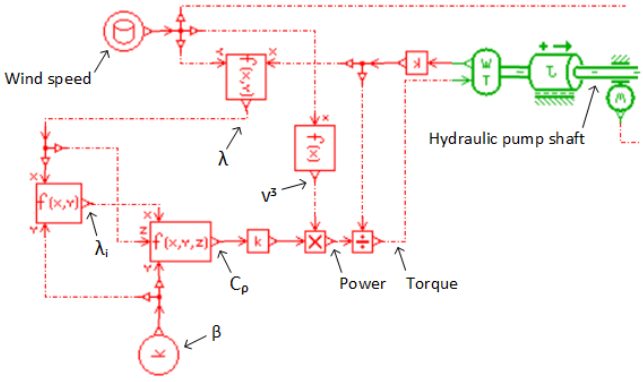

Figure 3.7: Model of the rotor and its interaction with the wind.

To model the characteristic wind power extraction of the rotor, Equation 3.1 is used which is based on a specific blade profile and Equation 2.47.

$$C_p = 0.258\left(\frac{100}{\lambda_i} - 0.4\beta - 2.164\right) \cdot exp\left(\frac{-15.21}{\lambda_i}\right) + 0.00571 \cdot \lambda \tag{3.1}$$

where λ_i is a help variable given by,

$$\lambda_i = \left(\frac{1}{\lambda + 0.08\beta} - \frac{0.035}{\beta^3 + 1}\right)^{-1} \tag{3.2}$$

In the model the wind speed goes together with the rotational speed of the rotor into the block with Equation 3.3 that calculates the tip speed ratio, λ.

$$\lambda = \frac{\omega_r R}{v} \tag{3.3}$$

where v is the wind speed. This tip speed ratio, λ, and the pitch angle, β, is then used first in the block with Equation 3.2 and then together with this result to calculate the power coefficient C_p in the block with Equation 3.1. With C_p, wind speed to the power of three, rotational speed of the rotor and the gain, from Equation 3.4, the torque is calculated according to Equation 2.48.

$$gain = \frac{1}{2}\rho\pi R^2 \tag{3.4}$$

The torque is then sent to the inertia where it, depending on the opposing torque from the hydraulic pump, will accelerate, decelerate or maintain the rotational

speed of the rotor. The inertia is the sum of inertias from the blades, hub, main shaft and bearings in the aerodynamic rotor. The rotational speed is then feedbacked into the block and the gain on this signal is simply to convert it from rpm to rad/s.

3.3.2 Model of hydrostatic transmission

The hydraulic system was modeled as presented in Figure 3.8. The hydraulic transmission is a closed circuit HST with one main fixed displacement pump and one main variable displacement motor. The hydraulic lines connecting outlet of pump/motor and inlet of motor/pump are called the main circuit and apart from the pump and motor a filter is attached to it. The filter is there to model its pressure drop. The system has a fixed rotational direction of both pump and motor so the line at the top of the figure is the high pressure line and the one at the bottom is the low pressure line. The system was sized for a nominal pressure of 200 bar and there is a pressure relief valve between the high and low pressure side with a cracking pressure of 230 bar that limits the maximum pressure. There is also a pressure relief valve from the low pressure line, via the charge circuit, to the tank with a cracking pressure of 25 bar that limits the pressure at the low pressure side.

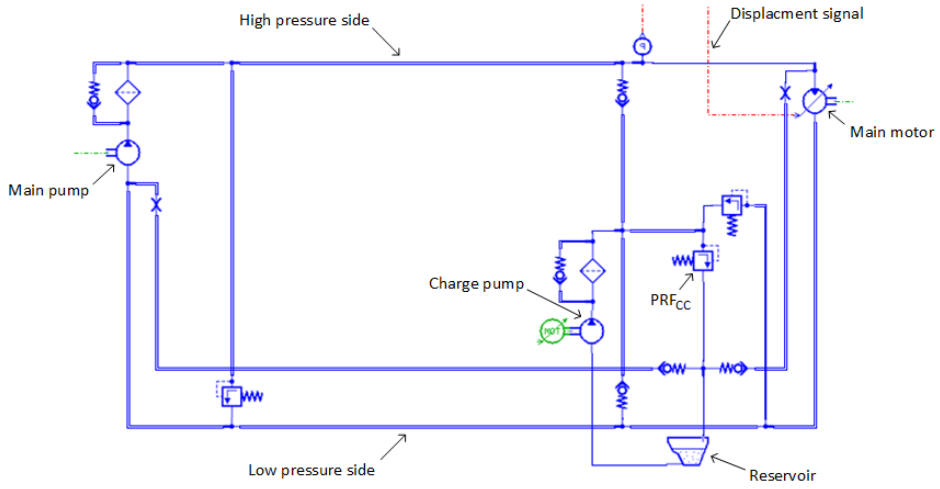

Figure 3.8: Model of the HST.

To model the efficiency of the main pump and main motor the mechanical efficiency is set to a fixed value of 93% inside the component models while the volumetric efficiency is divided and modeled in two parts, one that represent the external leakage and one the internal leakage. Both parts representing the volumetric efficiency was assumed to be equally large with an efficiency of 98.75% each. The internal parts consisting of cross port leakage, fluid compressibility losses and

timing-grove flow losses are modeled as a fixed value inside the component models. The external leakage of the volumetric losses are modeled by two hydraulic lines with sharp edged orifices that regulates the flow. These lines are going from the main line close to respectively machine inlet to the tank. The diameter of the orifices was chosen so that the flow to the tank corresponds to 1.25% of the total flow in the main circuit at rated power.

Apart from the main circuit there is a charging circuit. It consists of a charge pump, a filter and a pressure relief valve. The function of this system is to supply the main circuit with the oil that is leaking back to tank from the main machines and to prevent cavitation in the main pump. The charge system is connected to both the low and high pressure side and there are check valves in between the main and charge circuit to prevent high pressure in the charge circuit that otherwise could damage the components there. The connection to the high pressure side is to fill these lines of the system with oil at the first start up and after maintenance. The cracking pressure of the pressure relief valve PRF_{CC} in Figure 3.8 will set the pressure in the charge circuit and also the minimum pressure at the inlet of the pump. To avoid cavitation in the pump, the cracking pressure is therefore chosen, considering pressure drop in the line, high enough to ensure that the pressure at the pump inlet never drops below 1 *bar*.

3.3.3 Model of control system

This section describes how the control system, seen in Figure 3.9 was modeled.

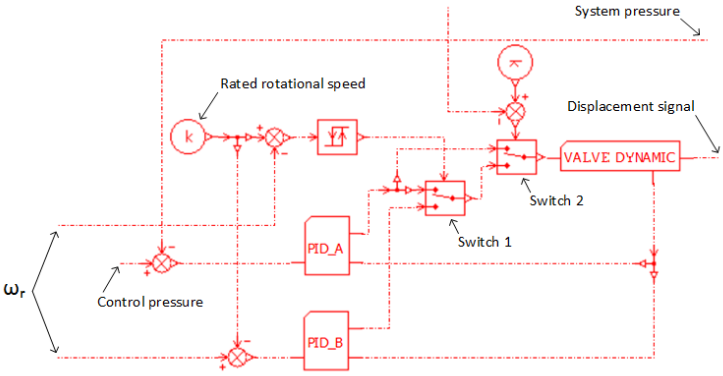

Figure 3.9: Model of the control system.

As described in Section 2.5.4 there is four main control regions. Where region 1 is the start up phase from standstill to connection with grid. Region 2a is from cut in speed of 4 m/s until the rotor has reached its rated rotational speed of 80 rpm, region 2b is from rated rotational speed to nominal power and region 3 is from the nominal power to cut-out speed. Region 1 and 3 are outside the scope of this study but the idea for region 3 is to use something called active pitch control or passive stall of the blades.

In region 2a the control strategy for Maximum Power Point Tracking (MPPT) $K\omega^2$ was used. As described in Section 2.5.4 the idea of this control strategy is to reach the optimal tip speed ratio, λ_*, i.e. reach the optimal C_p that yields maximum power extraction. This is done by calculating a control torque based on λ_* and $C_{p,ideal}$ for this specific wind turbine, together with the square of the current rotor rotational speed. The difference when using a HST instead of an electric drivetrain is that the torque can be recalculated to a control pressure, see Equation 3.5.

$$T_c = T_p = p_c D_p \eta_{hmp} \tag{3.5}$$

where

$$\begin{aligned} T_p &= \textit{pump torque } [Nm] \\ p_c &= \textit{pressure difference over the pump } [Pa] \\ D_p &= \textit{pump displacement } [m^3/rad] \\ \eta_{hmp} &= \textit{hydro mechanical efficiency of the pump } [-] \end{aligned}$$

This will together with Equation 2.49 give,

$$p_c = \frac{1}{D_p \eta_{hmp}} \cdot K\omega_r^2 \tag{3.6}$$

and with Equation 2.50 this gives the following new expression for K,

$$K = \frac{1}{2}\rho A R^3 \frac{1}{D_p \eta_{hmp}} \frac{C_{P,ideal}}{\lambda_*^3} \tag{3.7}$$

This K is then used in the control strategy to calculate a reference pressure, p_c. One PID controller, PID_A in Figure 3.9, is used to minimize the difference between the measured system pressure and the calculated reference pressure.

When the rotor reaches its rated rotational speed another PID controller, PID_B in Figure 3.9, steps in and takes over the control. PID_B regulates with the goal to keep the rotational speed fixed at the rated rotational speed. The speed is limited to protect the components in the turbine from being damaged.

The goal for both of the PID-controllers is to direct or indirect control the rotational speed of the rotor to a desired ideal value. But the output signal from them controllers is the displacement setting of the motor. By changing the displacement setting the pressure in the system will change, if the displacement setting is decreased the pressure in the system will increase and if it is increased the pressure will decrease. A change in pressure gives a proportional change of hydraulic torque. This torque opposes the aerodynamic rotor torque and when they differ the rotor will accelerate if the hydraulic torque is smaller than the generated torque from the wind and decelerate if it is bigger. Meaning that the controllers have ability to change the speed by regulating the displacement of the motor. But this only works due to the fact that the generator is connected to the grid which is an infinity-bus, meaning that it will keep the rotational speed of the generator

nearly constant and oppose with a torque equal to the torque from the hydraulic motor.

There are two switches that decide which one of the regulators that is active. Where the first, *Switch* 1 in Figure 3.9, switches from PID_A to PID_B when the rotor speed reaches just above 80 *rpm* and switch back when it drops below 80 *rpm*. The second switch, *Switch* 2 in Figure 3.9, switches from PID_A to the output of *Switch* 1 when the wind speeds reaches 10.7 m/s. This purpose of this switch is mainly to ensure a change back to the MPPT control when wind speed is reduced again, after reaching a high enough value to get the rotor to 80 *rpm*. Without this switch the regulator PID_B will at slow reduction of wind speed, keep 80 *rpm* even though a lower rpm would give the optimal TSR. It will continue until a very low wind speed is reached and during this time it will drift further and further away from the optimal TSR. Switching back to MPPT at a wind speed low enough to be sure that the optimal rotor speed is lower than 80 *rpm* but close to it will therefore prevent a loss in energy extraction which is the purpose of *Switch* 2.

Integral windup, also called reset windup, is a phenomenon that occurs in PI or PID controllers when the control signal saturates the actuator it is controlling. When this happens the integral part of the controller will keep growing, windup, because of the non-zero control error which result in large absolute value of the control signal while the actuator is still saturated. Even after a change of sign in the control error the controller might keep the actuator saturated for a long time because of the previous large integrated value. To prevent this an anti-windup can be added to the controller that prevents the integral part to grow when the actuator is saturated. The type of anti-windup that was implemented for both of the PID-controllers monitors if the output signal from the active regulator is saturated, i.e. higher than the maximum input signal to the displacement control valve. The difference between the signal from the active controller and the input signal to the control valve is then fed back to adjust the integration part of both controllers.

3.3.4 Model of generator and connection with the electrical grid

As stated above the synchronous speed of the generator is 1800 *rpm* when the generator is coupled to the grid which can be seen as an infinity bus. The grid will force the generator to run at this speed and since it is an infinity bus it can apply an infinite electrical torque to withheld this speed.

This fourth part models how changes in the torque from the hydraulic motor affect the generator speed and thereby the frequency of the delivered electric power. A schematic of the model is presented in Figure 3.10.

In this model the per-unit system, pu, is used meaning that the present value is divided with a base value to get the fraction from this base value. The torque from the hydraulic motor is first divided by the Base Torque. The base torque is given by Equation 3.8 and it is the torque given at nominal generator power and synchronous speed. In the calculation of this torque the efficiencies of the generator and transformer are included.

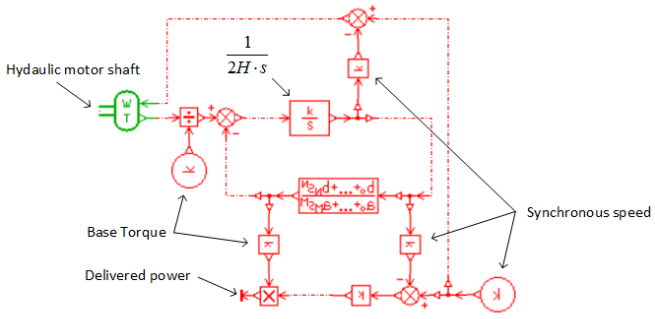

Figure 3.10: Model of the generator and its interaction with the grid.

$$T_{Base} = \frac{P_{nom,G} \cdot \eta_G \cdot \eta_{trans}}{\omega_{sync}} \tag{3.8}$$

The torque fraction is then subtracted by the electrical torque, also in pu, from the grid, divided by $2H$. The inertia constant H is used due to that the calculations are done in pu, for a deeper explanation of this see [2]. The signal is then integrated determine how much the rotational speed deviates from the synchronous speed and after that a gain transforms it to *rpm* and subtracts it from the synchronous speed. The resulting speed is fed back to the hydraulic motor. The deviation from the synchronous speed is also used to calculate the new electric torque fraction with Equation 3.9.

$$\bar{T}_e = \left(\frac{K_S}{s} + K_A \right) \bar{\omega}_G \tag{3.9}$$

where

$$\begin{aligned} K_S &= \textit{synchronizing torque coefficient} \\ K_A &= \textit{damping coefficient} \\ s &= \textit{Laplace variable.} \end{aligned}$$

This transfer function is an "oscillator" that models the interaction between a generator and the grid. It should have a frequency of 1 to 2 Hz and have a decay of 30% for every 4th cycle of a step input. In this model the frequency was chosen to 1.5 Hz and this was obtained with the values $K_s = 41$ and $K_A = 0.56$. Finally the rotational speed and the electric torque, see Equation 3.10, is used to calculate the electric power delivered to the grid.

$$T_e = T_{Base} \cdot \bar{T}_e \tag{3.10}$$

3.3.5 Hardware for simulation of aerodynamic rotor

At the start of the project it was predetermined that no real aerodynamic rotor would be used for the test platform. The reasons for this was cost, space availability and foremost the benefit of not being dependent on wind conditions during testing. Also the hardware needed to simulate the wind and rotor existed and was supplied by Reivax. The hardware consists of an electric motor of 56 kW, a frequency converter and a speed reducing gearbox. The frequency converter is able to control speed or torque of the electric motor. To reach the low rotational rotor speeds of 50-120 rpm a reducer gearbox with gear ratio of 12:1, capable of transferring power up to 100 kW, is available.

Chapter 4

Selecting system components

This chapter gives a detailed explanaiton of how the hydraulic components were selected for the test platform and implemented in the simulation model.

4.1 Hydraulic components

The hydraulic components was going to be supplied by Parker and a meeting with them at their facilities in Porto Alegre had been planned. All hydraulic components in the system had to be standard of the shelf components available from Parker's product portfolio. To have a good base to start from when attending the meeting an initial sizing of the main components were made. The components that were dimensioned before the meeting were the hydraulic motor, pump, charge pump, heat exchanger and also the high and low pressure accumulators. The hydraulic components were sized and chosen before the generator but the type of generator had already been decided, a four pole synchronous generator. To produce 60 Hz AC, a four pole synchronous generator must run at 1800 rpm and consequently this will be the speed of the hydraulic motor.

4.1.1 Initial sizing of components

The nominal power output $P_{nominal}$ of the system was intended to be 20 kW. To size the hydraulic components according to this power some assumptions and approximations were needed. Assuming that there are no pressure losses in the system gives that the pressure difference over both pump and motor are equal, $\Delta p_{pump} = \Delta p_{motor} = \Delta p$. The pressure difference, Δp, at the nominal power output was selected to be 300 bar. This pressure was selected due to a a brief field study of pumps and motors showing that their peak efficiencies commonly were around this pressure. With this assumption, and by approximating the efficiencies of all machines in the system, it was possible to size the main pump and motor in the transmission since their respective speed at nominal power were known. Their efficiencies was estimated according to Table 4.1.

Table 4.1: Estimated efficiencies used for sizing the system components.

Component	Overall	Volumetric	Hydromechanical
Electric generator	$\eta_g = 95$ %	-	-
Hydraulic motor	$\eta_{totm} = 90$ %	$\eta_{volm} = 95$ %	$\eta_{hmm} = 95$ %
Hydraulic pump	$\eta_{totp} = 90$ %	$\eta_{volp} = 95$ %	$\eta_{hmp} = 95$ %

The nominal hydraulic flow was calculated according to Equation 4.1, and gave a flow of 46.7 l/min.

$$q_{nominal} = \frac{P_{nominal,hydraulic}}{\Delta p} = \frac{P_{nominal}\frac{1}{\eta_{totg}\eta_{totm}}}{\Delta p} \tag{4.1}$$

where $P_{nominal,hydraulic}$ is the nominal hydraulic power i.e. flow times pressure. From the nominal flow the displacement of both pump and motor could be determined. The maximum speed of the rotor, and consequently the pump, is 120 rpm and gives a displacement of approximately 410 cm^3/rev. Similarly the maximum motor displacement of 25 cm^3/rev was calculated for the synchronous generator speed of 1800 rpm.

From the nominal flow it was also possible to approximate the leakage flow from the machines that determines the demands from the charging circuit. The purpose of a charging circuit in a closed HST is to avoid cavitation at the pump inlet and compensate for leakages that eventually would cause pressure drop due to decreased fluid volume in the system. As described in Section 2.1.2, the efficiency of a hydraulic machine is dependent on pressure, rotational speed and, if variable, the displacement setting. The volumetric losses consists of both internal and external losses in the hydraulic machines and it is the external losses, mainly drain flow from the machines, that the charge system needs to compensate for in a closed circuit HST. When sizing the charge circuit, a worst case scenario is considered to be when all volumetric losses are external leakage. With the volumetric efficiency of 95% on both pump and motor this gives a total external leakage of 4.79 l/min according to Equation 4.2.

$$q_{leakage} = q_{nominal}(1 - \eta_{volp}\eta_{volm}) \tag{4.2}$$

A common type of pump used in charge systems is the external gear pump type, because it has a relatively low cost. A negative aspect of the external gear pump is its low efficiency. Still it was considered that it was most likely that this type of pump would be the final component choice used on the test platform, therefore the dimensioning of the charge pump was done with respect to the efficiency of a external gear pump. A volumetric efficiency of 80% and a rotational speed of 1000 rpm gave a pump displacement of 6 cm^3/rev. Adding some safety margin to this it was concluded that a pump of approximately 7 cm^3/rev would be suitable for the system. The speed of 1000 rpm was considered to be a normal operating speed for a gear pump and since the electric motor powering the charge pump was not yet defined, the size of the charge pump remained flexible and could be selected in collaboration with Parker.

The idea is to place the charge circuit at the bottom of the wind turbine tower. The elevation between the pump in the nacelle and the charge circuit causes a pressure drop. This pressure drop can be approximated with the well known Bernoulli equation [14], which is reduced to Equation 4.3 assuming stationary and incompressible flow with no velocity difference in the line.

$$\Delta p_{drop} = \rho g \Delta h + \Delta p_{friction} \tag{4.3}$$

where ρ is the oil density, g is the acceleration of gravity, Δh is the height difference and $\Delta p_{friction}$ is the friction losses. The friction term $\Delta p_{friction}$ for a straight pipe and assuming laminar flow is calculated according to Equation 4.4.

$$\Delta p_{friction} = \frac{64}{Re}\frac{\Delta h}{d}\frac{\rho v^2}{2} \tag{4.4}$$

where v is the fluid velocity, d is the hydraulic line internal diameter and Re is the Reynolds number. With $\Delta h = 10\ m$, $\rho = 870\ kg/m^3$, $g = 9.91\ m/s^2$,$d = 25\ mm$ and the nominal calculated flow of 46.7 l/min and consequently a flow velocity of 1.59 m/s gives a pressure drop of approximately 1 bar. This means that to have 3 bar pressure at the inlet of the pump the charge circuit pressure needs to be set

somewhere around 4 *bar*. This pressure is set with a pressure relief valve placed after the pump in the charge circuit.

When the wind speed changes this will cause fluctuations in torque on the main pump, this will in turn cause pressure fluctuations in the HST which is, for slow dynamics, compensated for by the control system by regulating motor displacement. Though, at turbulent winds the dynamics of the wind could be faster than than those of the HST. This will cause short periods of pressure rise and pressure drops that will propagate via output torque to the generator and thereby affect the electric frequency output. Pressure fluctuations in hydraulic systems can be damped by using accumulators. Therefore the use of accumulators were considered to be a way to improve stability of the generator frequency output. Simulations were made with an accumulator placed close to the motor inlet on the high pressure line. It was positioned close to the motor to remain with the idea of placing as many components of the drivetrain as possible at the bottom of the tower to ensure easier maintenance. The results showed that with the use of an accumulator the pressure fluctuations during fast wind dynamics was damped a lot and thereby it also improved the generator frequency output. Figure 4.1 shows the difference in generator frequency output with and without a high pressure accumulator, for steps in wind speed.

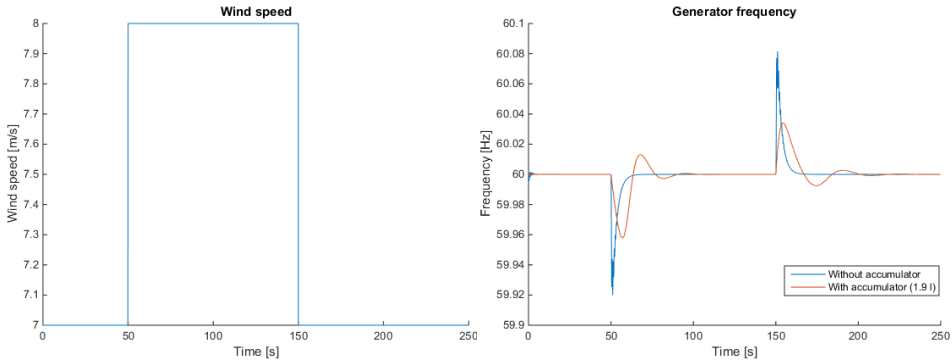

Figure 4.1: The right graph shows the generator frequency with and without an accumulator on the high pressure side for the wind profile given by the left graph.

The pressure fluctuations does not only occur in the high pressure line, as the pump is accelerated by increased wind speed, the inlet pressure drops and as it decelerates the inlet pressure rises. If these pressure drops are too high there is a risk for cavitation. Again simulations showed that connecting an accumulator to the low pressure line give less pressure oscillations and consequently a more stable supply pressure for the pump. Figure 4.2 shows the difference in pump inlet pressure with and without a low pressure accumulator, for the same wind profile as above in Figure 4.1.

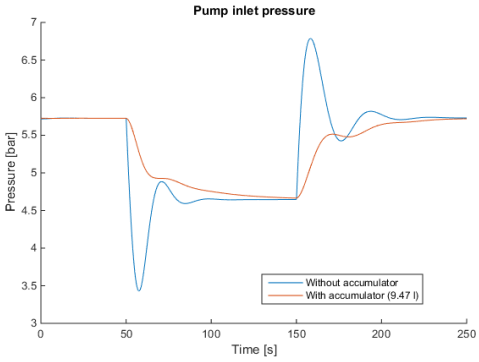

Figure 4.2: Pump inlet pressure with and without an accumulator on the low pressure side.

Simulations showed that the steady state pressures are independent on the use of accumulator but during fast pressure changes the pressure drop is faster and have more oscillation than without accumulator. To get an idea of what sizes that were suitable for the two accumulators, a series of simulations were made with help of the "batch" function in AMESim. This function allows to automatically run a series of simulation where component parameters can be changed automatically between the runs. First a couple simulations were made to determine the size of the high pressure side accumulator. An accumulator volume of around 2 liters was found suitable for the system. This size of accumulator gave a satisfying compromise between settling time and damping in electric frequency output. Figure 4.3 shows the result from a batch simulation with four different volumes of high pressure accumulator.

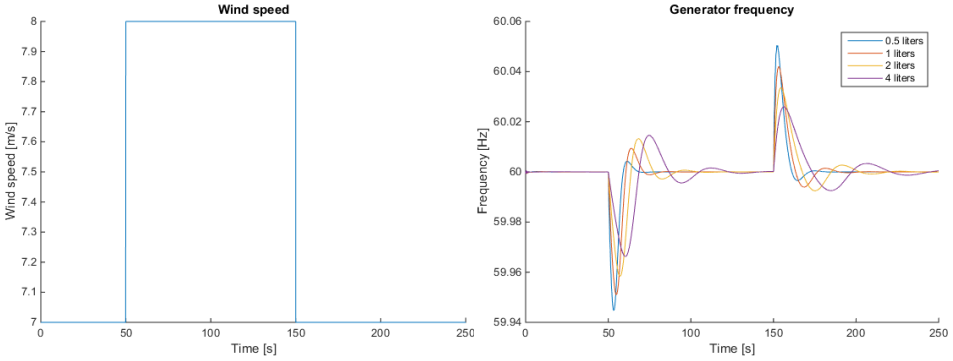

Figure 4.3: To the left the wind profile and to the right results from a batch simulation with four different sizes of accumulators on the high pressure side.

Same strategy was used to determine the size of the low pressure side accumulator. The simulations showed that the pump inlet pressure change is slower the larger the accumulator volume is, see Figure 4.4.

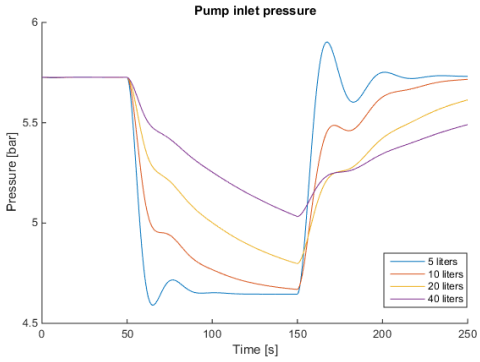

Figure 4.4: Results from a batch simulation with four different sizes of accumulators for the low pressure side.

A final component that had to be sized and included in the system was the heat exchanger. The heat exchanger was sized with respect to the predicted losses in the HST at nominal power. Again, the main losses in a HST are normally in the hydraulic machines and therefore, as an initial estimation, only these losses were considered. The demanded cooling capacity was estimated according to Equation 4.5.

$$P_{losses} = P_{nominal}\left(1 - \eta_{totp}\eta_{totm}\right) + P_{charge}\left(1 - \eta_{totp,charge}\right) \tag{4.5}$$

where P_{charge} is the input power to the charge pump at a rotational speed of 1000 rpm while maintaining a pressure of 4 bar with a hydromechanical efficiency estimated to 90%. $\eta_{totp,charge}$ is the total efficiency of the charge pump and was estimated to 72% ($\eta_{volp,charge} \cdot \eta_{hmp,charge}$). This resulted in estimated power losses of approximately 3.9 kW which could be used as a guidance when selecting a suitable heat exchanger for the system.

Sizing these components gave a good idea of the operating conditions in the HST such as flow rates and pressures in different parts of the system. Knowing these quantities enables determination of the other components in the system such as valves, reservoir, filters and hydraulic lines. As earlier mentioned this was just an initial estimation of components that could serve as a base when choosing the real components at the meeting with Parker. Because of this it was considered unnecessary to size the remaining components until the main components had been determined.

Figure 4.5 shows the layout of the system as it was designed after the initial sizing of the components. Comparing to the model that Flesch [2] designed, the changes made to the system was adding the high and low pressure accumulator number 4 and 12 in the figure and also move the high pressure filter, number 5, close to the motor. In that way it is placed on the bottom of the wind turbine which yields easier filter maintenance.

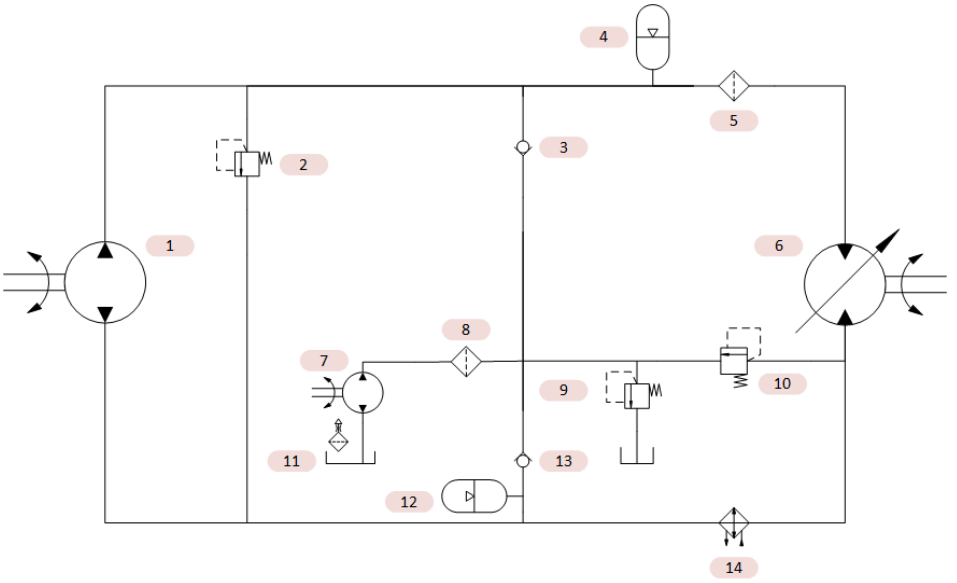

Figure 4.5: The hydrostatic transmission as it was designed before the meeting with Parker in Porto Alegre.

Table 4.2 lists the components in Figure 4.5 and the demanded specifications as calculated when doing the initial sizing. The calculated component parameters were implemented in the model and simulations were made to see that the system was working properly.

Table 4.2: Components their specifications from the initial sizing.

Index	**Component**	**Specification**
1	Fixed displacement piston pump	$\approx 410\ cm^3/rev$
2,9,10	Pressure relief valve	Not determined
3,13	Check valve	Not determined
4	High pressure accumulator	≈ 2 liters
5,8	Filter	Not determined
6	Variable displacement piston motor	$\approx 25\ cm^3/rev$
7	Fixed charge pump	$\approx 7\ cm^3/rev$
11	Reservoir	Not determined
12	Low pressure accumulator	As large as possible
14	Heat exchanger	Minimum capacity of 3.9 kW

4.1.2 Adapting system for commercially available products

At this time of the project a visit to Parker in Porto Alegre was made. The goal of the visit was to determine all the hydraulic components necessary to build the test platform. All the main hydraulic components had to be chosen from the existing product portfolio of Parker. Adding to this the parts also had to be produced or available in Brazil due to delivery and import time. Here follows a summation of how the components were selected in the chronological order.

The first component that was discussed was the transmission main pump that is connected to the rotor. Since the rotor have a relatively low maximum rotational velocity, 120 rpm, the pump needs to have a very large displacement, approximately 400 cm^3/rev, to a give sufficient flow . To have a good overall efficiency of the transmission it is essential that the efficiencies of the hydraulic machines are high. Therefore only piston machines were considered for the application of main pump and motor. Two different options with the demanded displacement existed in Parker's portfolio, one radial piston machine and one in-line variable piston pump. But cost and delivery time made them inappropriate for the test platform. Instead two different options were presented, one was the P1/PD pump series and the other one was the P2 pump series, both of variable displacement in-line piston type. These pumps exists in sizes from 18 to 145 cm^3/rev. Changing to either one of these would result in a complete resizing of the system. Simultaneously it was brought to knowledge that a variable bent-axis piston motor was available in stock. The model was a 60 cm^3/rev motor, model V12. With this information it was necessary to think about the concept and how it could be adapted to fit the suggested machine sizes.

Since the electric grid has a frequency of 60 Hz in the state of Santa Catarina in Brazil, a 4 pole generator direct coupled to the grid will run at 1800 rpm, see Equation 2.8. With the 60 cm^3/rev motor, this speed results in a flow demand of 108 L/min at full displacement and assuming 100% volumetric efficiency. In turn, this would result in a pump displacement of 900 cm^3/rev which would be even more costly. To be able to choose the available V12 type motor and a P1/PD or P2 series pump, either the pump speed had to be increased or/and the motor had to be running at partial displacement at nominal power. Running the motor at partial displacement means that the efficiency of the motor is decreased and since efficiency was considered as a weakness with the system, this was not considered to be an option. To reach the displacement range of the P1/PD or P2 pumps the only option then was to use a gearbox between the aerodynamic rotor and the pump to increase its rotational speed. As described in Section 3.3.5 the electric motor supplied by Reivax, that was going to simulate the torque from the aerodynamic rotor on the pump, had a speed reducer capable of powers up to 56 kW with a gear ratio of 12:1. The speed reducer enables the low input speeds below 120 rpm for the pump. Therefore the first idea was to remove the speed reducer and couple the electric motor directly with the pump shaft. This result in a nominal speed of 1440 rpm for the pump. It is important to see that in the test platform system this means that the speed reducer is removed but in a real wind turbine this would mean that a gearbox with gear ratio of 1:12 is added between the aerodynamic

rotor and the pump, compare Figure 4.6 and 4.7.

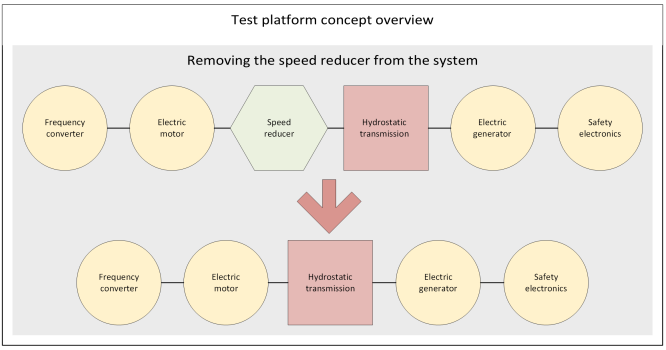

Figure 4.6: How the test platform concept changed when adding the gear box to the wind turbine concept.

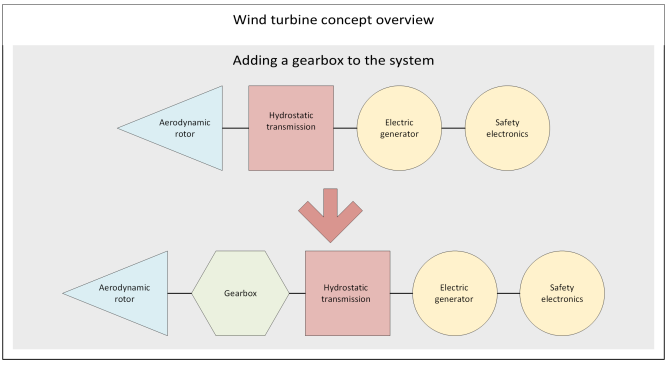

Figure 4.7: Overview of the wind turbine concept before and after adding a gear box to it.

A pump speed of 1440 rpm gives a pump displacement of 75 cm^3/rev which is in the middle of the pump displacement range of the suggested pump models. Considering this and knowing that it exists gearboxes with the 1:12 gear ratio capable of handling the high torque, the concept was changed by adding a gearbox. Figure 4.8 shows how the pump and motor displacement are correlated to each other for the two pump speeds of 120 rpm and 1440 rpm. The motor is running at a speed of 1800 rpm and 100% volumetric efficiency is assumed.

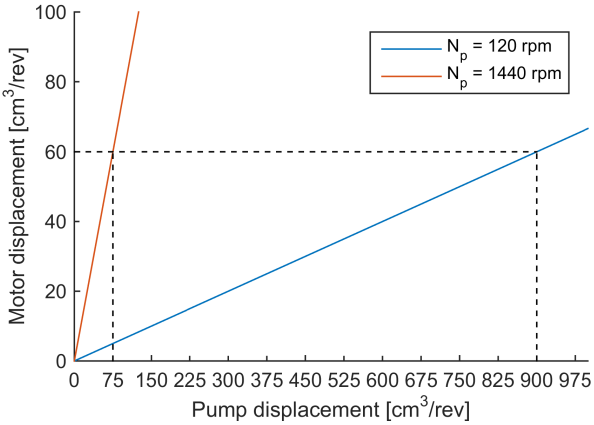

Figure 4.8: Correlation between pump and motor displacement with and without gearbox at nominal speed.

A perfect match for the new operating conditions of the pump was found to be the PD series 75 cm^3/rev variable piston pump. It has good efficiency in the operating speed range and have low cost. Though everything seemed fine with the new concept two problems appeared. Firstly the maximum continuous operating pressure for the PD pump is 280 *bar* meaning that it is impossible to run the system at 300 *bar* at nominal power. Secondly, changing the system nominal pressure to 250 *bar* would give a nominal power output of 40.5 kW considering the same efficiencies as the initial sizing. In theory it would have been possible to change the power of the test platform to 40.5 kW, since all parts that was already selected could handle this power, including the electric motor and frequency converter that will simulate the aerodynamic rotor. The decision had to be made by short notice, and due to insecureness of other problems that may occur, using twice as high power as the initial idea was not considered a good option. Also the generator and some hydraulic components would be more expensive, so it was decided to lower the pressure further. The final decision fell on 200 *bar* nominal pressure giving a nominal power output of 32.5 kW. But to remain with displacement controllability at nominal power the displacement setting must be $\varepsilon_m < 1$ and because of this the nominal power output was set to be 28 kW. This power gives a motor displacement of 51.7 cm^3/rev which corresponds to a displacement setting of approximately 0.85 and thereby leaves some safety margin both to remain with controllability slightly above nominal power and also for errors in estimated efficiencies. The lowered power also cause the pump displacement to decrease a bit to 71.6 cm^3/rev but it does not affect the choice of pump since it has variable displacement and can be set to any desired setting below 75 cm^3/rev.

At this point some major changes had been made to the system, the nominal power was increased from 20 kW to 28 kW, the pressure at nominal power was changed to 200 *bar* and a gearbox with gear ratio 1:12 had been added to the drivetrain. The new operating conditions of the hydrostatic transmission also

resulted in a more than doubled flow at nominal power of 98 l/min, instead of 46.7 l/min. Two system components had been selected, the hydraulic motor and the main pump. The motor was the Parker V12 variable displacement bent-axis motor of 60 cm^3/rev with electric proportional control and the pump was a Parker PD variable displacement in-line pump of 75 cm^3/rev.

The changes of system parameters were changed in the AMESim model and simulations were performed to ensure that the system characteristics and performance had not been changed. Simulations showed that the system performed satisfyingly and therefore it was concluded that the high pressure accumulator could remain at the same volume of 2 liters. Since the pressure is changing on the high pressure side from roughly 30 *bar* up to 200 *bar* this gives a minimum compression ratio of $\frac{200}{30} = 6.7$. It gives this minimum compression ratio since the precharge pressure needs to be set lower than the minimum working pressure and compression ratio is defined as $\frac{Max.workingpressure}{Prechargepressure}$. Parker bladder type accumulators are not an option for this system since they have a maximum compression ratio of 4. The diaphragm type accumulators can have up to 8 in compression ratio but only for accumulators with size up to 1.4 liters. This leaves only the option of piston accumulators. Piston accumulators have a slower response than bladder and diaphragm type but on the other hand they have very good serviceability, high temperature range and they can work with the high compression ratio. For a system pressure of 200 *bar*, Parker have the 3000 series piston accumulators that are rated to work at a continuous system pressure up to 207 *bar*. Closest volume to 2 liters in the 3000 series is a 1.9 liters accumulator which was selected as the high pressure accumulator.

For the low pressure line an accumulator with large volume was requested and available in stock at Parker was a 9.47 liters accumulator, also from the 3000 series piston accumulators. The reason for not choosing a larger accumulator on the low pressure side was to keep the cost of the drivetrain down.

A change in nominal flow to 98 l/min means that the leakage flow will change accordingly. Again with using the estimated efficiencies for the machines the nominal flow gives a leakage flow of 10.06 l/min. The charge pump was dimensioned to run at 1000 rpm and provide a flow of 7 l/min with a volumetric efficiency of 80%. Two options thereby existed, either increase the rotational speed or increase the displacement of the charge pump. The type of pump considered for the application of charge pump was external gear pumps, for two reasons, price and availability. Parker in Porto Alegre manufactures this type of pumps and therefore it could be provided on a very short notice. A decision was therefore made to wait with the determination of charge pump until the electric motor had been chosen so that the rotational speed would be known.

Hydraulic piston machines normally have an external leakage that goes from the pressurized side of the piston to the machine housing. This leakage is then drained from the machine through a drain port. The flow of oil inside the machine makes it self lubricated which is a reason for the long lifetime of hydraulic machines. In the machine housing, the case, it is recommended to have a low pressure to ensure proper lubrication. For the V12 motor this recommended case pressure is 2-4 *bar* and the PD pump have a maximum limit of 2 *bar* case pressure. To ensure

the correct case pressures two check valves were chosen to be installed on the drain lines. The drain lines goes from the drain port on the machines to the reservoir. The choice fell on a cartridge style check valve with a cracking pressure of 1.4 *bar*, model CVH103P. Pressure drop over the check valve increase with increased flow, Figure 4.9 shows pressure drop versus flow.

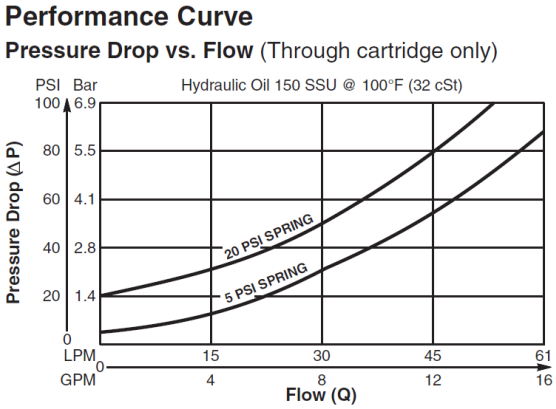

Figure 4.9: Pressure drop versus flow for the check valve, CVH103P. *Image courtesy of Parker Hannifin* [3]

The calculated leakage flow for the machines is 10.06 l/min and consequently a leakage of approximately 5.03 l/min from each machine. Assuming that 50% of this leakage is external, the drain flow would be around 2.5 l/min and would correspond to a pressure drop of approximately 1.5 *bar*.

These type of cartridge valves need to be installed in a special cartridge body, that also will cause a pressure drop. The type of body is selected by choosing a desired port size. A standard for the system was chosen to be 3/8" BSPG ports wherever possible. Figure 4.10 shows the pressure drop for different flows through the BSPG body.

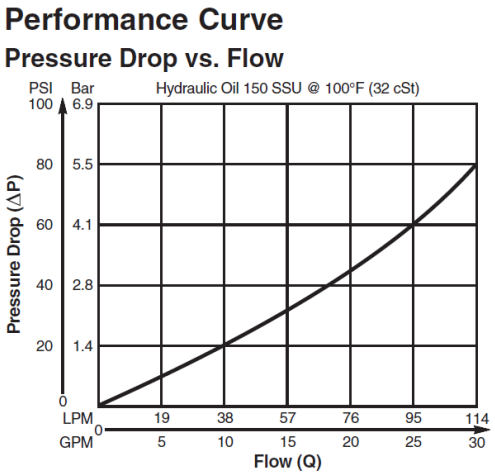

Figure 4.10: Pressure drop versus flow for the bodies used to the cartridge valves. *Image courtesy of Parker Hannifin* [3]

The flow of 2.5 l/min through the body gives a pressure drop of approximately 0.1 *bar* and thereby a total pressure drop through both check valve and body for a flow of 2.5 l/min would be 1.6 *bar*. This gives a case pressure well suited for the pump but slightly lower than the recommended for the motor. But though 1.6 *bar* is not the ideal case pressure it is well within the maximum and minimum limits for the motor working speed of 1800 *rpm*. The limits are 0-12 *bar* for 1500 *rpm* and 0.5-7 *bar* for 3000 *rpm* [43] and therefore it was considered a sufficient case pressure also for the motor. Two check valves are also needed for the charge circuit as explained in Section 3.3.2. Since the function of these valves only is to limit direction of flow it is desired to have a low pressure drop over these valve to minimize losses.

One of the check valves connects the charge circuit to the low pressure line. The charge system is designed to deliver a flow of at least 10.06 l/min which also will correspond to the highest flow through the charge circuit check valve. A CVH081P series check valve with a cracking pressure of 0.3 *bar* was chosen for this application and with a flow from 0-10 liters/min through this valve the pressure drop will be between 0.3-0.7 *bar* [3]. The check valves that are placed on the line which connects the charge system to the high pressure line only operates when filling up the system with hydraulic fluid. Therefore the performance of this valve is not essential for the system performance and was therefore simply chosen to be the same model as the other charge circuit check valve.

To ensure safety in hydraulic systems it is common to use pair of pressure relief valves if one fails. In the system it is required to have pressure relief valves at three different cracking pressure levels. One is connected between the high and low pressure side and should be set to limit the highest system pressure. During fast wind speed changes close to rated power the pressure may reach higher levels than 200 *bar*. If the cracking pressure of the relief valve is set to 200 *bar* this

means that the system will lose control over the aerodynamic rotor at this pressure. The reason for losing control is that the rotor speed no longer is related to the displacement setting of the motor. Under normal operating conditions this is of course undesired, and therefore the cracking pressure was chosen to be 225 bar. One thing to think about is that when a higher system pressure is allowed under short time periods, the output power will also be higher and the electric generator must therefore be dimensioned accordingly. This cracking pressure is one of two design parameters when choosing relief valve, the other one is flow capacity. Since the relief valve is connected to the high pressure line it needs to have capacity to handle the highest flow rate in the system which was calculated to approximately 98 l/min at the rated aerodynamic rotor speed of 120 rpm. Two equal valves were chosen for the application (one for safety) from the RAH101 series. These valves can handle flow rates up to 113 l/min and the chosen model have adjustable cracking pressure setting of 13.8-345 bar.

A maximum pressure of 25 bar was chosen for the low pressure side of the HST. The maximum flow in this line is the same as in the high pressure line and the RAH101 series relief valves was therefore suitable also for this application, but another pressure setting range of 6.9-69 bar was selected. Two relief valves were ordered, again one just for safety.

The third and last relief valve type is the valve that will be adjusted to set the charge circuit pressure. For this application a cracking pressure of around 5 bar was desired. The charge circuit was designed to deliver a maximum flow of around 9.5 l/min which also must be the capacity for the charge circuit pressure relief valve. The chosen valve was a A02B2 series valve with adjustable cracking pressure between 2-100 bar and a rated flow of 30 l/min.

Suitable filters were chosen by the engineers at Parker. Three filters were needed, one air filter that filters the air in the reservoir. Another filter that is placed directly after the charge pump and filters all oil entering the system from the reservoir, and a third filter that is placed on the main transmission line. Filters are determined by type of oil, fluid pressure, flow rate and the necessary filtration requirement that is determined by the system components. The main line filter was moved from the high pressure line to the low pressure line so that the filter would not have to endure such high pressure.

Considering the same efficiencies, a charge pump velocity of 1000 rpm, system running at nominal power and using Equation 4.5 the estimated cooling capacity needed for the 28 kW system was 5.35 kW. A ULDC-011 heat exchanger was chosen, Figure 4.11 shows the cooling capacity depending on entering temperature difference for the ULDC series heat exchangers.

Calculating the cooling capacity at nominal power with a flow of 98 l/min and a entering temperature difference of 20°C (fluid temperature of 45°C and air temperature of 25°C) with the cooling performance of ULDC 011 given in Figure 4.11 gave a cooling capacity of approximately 6.7 kW, for 340 Btu/hr/°F.

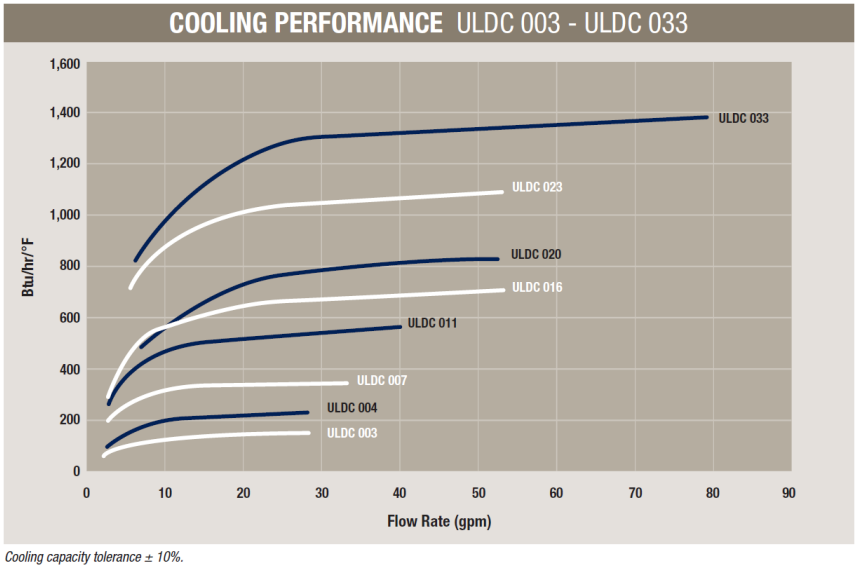

Figure 4.11: Cooling capacity of the ULDC 011 heat exchanger. *Image courtesy of Parker Hannifin* [4]

To simplify maintenance of the system two ball valves were selected and positioned to divide the components placed on the bottom of the wind turbine from the components placed in the nacelle. For the test platform system this means that the pump and the main part of the hydraulic lines running from pump to motor are separated from the rest of the components. The ball valves makes it unnecessary to empty all the fluid in the system when making a small changes or performing maintenance of the system. Also two ball valves were chosen to be fitted directly to the accumulators making it possible to test the system performance without accumulators.

The ball valves on the main transmission lines that divides the system also separates the high pressure line relief valves so another RAH101 valve with cracking pressure setting of 13.8-345 *bar* was added to the high pressure line below the ball valves for safety.

Finally a reservoir was needed, but before the meeting at Parker a reservoir of 100 liters was found at LASHIP that could be used. A rule of thumb for choosing reservoir size in hydrostatic transmissions is that the volume should be 3-4 times the volume that the charge circuit drains from the reservoir in one minute. The charge flow of 10 l/min gives that the reservoir should be in the range of 30-40 liters using this rule. What limits the minimum size of a reservoir is mainly that the fluid needs time for contaminant settling and deaeration before being pumped back into the system again. For the test platform space for placing the reservoir was not a problem plus that the shape of the reservoir gave a convenient surface for mounting some system components.

At this point all the main components of the hydraulic system had been deter-

mined that was going to be supplied by Parker. The only component from Parker that was not yet determined was the charge pump. Figure 4.12 presents the final schematic layout of the system with all the hydraulic components.

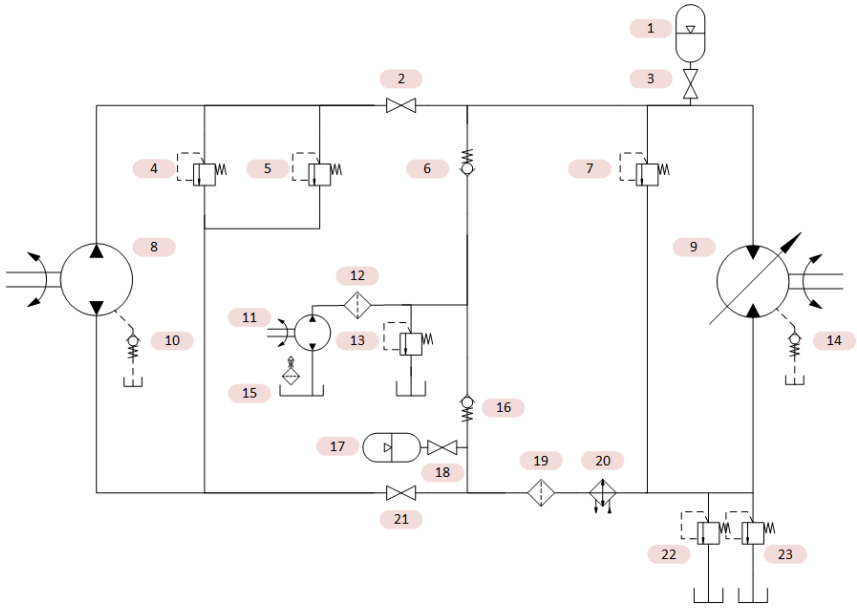

Figure 4.12: Final layout of the hydrostatic transmission.

Table 4.3 presents the system components supplied by Parker with indexing according to Figure 4.12.

Table 4.3: List of the components supplied by Parker.

Index	Component	Parker product number
1	Piston accumulator	A4N-0116D1K
2, 3	Ball valve	KH1X
4 ,5, 7	Pressure relief valve	RAH101K50-6B
6, 16	Check valve	CVH081P-6B
8	Variable in-line piston pump	PD075PS02SRU5AL00S0000000
9	Variable bent-axis piston motor	V12-060-MU-SV-S-000-D-0-
10, 14	Check valve	CVH103P20-6B
11	External gear pump	Not yet determined
12	Filter	FP10-010FV-068-LV3
13	Pressure relief valve	A02B2FZ-N-6B
15	Air filter	FAR76-010FV-06B/2
17	Piston accumulator	A4K-0578D1K
18, 21	Ball valve	KH3/4X
19	Filter	FP40-010FV-10B-LV3
20	Heat exchanger	LDC-011-A-000SB
22, 23	Pressure relief valve	RAH101K10-6B

Other components left to decide for the test platform was all the hydraulic lines including fittings and the flanges between the hydraulic machines and the electrical machines, but the determination of these components is not a part of this thesis work.

After the main components were chosen and confirmed with Parker the electric motor for the charge pump was selected. The motor selected was a 6 pole induction motor for 60 Hz with a nominal speed of 1130 rpm. It should be directly coupled to the grid without frequency converter to keep the cost down, meaning that the motor speed can not be adjusted. Looking into the volumetric efficiencies for the main hydraulic machines a more accurate data, then the assumption that they both had 95%, was found in catalogs [44]. The catalogs showed that both machines had lowest volumetric efficiencies at rated power and confirmed that the assumption of 95% as lowest efficiency was good for the pump but a bit low for the motor which efficiency only dropped to approximately 98.5%. This gives a reduced total leakage flow from 10.06 l/min to $5.16 + 1.47 = 6.63$ l/min. To get some safety margin a charge pump with a displacement of 8 cm^3/rev was selected which gives, with an volumetric efficiency of 80%, a flow of 7.23 l/min. The safety margin is only around 10% and it may look small but with the assumption that all volumetric losses goes as flow to tank. This is not the real case and a decreased leakage flow will give a bigger margin and therefore it was decided to be sufficient.

4.1.3 Generator and safety electronics

As mentioned earlier, the type of generator was chosen in advance since its speed is one parameter that has to be known when sizing the hydrostatic transmission. The type chosen was a four pole synchronous generator that, connected to a 60 Hz grid, will run at 1800 rpm. Choosing generator model for the test platform was not a part of this thesis work but was performed simultaneously. The chosen generator is rated at a continuous apparent power of 36 kVA which, for a power factor of 0.8, generates an active power of 28.8 kW, see Section 2.3. It is a four pole, three phase, synchronous generator with built in voltage regulation. It also has an internal exciter stator with permanent magnets which means that no external power supply is needed for the built-up of the alternator.

As described in Section 2.3 four conditions must be met in order to synchronize a generator to the grid, phase sequence, voltage magnitude, frequency and phase angle. The phase sequence can only be wrong if the generator is not properly installed and the voltage magnitude is controlled by the built in voltage regulator. But frequency and phase angle must be synchronized every time a connection with grid is to be made.

To ensure that the generator parameters are synchronized with the electrical grid, a synchronizer device supplied by Reivax will be used. The device is called a "Generators automatic synchronizer" and the product name is $SNX100$. It measures the difference in phase angle, voltage amplitude and frequency between the generator and the grid and when the synchronization criteria is fulfilled it outputs an "enabling signal". The criteria needed to be fulfilled are [45],

- Phase difference $< 6°$.

- Frequency difference $< 0.1\%$ *or* 0.2%.
- Voltage difference $< 0.1\%$ *or* 0.2%.

This means that to enable synchronization the speed of the hydraulic motor must be controlled in such a way that these criteria are fulfilled. The actual synchronization process and how to control the hydraulic motor for this purpose is not a part of this thesis work.

4.2 Adapting the model for the test platform

To improve the AMESim model and make it more representative for the test platform some changes and improvements were made to the model. This chapter will go through the most important changes and explain them in detail. All parameters used for the different submodels in AMESim can be found in Appendix A.

4.2.1 Efficiency models

As described in Section 3.3.2 the efficiencies of the main hydraulic machines were partly modeled as a fixed value and partly modeled to be dependent on the pressure. A decision was made to model the machines with a more profound efficiency model which makes both the volumetric and mechanical efficiencies variable.

The model that was used can be found in [46]. These models are given in Equation 4.6 to Equation 4.9. For the pump the hydromechanical (η_{hmp}) and the volumetric (η_{volp}) efficiencies are,

$$\eta_{volp} = 1 - k_{L1}\left(\frac{p_p}{p_{p,nom}}\right)^{k_{LP}}\left(\frac{\varepsilon_p}{\varepsilon_{p,max}}\right)^{k_{LD}}\left(\frac{\omega_p}{\omega_{p,nom}}\right)^{k_{L\omega}} \tag{4.6}$$

$$\eta_{hmp} = \frac{1}{1 + k_{F1}\left(\frac{p_p}{p_{p,nom}}\right)^{k_{FP}}\left(\frac{\varepsilon_p}{\varepsilon_{p,max}}\right)^{k_{FD}}\left(\frac{\omega_p}{\omega_{p,nom}}\right)^{k_{F\omega}}} \tag{4.7}$$

and for the motor they are given as,

$$\eta_{volm} = \frac{1}{1 + k_{L1}\left(\frac{p_m}{p_{m,nom}}\right)^{k_{LP}}\left(\frac{\varepsilon_m}{\varepsilon_{m,max}}\right)^{k_{LD}}\left(\frac{\omega_m}{\omega_{m,nom}}\right)^{k_{L\omega}}} \tag{4.8}$$

$$\eta_{hmm} = 1 - k_{F1}\left(\frac{p_m}{p_{m,nom}}\right)^{k_{FP}}\left(\frac{\varepsilon_m}{\varepsilon_{m,max}}\right)^{k_{FD}}\left(\frac{\omega_m}{\omega_{m,nom}}\right)^{k_{F\omega}} \tag{4.9}$$

where k_{XX} are constants, derived from measured data.

This model was chosen because it contains three of the main parameters that influence the efficiency, displacement setting ε, rotational speed ω and pressure difference over the component Δp. It does not however take the fluid parameters into account.There are more complex model present for example in [15]. But the increased complexity of these did not seem to be necessary, partly because limited efficiency data for the pump and partly because the chosen model gave satisfying accuracy in the working range of the machines.

Least square optimization was used to set the unknown parameters, k_{xx}, in the efficiency models for the machines. Meaning that the parameters was optimized to give as little absolute deviation as possible from the given efficiency data. The data for the main pump was extracted from its data sheet [44] meanwhile Parker supplied more extensive efficiency data for the hydraulic motor.

Data points of the efficiencies in three dimensions depending on pressure, rotational speed and displacement setting was used for the main motor. For the main

pump only the pressure and the rotational speed was used. The displacement setting was not considered for the pump because it is used as a fix displacement machine and therefore there is no need to derive a parameter for the displacement setting dependency. The resulting parameters are given in Table 4.4 and Table 4.5. Figure 4.13 to Figure 4.16 show how well the model correlates to the efficiency data with the derived parameters. They show that the model gives a good overall representation of the efficiencies, especially for the volumetric efficiencies. The models of the mechanical efficiencies deviate a bit more at low pressures.

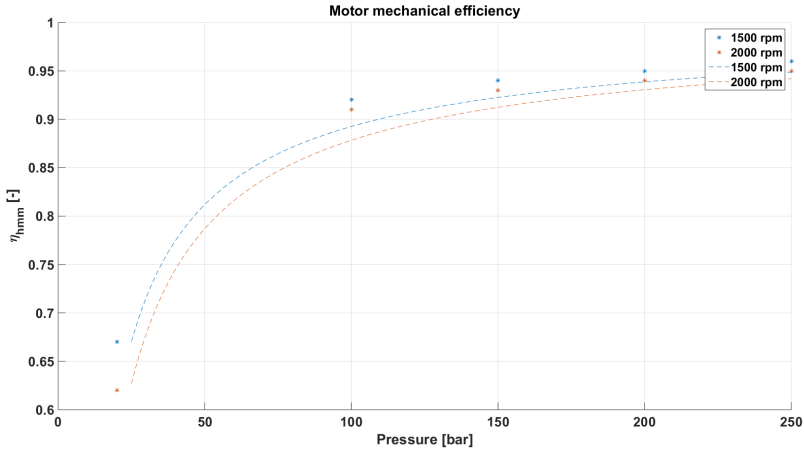

Figure 4.13: Comparison between the mechanical efficiency model for the motor (dotted line) and its given data (dots).

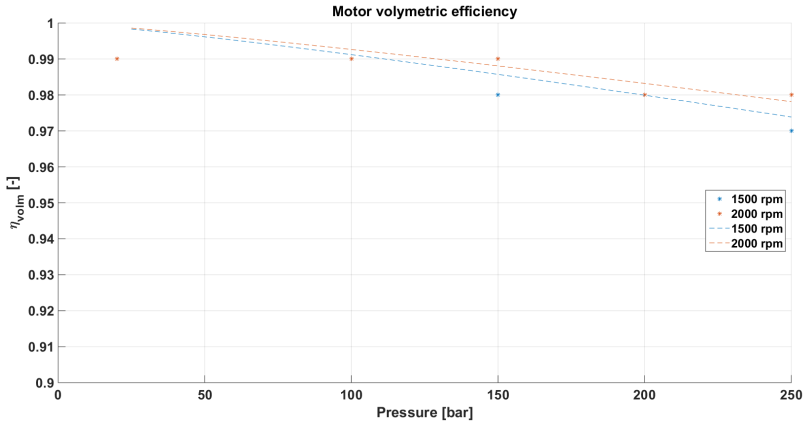

Figure 4.14: Comparison between the volumetric efficiency model for the motor (dotted line) and its given data (dots).

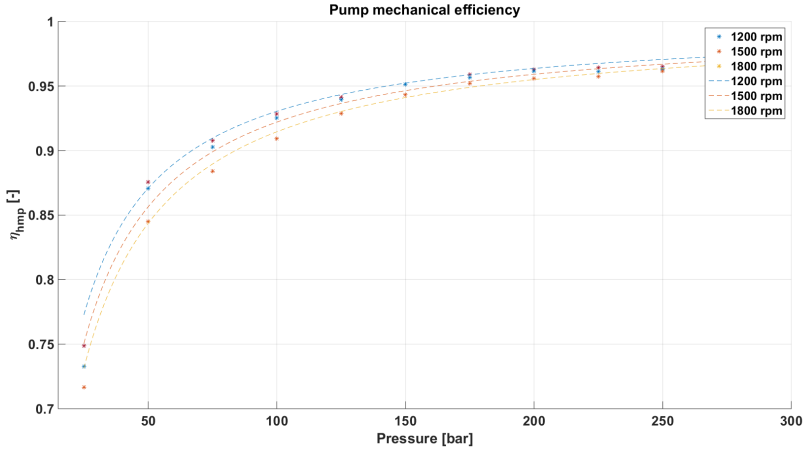

Figure 4.15: Comparison between the mechanical efficiency model for the pump (dotted line) and its given data (dots).

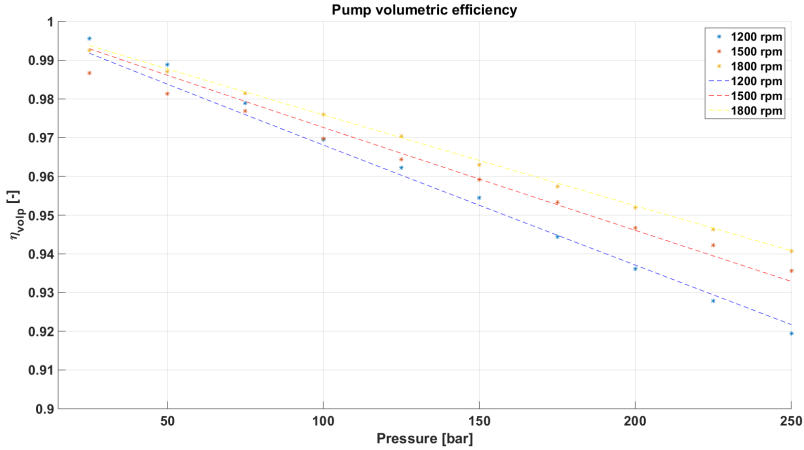

Figure 4.16: Comparison between the volumetric efficiency model for the pump (dotted line) and its given data (dots).

Table 4.4: Derived parameters for the mechanical efficiency models.

Machine	F_1	F_p	F_D	F_ω
Pump	0.033789	0.97954	-	0.54873
Motor	0.034184	-0.80839	-0.60465	0.43201

Table 4.5: Derived parameters for the volumetric efficiency models.

Machine	L_1	L_p	L_D	L_ω
Pump	0.066138	0.97954	-	-0.68917
Motor	0.013673	1.2068	-0.95794	-0.63237

4.2.2 Hydraulic lines

Choosing and sizing the hydraulic lines of the test platform was not a part of this thesis work but to have a good compliance between the real system and the simulation model it is important that the hydraulic lines are modeled properly. Two decisions about the hydraulic lines were made. The main circuit hydraulic machines will have hoses connected at inlet and outlet to reduce propagation of structural vibrations through hydraulic lines. The other decision was that steel pipes will be used for the elevation difference between pump and motor in the main circuit. At this point of the project an internal diameter of 19 mm for the high pressure line and 25 mm for the low pressure line was set. Because the knowledge of the platform layout and design was limited to these fact at this point, it was decided to only model the influence of the hoses and the long steel pipes with elevation difference. Figure 4.17 shows the hydraulic circuit as modeled in

AMESim and points out the hoses and pipes that were modeled to influence the system.

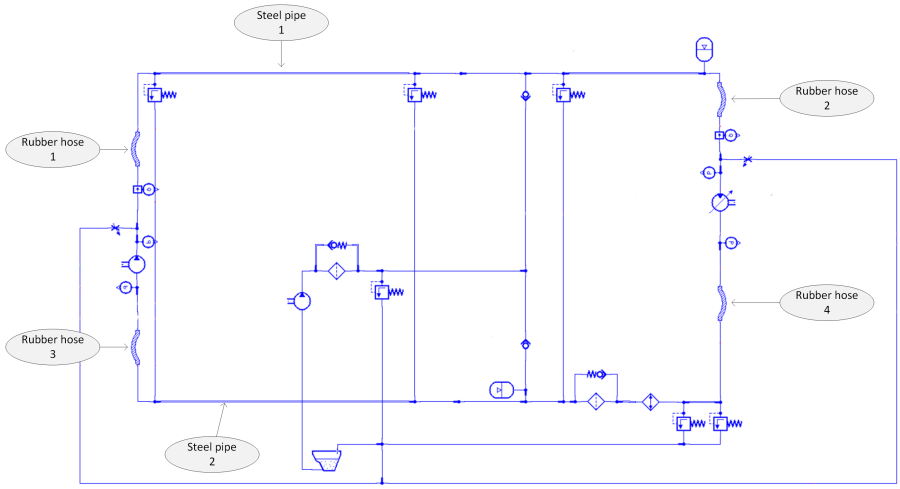

Figure 4.17: AMESim model of the hydraulic circuit.

Simple hydraulic line models were chosen to reduce simulation time. The models only calculates static friction, influence of gravity and compression. The friction in the lines are calculated by Reynold's number and relative roughness. The relative roughness rr is defined as the absolute roughness divided by the pipe/hose diameter. For the hoses an absolute roughness of $1.85e^{-4}$ was used [47] and for the steel pipes a absolute roughness of $8.25e^{-5}$ was used [48]. The line models also calculates the wall volumetric compliance as a function of internal diameter, wall thickness and Young's modulus for the material. The wall thickness of the pipes was measured to 3 mm and the wall thickness of the tubes was set to 5.2 mm referring to a Parker 302 $Hydraulic\ Worldwide$ [49] hose with internal diameter of 19 mm. Young's modulus were set to AMESim recommended values. Table 4.6 presents the model parameters for the hoses with indexing referring to Figure 4.17.

Table 4.6: Model parameters used for the hoses.

Parameter	Steel pipe 1	Steel pipe 2	Rubber hose 1	Rubber hose 2	Rubber hose 3	Rubber hose 4
Internal diameter [mm]	19	25	19	19	25	25
Pipe length [m]	8	8	3	3	3	3
Relative roughness	0.0043	0.0033	0.0097	0.0097	0.0097	0.0097
Wall thickness [mm]	3	3	5.2	5.2	5.2	5.2
Young's modulus [GPa]	206	206	52.5	52.5	52.5	52.5
Elevation [m]	8	8	0	0	0	0

The remaining lines were set to direct connections with the exception of four lines that AMESim required friction and compression models for to function. These four lines were set to the same parameters as the steel pipes but with a length of 0.01 m which almost eliminates their influence in the system.

4.2.3 Aerodynamic model and rotor inertia

In the aerodynamic model, see Section 3.3.1, there are two parameters that depends on the shape and size of the rotor, the power coefficient C_p and disc area A. C_p is dependent on the shape and radius of the blades. An assumption was made that the blade could have the same C_p performance as the larger rotor model that Flesch [2] used and that the only thing that would change is the radius of the rotor. Changing the radius then affects two parameters in the calculated power extraction from the wind, tip speed ratio λ and again the rotor disc area A. The radius was sized so that at a wind speed of 10 m/s, the nominal output power from the generator would be 28 kW. The extracted power from the wind was calculated backwards from the output power,

$$P_{rotor} = \frac{P_{G,nominal}}{\eta_G \cdot \eta_{m,tot} \cdot \eta_{p,tot}} \tag{4.10}$$

This resulted in an extracted power from the wind of 36.186 kW. From Equation 2.36 the area of the disk can be extracted,

$$A = \frac{2 \cdot P_{rotor}}{\rho \cdot C_{p,ideal} \cdot v^3} \tag{4.11}$$

where $C_{p,ideal} = 0.496$ is the maximum power coefficient possible to reach for the given design parameters of the blade. This resulted in a rotor area of approximately 119.1 m^2 and thereby a radius of 6.16 m.

Another parameter that changes when downsizing the aerodynamic rotor is, of course, the inertia. It was hard to find inertia data for rotor diameter of this size. S.M. Muyeen, Junji Tamura and Naoto Kakimoto [50] proposed that a simple estimation of the mass moment of inertia could be estimated with the inertia of a thin disc,

$$J_r = \frac{3 \cdot m_{blade} \cdot r^2}{2} \tag{4.12}$$

where the mass m of one blade can be approximated from the rotor radius according to the following relation [51],

$$m_{blade} = 2.95 \cdot r^{2.13} \tag{4.13}$$

The rotor radius of 6.16 m gives $J_r = 8070\ kg \cdot m^2$.

The last change made to the model of the rotor was that the inertia model on the rotor shaft in AMESim was changed to an inertia model that is compatible with viscous friction. A rough estimation of the friction, windage and oil churning losses in a wind turbine rotor and gearbox at rated power was found to be 1% [52]. These losses were assumed to be proportional to the rotational speed of the shaft and was therefore modeled as a viscous friction coefficient giving approximately 1% torque losses at nominal power with a rotor speed of 120 rpm.

4.2.4 Valve characteristics

All valves in the system, both check valves and pressure relief valves have a pressure drop that is dependent on the flow through the valve. This relation is measured by the producer and can be found in the component data sheet. In AMESim it is possible to model this relation linearly by adjusting a parameter called flow rate pressure gradient which corresponds to the linear relation between flow and pressure. Figure 4.9 in Section 4.1.2 shows the relation between flow and pressure drop for one of the check valves. The flow rate pressure gradient were approximated for all valves by taking two points on their respective curve and calculate the gradient between them. The obtained gradient values also used in the simulation model are presented in Table 4.7.

Table 4.7: Gradient values used in the model for the different valves. (PRV = Pressure Relief Valve, CV = Check Valve)

Product name (Type of valve)	Pressure gradient [lpm/bar]
RAH101K10 (PRV), RAH101K50 (PRV)	3.4978
A02B2FZ (PRV)	1.2
CVH081P (CV)	20.6364

It is also possible to model the dynamics of the pressure relief valve as a first or second order transfer function but since no data was available this was not done.

4.2.5 Proportional control of motor displacement

The hydraulic bent axis motor, Parker V12, that was planned to use in the test platform is equipped with electrohydraulic proportional control of the displacement. This type of control consists of a DC solenoid that regulates the motor displacement proportional to the input current. Since the dynamic behavior of the electrohydraulic control system was unknown it was decided to only model the displacement control dynamics as the dynamics of a solenoid. A solenoid can be modeled as a first order lag with a time constant of 15-35 ms [53]. The time constant of the actual solenoid was unknown and therefore the time constant was chosen to be in the middle of the interval, 25 ms.See Appendix A.2 for submodel parameters.

At a late stage of the project it came to knowledge that the test platform would utilize another type of control for the motor displacement, a hydraulic proportional control. This type of control changes the motor displacement proportionally to an external pilot pressure. In turn this pilot pressure needs to be controlled to a desired level which introduces more dynamics to the control system. Due to lack of time a decision was made to continue evaluating the system for electrohydraulic proportional control instead of hydraulic proportional control.

4.2.6 Generator and grid model

One parameter change was needed to be made in the generator model, the base torque of the generator, see Section 3.10. The base torque is the torque that the hydraulic motor feels from the generator when the generator is running at nominal power and it is calculated as follows,

$$T_{G,Base} = \frac{P_{nominal}}{\eta_G \omega_{G,nominal}} \tag{4.14}$$

where η_G is the generator efficiency of 95% and $\omega_{G,nominal}$ is the nominal or synchronous speed of the generator of 1800 rpm. With a nominal power of 28 kW this gives $T_{G,Base} = 156.4\ Nm$.

Chapter 5

Control strategies

This section explain the different control strategies that were developed and evaluated for the system. In total four different strategies were studied. The original $K\omega^2$, one other Direct TSR/MPT method and both methods togehter with feedforward.

PID-controllers were used for the feedback control of all the presented strategies. This was partly because they are simple and cheap controllers that are widely used in the industry, and partly because it should be easier to compare the different strategies against each other.

The PID controllers were designed using the non-interacting form as described by Equation 5.1,

$$u(t) = K_p\Big(e(t) + \frac{1}{T_i}\int_0^t e(\tau)d\tau + T_d\frac{d}{dt}e(t)\Big) \tag{5.1}$$

where K_p is the Proportional gain, T_i is the Integral time constant and T_d is the Derivative time constant.

5.1 Kω^2 control

As described in Section 2.5.4 one of the most common control strategies for wind turbines are the so called $K\omega^2$ control, see Figure 5.1. It was also this strategy that was used in the AMESim model developed by Flesh [2], that was the base for this study. These are the reasons for it to be one of the control strategies evaluated in this study and it has also served as performance reference for the other control strategies.

The value of the K was updated with the new values of rotor radius and pump displacement while the optimal tip speed ratio, λ, and $C_{P,ideal}$ was keep as in the previous study [2]. The resulting value was,

$$K = 1.3131 \cdot 10^6 \ [Ns^2/m^2] \tag{5.2}$$

The switching of controllers between *Region* 2*a* and *Region* 2*b* was done the same way as the original model with two switches. They operate like described in Section 3.3.3. But a method to get a bumpless transfer when switching between controllers was added. This technique is explained in Section 5.4.

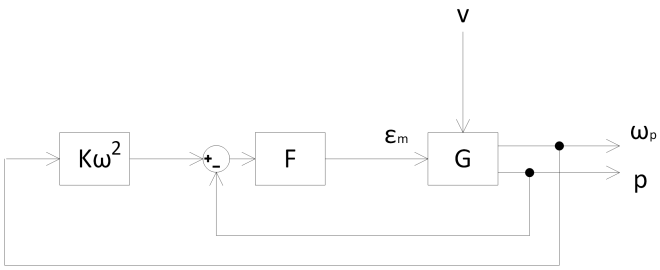

Figure 5.1: A block scheme of the $K\omega^2$ control strategy. Where F is the controller and G is the system.

5.2 Direct Tip Speed Ratio Tracking, DTSRT

The $K\omega^2$ is a quite slow TSR Tracking that also depends on the accuracy of the model of the turbine used to calculate the K. Therefore an idea arose to control directly on the error of TSR, this still uses the same C_P model as the $K\omega^2$ to decide what value the optimal TSR has. It was thought to be able to faster track the optimal TSR which would give a higher energy extraction from the wind and hence give a larger total delivered output energy. The control strategy was named Direct Tip Speed Ratio Tracking ($DTSRT$), see Figure 5.2. In this control strategy the wind speed is measured and then converted to the corresponding optimal rotational speed of the rotor. Meaning that a rotational speed will be the reference meanwhile the difference between the reference and the actual rotational speed will be the control error. For this control strategy it is simple to implement the constraint of the maximum rotational speed of 120 rpm. The only thing needed is a saturation

with this speed on the reference signal, which means that the reference will be the rotational speed for optimal TSR up to 120 *rpm* but for higher wind speeds the saturation will keep the reference at 120 *rpm*. This reduces the complexity of the control system compared to the $K\omega^2$ since only one PI/PID-controller and no switches are needed. It also makes the tuning easier not only because it has one less PI/PID-controller. Other advantages are that there no longer is a need for tuning the switching between the controllers to get a bumpless transfer neither to make sure that the constraint of maximum rotational speed is not violated.

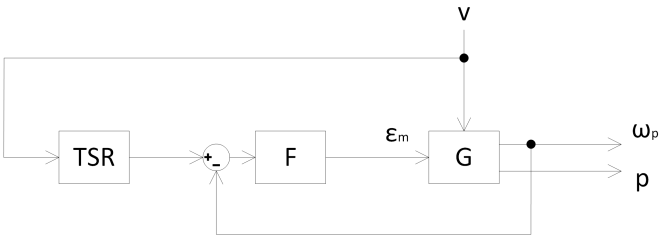

Figure 5.2: A block scheme of the *DTSRT* control strategy. Where F is the controller and G is the system.

5.3 Feedforward

A method that can be used when a fast reference tracking with good stability margins is sought for is Feedforward (FF). Therefore it was interesting to implement the FF together with the other control methods to see if there reference tracking could be faster. FF can be seen as an attempt to predict how the system will react to a input signal. The input signal can be from the reference signal and/or from a measurable disturbance [54]. The idea for $FF\ from\ reference$ is to use knowledge of the system and then let the reference be fed through the inverse of the known system, $G_{FF,r}(s) = 1/G(s)$. The idea is similar for the $FF\ from\ disturbance$ but here the knowledge of how a measurable disturbance affect the system is used and the measured disturbance is fed through the inverse of this known influence, $G_{FF,d}(s) = 1/H(s)$. The G_{FF} links demands that the inverse of the transfer functions describing either system $G(s)$ or disturbance $H(s)$ are proper[1]. If this is not the case they have to be adjusted so that they turn out proper, otherwise there will be an exact derivative which for real systems are not suitable, why is described in Section 5.5. One way to make G_{FF} proper is to add the same amount of poles to the G_{FF} links as the degree differ between the denominator and numerator. The poles can either be chosen as a duplication of some already existing pole/poles or be placed to give the FF desired characteristics.

A mathematical system model of a similar HST in a wind turbine was done by the Offshore Wind Group at TU Delft [55], Equation 5.3 to 5.11 refers to this work.

[1]Proper = Degree of the denominator polynomial $\geq$ degree of the numerator polynomial

The total leakage flow of a hydraulic machine, q_l, is assumed to be proportional to the pressure difference over the machine, p, with respect to a laminar leakage coefficient, C_v.

$$q_l = C_v \cdot p \tag{5.3}$$

Effective shaft torque from the pump, T_p, is assumed to be given by,

$$T_p = D_p \cdot p + B_p \omega_p + C_f D_p \cdot p \tag{5.4}$$

where D_p is the pump displacement, B_p is the viscous damping coefficient of the pump and C_f is a constant Coulomb friction coefficient. The hydraulic capacitance, C_h of the line between the pump and motor is defined as,

$$C_h = \frac{V_h}{E_{eff}} \tag{5.5}$$

where V_h is the total volume of the line and E_{eff} is the effective bulk modulus. The effective bulk modulus will depend on if the high pressure accumulator is connected to the line or not. Though this was known a decision to not model the accumulator was made to simplify the equations. Considering fluid stiffness, material compliance and entrapped air in the hydraulic lines gives the effective bulk modulus,

$$E_{eff} = \frac{1}{E_{fluid}} + \frac{1}{E_{pipe}} + \frac{\alpha}{1.4 p_{ref}} \tag{5.6}$$

where α is the percentage of entrapped air in the line volume at a reference pressure p_{ref}, E_{fluid} is the bulk modulus of the fluid and E_{pipe} is the bulk modulus of the pipe calculated according to Equation 5.7 [56] in terms of Young's modulus $E_{Young,pipe}$ and the Poisson's ratio ν.

$$E_{pipe} = \frac{E_{Young,pipe}}{3(1 - 2\nu)} \tag{5.7}$$

The pressure losses in the lines can be defined as proportional to the flow times a hydraulic resistance, R_h. Assuming laminar flow the hydraulic resistance can be expressed as,

$$R_h = \frac{128 \mu L}{\pi D^4} \tag{5.8}$$

where μ is the dynamic viscosity, L is the length and D the diameter of the pipe.

With these equation it is possible to represent the system with two equations. The first one is given from a torque balance on the aerodynamic rotor shaft,

$$J_r \dot{\omega}_r = T_a - B_r \omega_r - T_p \tag{5.9}$$

where T_a is the torque generated by the wind acting on the rotor and B_r is the viscous friction in the rotor. But since a gearbox with gear ratio, U, is used in the

system between the rotor and pump the Equation 5.9 becomes when considering torque balance on the pump side of the gearbox,

$$\begin{aligned}\frac{J_r}{U^2}\dot{\omega_p} &= \frac{T_a}{U} - \frac{B_r}{U^2}\omega_p - T_p \\ &= \frac{T_a}{U} - \big(\frac{B_r}{U^2} + B_p + D_p^2(1+C_f)R_h\big)\omega_p - D_p\big(1+C_f\big)p\end{aligned} \tag{5.10}$$

where $J_r$is the aerodynamic rotor inertia. The second equation is held from the flow continuity equation on the high pressure line between pump and motor,

$$C_h\dot{p} = D_p\big(1 - R_hC_{v,p}\big)\omega - \big(C_{v,p} + C_{v,m}\big)p - \varepsilon_m D_m\omega_m \tag{5.11}$$

where ε_m is the motor displacement setting, D_m the motor displacement and ω_m the motor rotational speed.

Assuming that the motor speed is constant, linearizing at steady state point $(T_{a,0}, \omega_{p,0}, p_0, \varepsilon_{m,0})$ and taking the LaPlace transform of Equation 5.10 and 5.11 gives the following equations,

$$\frac{J_r}{U^2}\Delta\omega_p s = \frac{\Delta T_a}{U} - \big(\frac{B_r}{U^2} + B_p + D_p^2(1+C_f)R_h\big)\Delta\omega_p - D_p\big(1+C_f\big)\Delta p \tag{5.12}$$

$$C_h\Delta p s = D_p\big(1 - R_hC_{v,p}\big)\Delta\omega_p - \big(C_{v,p} + C_{v,m}\big)\Delta p - \Delta\varepsilon_m D_m\omega_m \tag{5.13}$$

where $\Delta\omega_p = \omega_p - \omega_{p,0}$, $\Delta\varepsilon_m = \varepsilon_m - \varepsilon_{m,0}$ and $\Delta T_a = T_a - T_{a,0}$.

The wind torque T_a is a variable that is dependent on the wind speed v and the rotor speed ω_r. With Equation 2.36 in Section 2.5.2 and $\omega_r = \frac{\omega_p}{U}$ the wind torque can be expressed as,

$$\begin{aligned}T_a &= \frac{P_{rotor}}{\omega_r} = \frac{P_{rotor}U}{\omega_p} \\ &= \frac{1}{2}\rho A C_p U\frac{v^3}{\omega_p}\end{aligned} \tag{5.14}$$

C_p is variable and depends on the pitch angle β, the wind speed v and the rotor speed ω_r. As explained in Section 2.5.2, for one blade design there is an optimal tip speed ratio that gives the maximum power coefficient $C_{p,ideal}$. Assuming that $C_p = C_{p,ideal} = constant$ and linearizing Equation 5.14 at the steady state point $(v_0, \omega_{p,0})$ gives,

$$\begin{aligned}\Delta T_a &= \frac{3\zeta U v_0^2}{\omega_{p,0}}\Delta v - \frac{\zeta U v_0^3}{\omega_{p,0}^2}\Delta\omega_p \\ where \quad \zeta &= \frac{1}{2}\rho A C_{p,ideal}\end{aligned} \tag{5.15}$$

Taking Equation 5.15 and putting into Equation 5.12 results in,

$$\frac{J_r}{U^2}\Delta\omega_p s = \frac{3\zeta v_0^2}{\omega_{p,0}}\Delta v - \left(\frac{\zeta v_0^3}{\omega_{p,0}^2} + \frac{B_r}{U^2} + B_p + D_p^2(1+C_f)R_h\right)\Delta\omega_p - D_p\big(1+C_f\big)\Delta p \tag{5.16}$$

Equation 5.13 and 5.16 are two linear functions that represents the system in the frequency domain. The system has four different variables $\Delta\omega_p, \Delta v, \Delta p$ and $\Delta\varepsilon_m$. With two equations this means that it is possible to express one variable as a function of two other. The output from the controller is the motor displacement ε_m and consequently the feedforward controller should output a desired motor displacement for two given reference signals. It was chosen to feedforward the wind speed and pressure. Solving Equation 5.16 and 5.13 for $\Delta\varepsilon_m(\Delta p, \Delta v)$ gives,

$$\begin{aligned}\Delta\varepsilon_m = &\frac{3v_0^2\zeta D_p U^2(1-C_{v,p}R_h)}{\omega_{p,0}D_m\omega_m J_r}\cdot\frac{1}{s+\frac{U^2Y}{J_r}}\cdot\Delta v \\ &-\frac{C_h}{D_m\omega_m}\cdot\frac{\left(s^2+\frac{U^2YC_h+XJ_r}{J_rC_h}s+\frac{U^2D_p^2\left(1+C_f\right)\left(1-C_{v,p}R_h\right)+XY}{J_rC_h}\right)}{s+\frac{U^2Y}{J_r}}\cdot\Delta p\end{aligned} \tag{5.17}$$

where,

$$\begin{aligned}Y &= B_p+\frac{B_r}{U^2}+D_p^2R_h(1+C_f)+\frac{\zeta v_0^3}{\omega_{p,0}^2}\\ X &= C_{v,m}+C_{v,p}\end{aligned}$$

and thus we get the transfer function from wind speed to motor displacement $G_{v,\varepsilon}$:

$$G_{v,\varepsilon} = \frac{3v_0^2\zeta D_p U^2(1-C_{v,p}R_h)}{\omega_{p,0}D_m\omega_m J_r}\cdot\frac{1}{s+\frac{U^2Y}{J_r}} \tag{5.18}$$

and the transfer function from pressure to motor displacement $G_{p,\varepsilon}$:

$$G_{p,\varepsilon} = -\frac{C_h}{D_m\omega_m}\cdot\frac{\left(s^2+\frac{U^2YC_h+XJ_r}{J_rC_h}s+\frac{U^2D_p^2\left(1+C_f\right)\left(1-C_{v,p}R_h\right)+XY}{J_rC_h}\right)}{s+\frac{U^2Y}{J_r}} \tag{5.19}$$

$G_{p,\varepsilon}$ is not a proper transfer function since the numerator has one order higher than the denominator. Therefore another pole was added to make it proper. The pole was chosen to be in the same point as the already existing pole $(-\frac{U^2Y}{J_r})$. This can be regarded as adding a first order low pass filter to the transfer function and by choosing the position of this pole it is possible to change the dynamic response of the FF-transfer function. Choosing a double pole in $(-\frac{U^2Y}{J_r})$ gave good simulation results. To have the both feedforward links equally fast the same pole was added to $G_{v,\varepsilon}$. After adding the pole to both transfer functions the FF links are ready to be implemented in the model. The FF links are shown in Equation 5.20 and 5.21.

$$G_{FFv,\varepsilon} = \frac{3v_0^2\zeta D_p U^2(1-C_{v,p}R_h)}{\omega_{p,0}D_m\omega_m J_r}\cdot\frac{1}{\left(s+\frac{U^2Y}{J_r}\right)^2} \tag{5.20}$$

$$G_{FFp,\varepsilon} = -\frac{C_h}{D_m \omega_m} \cdot \frac{\left(s^2 + \frac{U^2 Y C_h + X J_r}{J_r C_h} s + \frac{U^2 D_p^2 \left(1+C_f\right)\left(1-C_{v,p} R_h\right) + XY}{J_r C_h} \right)}{\left(s + \frac{U^2 Y}{J_r} \right)^2} \tag{5.21}$$

Figure 5.3 shows the dynamic difference between $G_{v,\varepsilon}$ and $G_{FFv,\varepsilon}$.

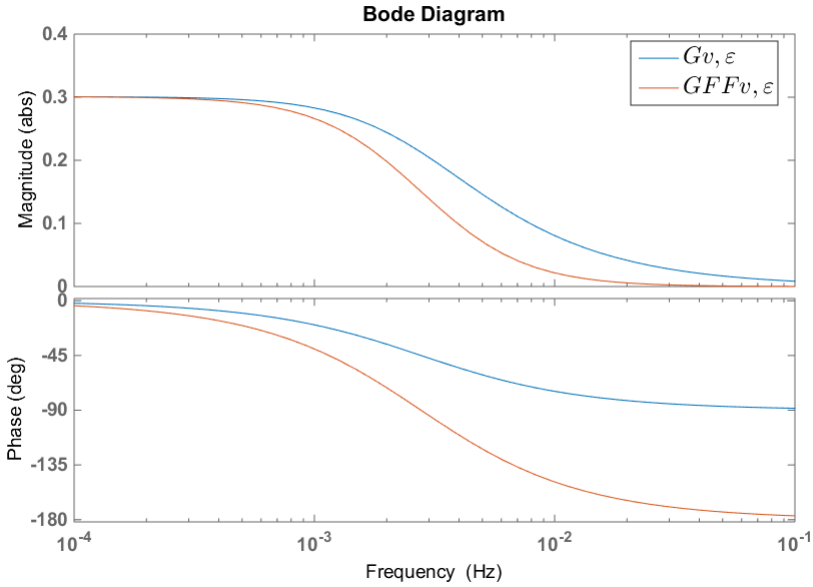

Figure 5.3: A bode diagram to point out the dynamic difference between $G_{v,\epsilon}$ and $G_{FFv,\epsilon}$.

Adding the pole to the transfer function gives a lower break frequency and a slightly larger delay but the static amplification remains the same. Figure 5.4 displays the block diagram of the feedforward control implemented together with the $K\omega^2$ control strategy.

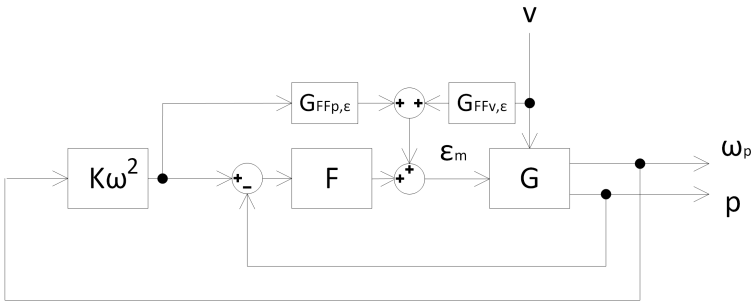

Figure 5.4: A block scheme of the feedforward implemented with the $K\omega^2$ control strategy. Where F is the controller and G is the system.

To implement the FF together with DTSRT another approach was needed. Since the reference signal is the rotor speed ω_r and the FF links calculates motor displacement from wind speed and pressure two options existed. Either to solve Equation 5.13 and 5.16 for ε_m as a function of v and ω_p or to use the $K\omega^2$ method to calculate an ideal pressure from the rotor speed. The latter option was chosen to have more similarities between the both FF implementations. Figure 5.5 shows how the FF links are implemented together with the DTSRT control strategy.

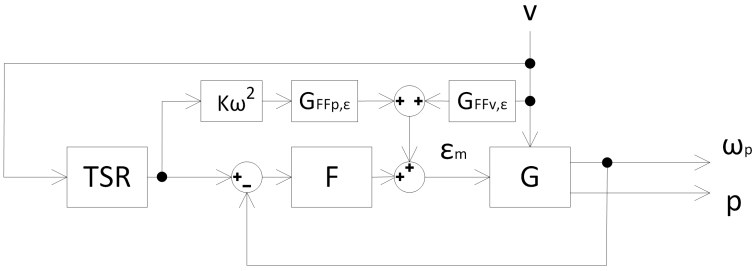

Figure 5.5: A block scheme of the feedforward implemented with the DTSRT control strategy. Where F is the controller and G is the system.

It is important to notice that the transfer functions calculates $\Delta\varepsilon_m$ from Δv and Δp which are the deviations from their respective linearization equilibrium values. Therefore input signals and output signal must be calculated accordingly. See Equation 5.22 for how the input signals v and p are adjusted with their equilibrium values and that the motor displacement equilibrium value is added to give the right output value from the controller.

$$\varepsilon_m = \varepsilon_{m,0} + G_{FFp,\varepsilon} \cdot (p - p_0) + G_{FFv,\varepsilon} \cdot (v - v_0) \tag{5.22}$$

The linearization was chosen to be done around the equilibrium point given at 7 m/s wind speed when the system is running at optimal TSR. This could

be done by simulating until steady state values were reached for a constant wind speed input of 7 m/s and using the DTSRT controller. The obtained equilibrium values were,

$$v_0 = 7\ m/s, \quad p_0 = 91.28\ bar, \quad \varepsilon_{m,0} = 0.6971 \quad and \quad \omega_{p,0} = 114.7\ rad/s \tag{5.23}$$

The reason for chosing 7 m/s as linearization point was that it is in the middle of the operating range of the hydrostatic transmission (4-12 m/s) and should thereby give the best overall estimation.

5.4 Mode switching with bumpless transfer

When switching between different controllers some problem may occur. When switching between one regulator, Regulator A, to another, Regulator B, there can be a large step between the output signal for the two regulators meaning that the signal to the system makes a large step when the switching is done. This can give large shock forces in the system due to abrupt changes and also induce oscillations to the system.

For example if both Regulator A and B have I-parts. The difference in output between the controllers occurs because for example Regulator B was inactive until the point of switching and could not control the system, the I-part of this regulator kept integrating its error. Thus the integrated value become very large since the active regulator kept the system quantities away from the inactive Regulator B's reference. When then switching back to Regulator B the signals does not match and a control signal step occurs. To prevent this and the risk of making a large step in the control signal some sort of adjusting or reset of the I-part must be done. One way to adjust the I-part is to add a type of tracking mode to the controllers, see Figure 5.6.

If the tracking mode is added to the system it feedback the difference between the regulators output signal and the active regulator output signal to the integral part of respective regulator. So for the active controller the tracking signal will be zero. But the tracking signal will force the output signals from inactive regulators to adjust to the output signal of the active regulator. Which yields that when switching from one regulator to another the new active regulator will start with the same regulator output signal as the old active one just had and from there regulate the system towards its reference. So the abrupt step in the output signal is removed and a bumpless transfer between the controllers is obtained, giving a smoother control of the system. This method of bumpless transfer is more commonly used in control system that, apart from a regulator, have a manual mode to give a smooth transit when changing between the modes.

The tracking signal that is feedbacked to the regulators can also be used to prevent wind-up in the active controller. If the known saturation is added into the controller and the signal after this saturation is feedbacked to the controllers, this will prevent wind-up hence it adjust the integral part of the active regulator when

its output signal is saturated. In this way it prevents the value of the integral part from increasing undesirably.

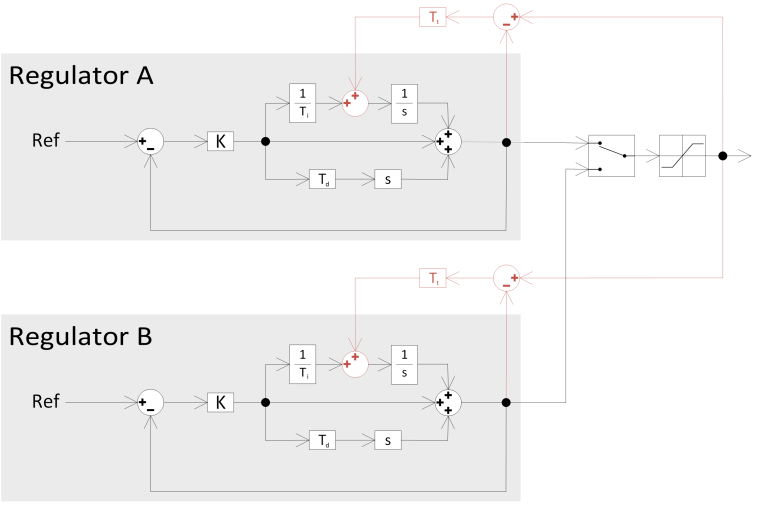

Figure 5.6: How the control system looks after the tracking mode was added (New parts and lines marked with red).

5.5 Filtering the derivative part of PID

In the original model both of the PID controllers had an ideal Derivative part, D-part. In a real system when controlling on measured signals, where noise almost always are present, an ideal D-part would amplify this noise and give a poor control of the system. This is why some kind of modifications have to be done to the D-part to give good control of real systems, unless the measured signal have low noise. One way is to add a low pass filter to the D-part, see Equation 5.24. This means that low frequencies will be let through so that they are derived almost exactly meanwhile high frequency noise will only have a gain of $1/\mu$. For an ideal D-part the gain otherwise will go towards infinity when frequency goes towards infinity. The lower the value chosen for μ the more the D-part will act like a pure ideal drivative which gives a more precise derivative of the signal but with more and more noise passing through.

$$G_{D-part} = \frac{1}{\mu T_d s + 1} \tag{5.24}$$

where T_d is the derivative time constant and μ is the filter constant.

When adding the filter to the D-part the full PID-controller will have a transfer function looking like Equation 5.25.

$$F(s) = K\left(1 + \frac{1}{T_i s} + \frac{T_d s}{\mu T_d s + 1}\right) \tag{5.25}$$

where K is the proportional gain, T_i is the integral time constant, T_d is the derivative time constant and μ is the filter constant.

5.6 Optimizing the PI and PID parameters

To be able to compare the results from the different control strategies the parameters in the controllers had to be chosen in a similar way. There is a lot of different approaches to tune a controller, everything from trial and error tuning, to optimizing the parameters for model of the system. Since the system is complex and a simulation model already existed the optimization method was considered a good option. Using the same optimum and limits also gives a good base for comparison of the different control strategies.

The parameters in the PID controllers was optimized using an optimizing algorithm called Genetic Algorithm, GA. This is an optimizing algorithm that is based on natural selection and Darwin's theory, survival of the fittest. It starts with a population of randomly generated solutions, called individuals, that evolves over time towards the optimal solution. [57, 58]

As objective function the deviation from optimal TSR and deviation from generator frequency was chosen to be minimized. Since being at optimum TSR yields a larger power extraction from the wind and being at the right frequency gives a better quality of the electric energy that is delivered to the grid. For both of them the absolute value of their deviation was first normalized with their optimal value and then integrated. They were also weighted against each other with a factor. The weight factor was set to 5000. With a low value the controller got too aggressive, with a large I-part that made the system unstable at low wind speeds where the damping is low. A to high factor resulted in an optimal solution with almost no TSR tracking at all. The only constraint used was that the frequency deviation had to be within 1% all the time. For 60 Hz this mean a deviation of maximum ± 0.6 Hz.

In the optimization K and T_i were optimized for the PI controllers. The PID controllers were optimized in two different ways. One where all the three parameters, K, T_i and T_d, were optimized at the same time and the other way was to first optimize it as a PI controller and after that the T_d parameter was optimized in a separate run. The parameter μ was not optimized for the PID-controllers because this value should, as stated above, be chosen to prevent the controller from regulating on noise in the measured feedback signal. But since no noise was modelled on this signal the value of this parameter was set to a fixed value of 1/14, which is in the middle of a recommended range $1/20 - 1/8$ [59].

For the $DTSRT$ and $DTSRT$ with FF with only one PID/PI-controller the T_t were chosen to be the same as T_i since no faster or slower tracking of the I-part at saturation of the signal was needed. For the $K\omega^2$ where a fast tracking is needed to minimize the bump in the control signal when switching between the two PI-controllers T_t was tuned to give a satisfying result and $T_t = 0.1$ was found to be a good value.

For the feedforward strategies the FF links was implemented without tuning

since they gave good results and any model error in them should be handled by the PI/PID-controller.

The complete optimization set that was used to optimize the parameters in the controllers is given in Equation 5.26.

$$
\begin{aligned}
min\ S(\mathbf{X}) = \ & Integrated\ TSR\ error(\mathbf{X}) + 5000 \cdot Integrated\ Frequency\ error(\mathbf{X}) \\
& s.t. \\
& Maximum\ Frequency\ Deviation(\mathbf{X}) - 0.6 \leq 0 \quad [Hz] \\
& 0.001 \leq K_1, K_2 \leq 0.1 \\
& 10 \leq T_{i1}, T_{i2} \leq 100 \\
& 0.1 \leq T_{d1}, T_{d2} \leq 10 \\
where \quad & \mathbf{X} = [K_1\ K_2\ T_{i1}\ T_{i2}\ T_{d1}\ T_{d2}]'
\end{aligned}
\tag{5.26}
$$

This set was used for all of the optimizations except for the optimization of the complete PID controller for the $DTSRT$ where the range of T_i was adjusted to $[10, 100]$. This was done because it tended to get stuck in a local optimum with a value of $T_i \approx 200$ which gave almost no TSR tracking.

The wind profile that was used for the optimization was steps of 2 m/s from the cut-in speed, 4 m/s, up to nominal wind speed, 10 m/s and then down again to the cut-in speed where it was kept for a quite long time. This was done to penalize unstable and poorly damped solutions that otherwise tended to break through as the optimal solution. The wind profile is presented in Figure 5.7.

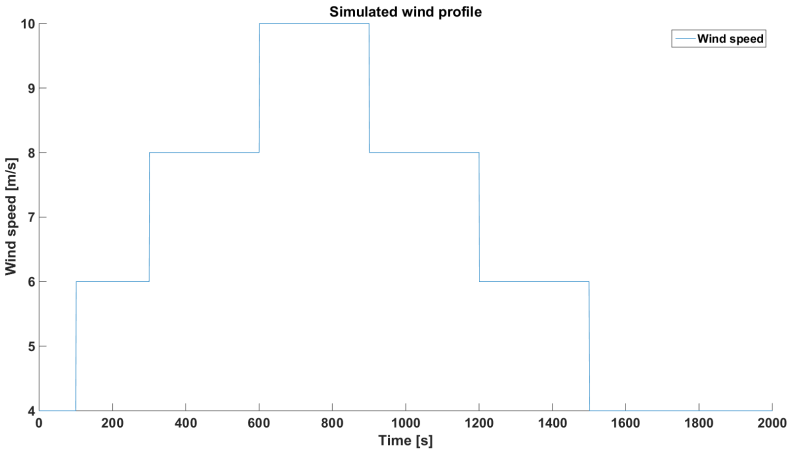

Figure 5.7: Wind profile used for the optimization.

Chapter 6

Dynamic analysis

To have a better understanding of the system brief dynamic analysis was made. Wave propagation in the high pressure line between the pump and motor was analyzed and how the wind dynamics affects the system. Wave propagation was analyzed because of two reasons, one is to see if the natural frequencies of the system may be triggered by flow pulsations from pump or motor. This may cause high noise levels from the system. The other reason is to see if the time delay in the lines, meaning the time it takes for a pressure buildup at one side of the line (pump outlet) to travel to the other side of the line (motor inlet), may significantly change affect the response time of the system. The time delay may cause stability problems in closed loop control of the system [60].

6.1 Comparison of different hydraulic line models

The first thing that was done was to compare different types of line models to make sure that the model gives as good results as possible but to the lowest computational cost. A well known technique that has been proved to be efficient is the Transmission Line Method (TLM) that uses delay elements to represent wave propagation. Nigel Johnston [61] have developed such a model and showed that it is a robust and reliable model. Also the simulation software Hopsan, developed at Flumes (Linköping University) uses TLM to model wave propagation. It models laminar flow in pipes and also calculates the effect of frequency dependent friction. The model has been developed in Matlab/Simulink and since it was desired to model the lines in AMESim it has therefore only been used as a reference when choosing model in AMESim.

In AMESim several options exist when choosing type of line model. The most simple and least computationally demanding only calculates static friction losses and fluid compression, therefore this model is not suitable for wave propagation analysis. Two models use the Lumped Element Method (LEM), one is a single element LEM and the other is a so called distributed LEM. The difference is that the distributed LEM divides the hydraulic line in an optional number of elements whilst the other LEM only use one element that represents the line. Each element is modeled as a resistance, inductance and capacitance and, when using the distributed LEM, a higher number of elements is assumed to give a better result, but a higher number of elements also increase the computational burden [62]. The last model that was evaluated was the $CFD\ 1D\ Lax-Wendroff$ model here after called just CFD. This model solved the 1D Naiver-Stokes equations using a Lax-Wendroff 2nd order numerical scheme in space [63]. Both the LEM models and the CFD model calculates frequency dependent friction, just as the TLM model.

Initially tests were performed, trying to using the different line models in the AMESim model that represents the whole system. When changing to a more complex line model such as the distributed LEM or the CFD model, the computational time became too long. A simplified model of the system was needed to be able to perform the desired frequency analysis. The wind turbine drivetrain system operation is different compared to the normal operation of a HST. Commonly the pump is driven by an internal combustion engine or electric motor running at a constant speed and the motor is coupled to a load that oppose a certain torque. This can be seen as that the pump is a flow source and the motor is a pressure source. In the wind turbine system it is the other way around. The wind speed defines a torque on aerodynamic rotor which via the gearbox gives a proportional torque on the pump. Torque on the pump is proportional to pressure and thus the pump can be considered as a constant pressure source for a certain wind speed. The generator, when coupled to the electrical grid, runs at a constant speed and thus the hydraulic motor will run at the same speed. Hydraulic motor speed is proportional to flow and thus the motor can be seen as a constant flow source when running at a specific displacement setting. Regarding this and limiting the frequency analysis to only be performed on the high pressure line between the

pump and motor makes it possible to model the system with a constant pressure source as pump and the motor as a constant flow source, see Figure 6.1.

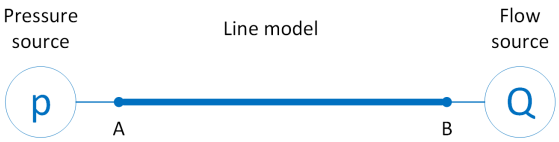

Figure 6.1: Simple model used to validate the different line models.

To better understand how the different line model parameters affect the dynamics of the system some different simulation were made. The first test was to see how the number of states for calculating frequency dependent friction in the LEM models affect the wave propagation in the lines. The pressure source was set to a constant pressure of 100 *bar* and the flow source was set to start with a flow of 50 l/min and make a step after 1 second to 40 l/min. The line model was chosen as to be a distributed LEM model with two elements. Five different number of states for calculating frequency dependent friction were evaluated 0,1,2,3 and 4 number of states. Zero number of states corresponds to just calculating static friction losses [64]. The line model parameters were set to the ones of *Steelpipe*1 in Table 4.6 with the exception of no elevation and the oil properties used for all frequency analysis are presented in Table 6.1.

Table 6.1: Line model parameters used in the simulations.

Parameter	**Value**	**Unit**
Density	870	kg/m^3
Bulk modulus	1500	MPa
Absolute viscosity	27.78	cP
Saturation pressure	0	Pa
Air/gas content	0.1	%
Temeperature	40	$°C$
Polytropic index	1.4	-
Absolute viscosity of air/gas	0.02	cP

The results showed that the natural frequencies for the line are not affected whilst the damping is strongly related to the number of frequency dependent friction states. A comparison of the different line models were then made to see what model that gives the least deviation from the TLM reference. Since the TLM was modeled in Matlab/Simulink a co-simulation between AMESim and Simulink was made with the *SimulinkCosim* interface that is included in AMESim. The input parameters to TLM model are pipe length, internal diameter of pipe, fluid density, kinematic viscosity of the fluid and fluid bulk modulus. It is noticeable that the relative roughness is not a changeable parameter in the TLM model. Both the TLM model and the CFD model does not care of wall compliance. To make

them comparable to the LEM models the effect of wall compliance were neglected also in the LEM models. The simulation models can be seen in Figure 6.2.

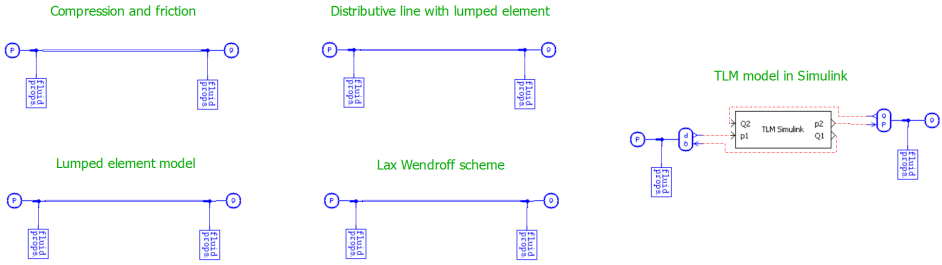

Figure 6.2: The five different line models that was evaluated.

Again the parameters in the model was chosen as the *Steelpipe*1 in Table 4.6 with exception of no elevation. The number of states for frequency dependent friction was chosen to be 4 in the TLM and LEM models. Number of states is not optional in the CFD model. Number of elements in the distributed LEM and CFD model were set to 100. Pressure and flow was similar to previous test, constant 100 *bar* and a step in flow from 50 to 40 l/min. Figure 6.3 and 6.4 shows the resulting pressure in point B, referring to Figure 6.1, for the different hydraulic line models.

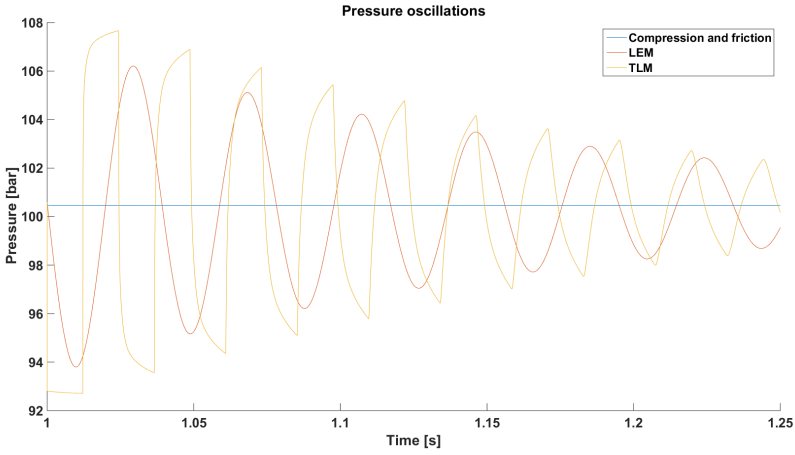

Figure 6.3: Resulting pressure in point B for the three line models Compression and friction, LEM and TLM.

Simulation results show that the simple compression and friction model does not show any wave propagation at all, as predicted. It also shows that the LEM model with a single element is not able to calculate the right frequency response for this specific line parameters.

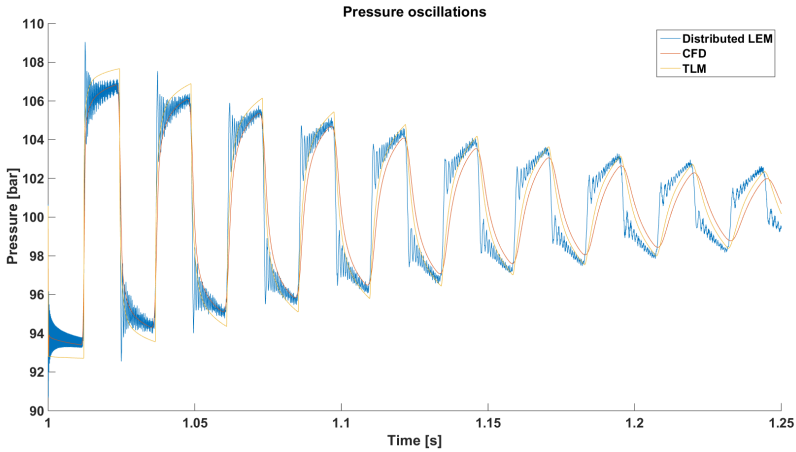

Figure 6.4: Resulting pressure in point B for the three line models Distributed LEM, CFD and TLM.

Comparing the CFD and distributed LEM to the TLM model, shows that both methods gives good correlation both in damping and frequency. But the distributed LEM suffers from high frequency disturbances and also that it deviates more and more in frequency with time. One can also assume that since the relative roughness is not changeable in the TLM model, the static amplification does not match due to difference in static friction. Another difference between the distributed LEM and the CFD is the computational time, the CFD simulation have less than half the CPU time compared to the LEM simulation for this setup. From these results it was therefore decided to analyse the wind turbine system using the CFD model.

6.2 Resonance frequencies of transmission lines

The high pressure line of the system was then modeled using the CFD model. Since the length, type and placement of the hydraulic lines for test platform still was not decided, they had to be estimated. The same lengths and parameters as *Steelpipe*1, *Rubberhose*1 and *Rubberhose*2 in Table 4.6 was used but also one meter steel pipe with no height difference was added. The other parameters of the one meter pipe was set equal to *Steelpipe*1. The test platform will have the ability to turn off the accumulator with a ball valve. Therefore two models were made one with an accumulator and one without, to compare the difference, see Figure 6.5. The parameters for the high pressure accumulator can be seen in Appendix A.1. Simulation was then run in the same manner as when evaluating the line models. The pressure was set to a fixed value corresponding to a fixed wind speed and a step was made in flow that can represent doing a step in displacement setting of the motor.

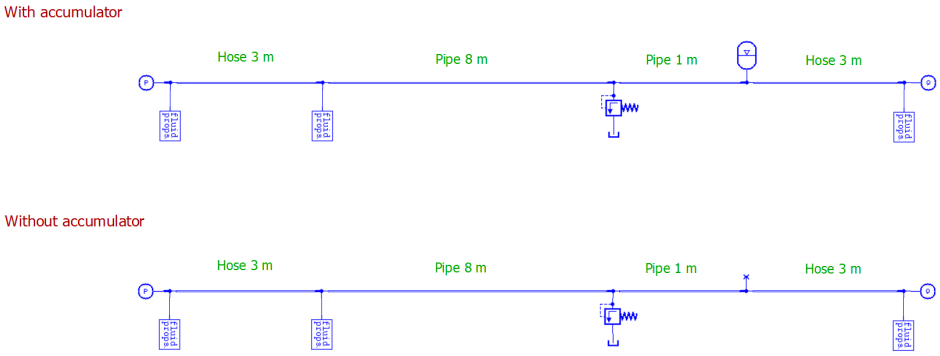

Figure 6.5: The two different system model used for the wave propagation analysis.

To evaluate the results the resonance frequencies were compared to the analytical solution of pressure waves in a pipe with one open end and the other one closed. An open end have a fixed pressure which can be compared to the pump side of the high pressure line and a closed end have variable pressure (constant flow) which is comparable to the motor side [65]. The resonance frequencies $f_{resonance}$ for such a pipe can be calculated according to Equation 6.1 [14].

$$f_{resonance} = a \cdot \frac{k + \frac{1}{2}}{2L} \quad for \quad k = 0, 1, 2... \tag{6.1}$$

where L is the pipe length and a is the wave propagation speed in a pipe filled with fluid which corresponds to,

$$a = \sqrt{\frac{\beta_e}{\rho}} \tag{6.2}$$

where β_e is the effective bulk modulus and ρ the density of the fluid.

A fluid density of $\rho = 870\ kg/m^3$ and a pipe length of 15 meters, giving a pipe volume $V_c = 4.3\ liters$ for an internal diameter of 19 mm, was used for the calculations. When estimating the frequencies for the system without accumulator the effective bulk modulus used was $\beta_e = \beta_{fluid} = 1500\ bar$. For the system with accumulator an effective bulk modulus was calculated according to Equation 6.3 [66].

$$\beta_e = \left(\frac{V_p}{V_p + V_a} \cdot \frac{1}{\beta_{fluid}} + \frac{V_a}{V_p + V_a} \cdot \frac{1}{p} \right)^{-1} \tag{6.3}$$

where V_a is the gas volume at a given precharge pressure and p is the system pressure. This means that the effective bulk modulus with an accumulator in the system will change with pressure.

The resonance frequencies were then compared to the pulsations from the pump and motor to see if they were in the same frequency range and thereby risking high noise from the system.

6.3 Aerodynamic rotor dynamics

Another thing found interesting to investigate was how the wind dynamics will affect the system. It is of great interest since these dynamics defines how fast the controller must respond to change in wind speed. It is also interesting to see if the wind can trigger the natural frequencies of the pipe and cause noise or instability.

The earlier derived equations in Section 5.3, Equation 5.12 and 5.13 can be used to express a transfer function from wind speed and pressure difference over the pump to pump speed. But when linearizing the wind torque ΔT_a in Equation 5.15 an assumption was made that $C_p = C_{p,ideal}$. This is a valid assumption if the TSR (λ) is close to ideal. To have a better estimation of the rotor speed, also when λ is far from ideal, the wind torque was therefore linearized again for $C_p \neq constant$. From Equation 3.1 in Section 3.3.1 for pitch angle $\beta = 0$ the power coefficient is calculated as,

$$C_p = 0.258(100(\lambda - 0.035) - 2.164)e^{-15.21(\lambda - 0.035)} + 0.00571\lambda \tag{6.4}$$

where $\lambda = \frac{\omega_r r}{v} = \frac{\omega_p r}{Uv}$.

Taking Equation 6.4 and putting into Equation 5.9 gives,

$$\begin{aligned} J_r\dot{\omega}_p = {} & 25.8 \cdot CU^3 \frac{v^4}{\omega_p^2 r} \cdot e^{-15.21(\frac{Uv}{\omega_p r} - 0.035)} - 1.4613 \cdot CU^2 \frac{v^3}{\omega_p} \cdot e^{-15.21(\frac{Uv}{\omega_p r} - 0.035)} \\ & + 0.00571 \cdot CUrv^2 - B_r\omega_p - U^2 T_p \end{aligned} \tag{6.5}$$

for

$$C = \frac{1}{2}\rho A \tag{6.6}$$

and considering that

$$T_p = D_p p \frac{1}{\eta_{hmp}} \tag{6.7}$$

Linearizing in (v_0, ω_{p0}, p_0) and taking the LaPlace transform then gives,

$$\begin{aligned} J_r\Delta\omega_p s = {} & J_r \cdot \left.\frac{\partial\dot{\omega}_p}{\partial v}\right|_{v_0,\omega_{p0},p_0} \Delta v \\ & + J_r \cdot \left.\frac{\partial\dot{\omega}_p}{\partial\omega_p}\right|_{v_0,\omega_{p0},p_0} \Delta\omega_p \\ & + J_r \cdot \left.\frac{\partial\dot{\omega}_p}{\partial p}\right|_{v_0,\omega_{p0},p_0} \Delta p \end{aligned} \tag{6.8}$$

where

$$\begin{aligned} J_r \cdot \left.\frac{\partial \dot{\omega}_p}{\partial v}\right|_{v_0,\omega_{p0},p_0} &= K_1 = \frac{-CU^3 v_0^3}{\omega_{p0}^2 r}\left(\frac{U v_0}{\omega_{p0} r} - 4\right) \cdot e^{-15.21(\frac{U v_0}{\omega_{p0} r} - 0.035)} \\ &+ 1.4613 \cdot \frac{CU^2 v_0^2}{\omega_{p0}}\left(\frac{U v_0}{\omega_{p0} r} - 3\right) \cdot e^{-15.21(\frac{U v_0}{\omega_{p0} r} - 0.035)} \\ &+ 0.01142 \cdot CU r v_0 \end{aligned} \tag{6.9}$$

$$\begin{aligned} J_r \cdot \left.\frac{\partial \dot{\omega}_p}{\partial \omega_p}\right|_{v_0,\omega_{p0},p_0} &= K_2 = \frac{CU^3 v_0^4}{\omega_{p0}^4 r}\left(\frac{U v_0}{r} - 2\omega_{p0}\right) \cdot e^{-15.21(\frac{U v_0}{\omega_{p0} r} - 0.035)} \\ &- \frac{CU^3 v_0^4}{\omega_{p0}^3 r}\left(\frac{U v_0}{r} - \omega_{p0}\right) \cdot e^{-15.21(\frac{U v_0}{\omega_{p0} r} - 0.035)} \\ &- B_r \end{aligned} \tag{6.10}$$

$$J_r \cdot \left.\frac{\partial \dot{\omega}_p}{\partial p}\right|_{v_0,\omega_{p0},p_0} = K_3 = -U^2 D_p \frac{1}{\eta_{hmp}} \tag{6.11}$$

Equation 6.8 to 6.11 then gives the transfer function from pressure Δp and wind speed Δv to rotor pump speed $\Delta\omega_p$ as,

$$\begin{aligned} \Delta\omega_p &= \frac{1}{J_r s + K_2}\left(K_1 \Delta v + K_3 \Delta p\right) \\ &= \frac{1}{\frac{J_r}{K_2} s + 1}\left(\frac{K_1}{K_2}\Delta v + \frac{K_3}{K_2}\Delta p\right) \end{aligned} \tag{6.12}$$

where

$$\frac{1}{\frac{J_r}{K_2} s + 1} \tag{6.13}$$

can be considered as a first order low pass filter with break frequency $\omega_c = \frac{K_2}{J_r}$ that filters the wind speed and pressure.

Chapter 7

Results

7.1 Control strategy performance

All together there were six different controllers investigated. The original $K\omega^2$, the $DTSRT$ with three different controllers, the $K\omega^2$ with feedforward and the $DTSRT$ with feedforward. The $DTSRT$ was evaluated with a PI-controller, with the PI-controller with a D part added and optimized separately and finally with a full PID-controller. The resulting control parameters from the optimizations of the six different runs with the wind profile in Figure 5.7 are presented in Table 7.1. The four performance categories integrated TSR error ($\int \Delta$TSR), integrated frequency error ($\int \Delta$Freq), maximum peak frequency deviation (Max ΔFreq) and extracted energy are displayed in Table 7.2.

Table 7.1: The controller parameters found with optimization.

	K_1	Ti_1	Td_1	K_2	Ti_2
$K\omega^2$	$6.767e^{-2}$	22.73	-	0.02584	271.8
DTSRT PI	$9.945e^{-3}$	12.73	-	-	-
DTSRT PI+D	$9.945e^{-3}$	12.73	0.1134	-	-
DTSRT PID	$9.209e^{-3}$	11.21	0.4345	-	-
FF $K\omega^2$	$9.837e^{-2}$	264.1	-	0.01006	178.9
FF DTSRT	$9.367e^{-3}$	10.86	-	-	-

Table 7.2: Performance results with the optimal control parameters.

	$\int \Delta$**TSR**	$\int \Delta$**Freq**	**Max** Δ**Freq**	**Energy [kWh]**
$K\omega^2$	120.5	264.3	0.1	5.089
DTSRT PI	152.6	572.1	0.5627 (0.1663)	5.032
DTSRT PI+D	152.6	576.8	0.5700 (0.1662)	5.032
DTSRT PID	145.6	594.7	0.5490 (0.2216)	5.037
FF $K\omega^2$	75.07	265.5	0.08772	5.111
FF DTSRT	127.1	563.1	0.1756	5.084

The table data shows that $K\omega^2$ with FF is the method that performs the best in three of the four performance categories and second best in the fourth one, where the pure $K\omega^2$ performs a little bit better. It is also noticeable that the two control methods with $K\omega^2$ gives more than 50% less integrated frequency error then the methods with $DTSRT$. Adding FF to the control systems gives a better TSR tracking, which gives some but not so much more delivered energy. It gives a better tracking without improving or deteriorating the integrated frequency error.

Comparing $DTSRT$ with its different controllers the one with a PI-controller with a D-part added afterwards got the worst overall performance. Meanwhile if comparing the PI-controller and the PID-controller the PID-controller got a bit smaller integrated TSR error with the cost of a bigger integrated frequency error than the PI-controller. For all these three controllers the maximum frequency deviation is very close to the hard limit in the optimization set of 0.6 Hz. This comes from the fact that the high pressure accumulator gets emptied at one instance of the cycle. It occurs when the pressure on the high pressure side goes below the precharge pressure of the accumulator. After the accumulator is emptied the

pressure falls quicker, even below the low pressure side for a short moment and this gives the large peak in frequency deviation. The numbers inside the brackets shows the maximum frequency deviation from the rest of the cycle.

To better display the characteristics of the four control strategies the wind profile in Figure 7.1 was used. It covers the whole wind speed range of the two control regions *Region* 2*a* and *Region* 2*b* for the evaluated HST. In Figure 7.2 and 7.3 the corresponding generator frequencies are presented for the $K\omega^2$ and the $DTSRT$ control strategies. For the results of the FF control strategies see Appendix B.1.1. These figures shows that the frequency deviation from 60 Hz and frequency oscillations are much bigger for the two control strategies using the $DTSRT$ than the two using $K\omega^2$, which agrees with the data in the result table.

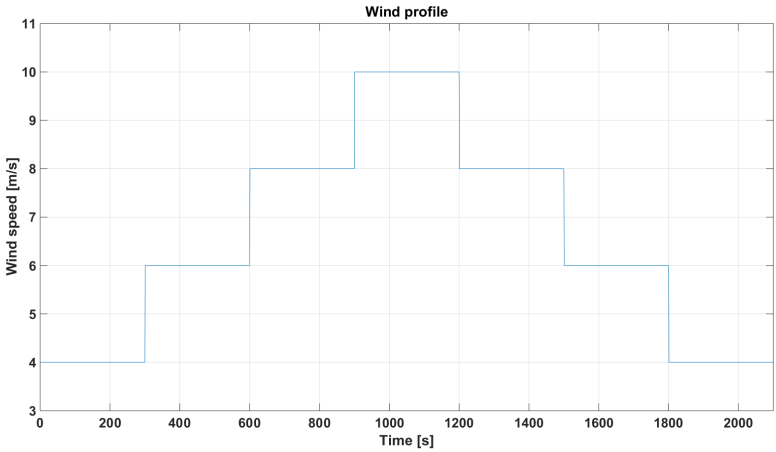

Figure 7.1: Step wind profile used to display the performance of the different control strategies.

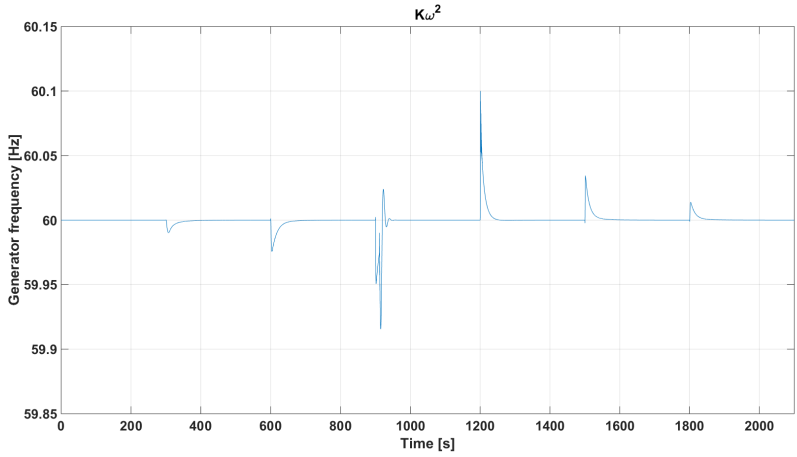

Figure 7.2: Generator frequency for the $K\omega^2$ control strategy.

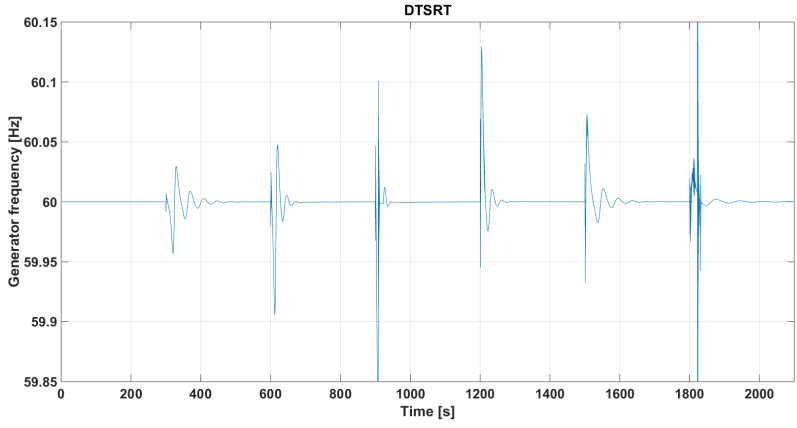

Figure 7.3: Generator frequency for the $DTSRT$ control strategy.

If focusing only on the frequency from the $K\omega^2$ shown in Figure 7.2 it takes the frequency back to 60 Hz really smooth for all wind speed steps but one peak. This oscillating peak occurs when the wind speed goes up to 10 m/s. Before it reaches the optimal TSR for this wind speed the rotor will reach its rated rotational speed of 120 rpm and then switch from the $K\omega^2$ controller to the safety controller that keeps the rotational speed at 120 rpm. This controller has a more oscillating characteristic and look a bit like the $DTSRT$. The similarity is even more distinct when looking at the pressure, see Figure 7.4.

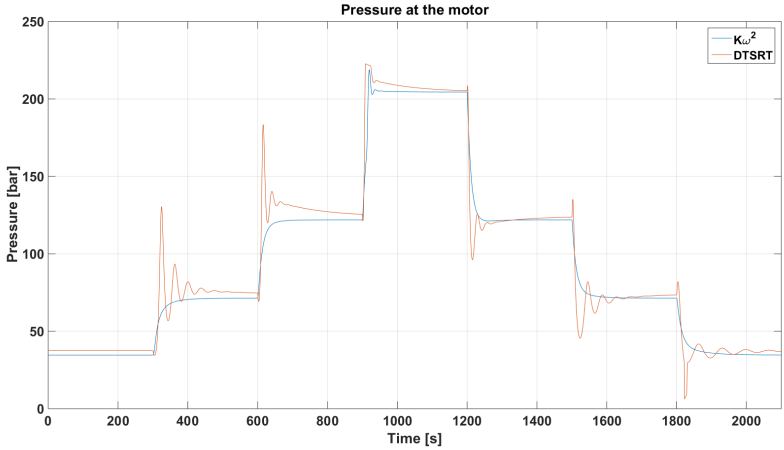

Figure 7.4: System pressure for the $K\omega^2$ and the $DTSRT$ control strategies.

The pressure graph also shows very clearly the oscillations that the $DTSRT$ strategy has compared with the $K\omega^2$. At the end of the cycle the quick drop in pressure, mentioned above, that happens when the accumulator is empty can be seen for the $DTSRT$. The pressure graph for the two FF strategies looks basically the same as their respective strategy without the FF. The only difference is that the FF slightly suppress some oscillations for the $DTSRT$, see Appendix B.1.2.

The TSR tracking of the different methods are presented in Figure 7.5 and 7.6. Comparing $K\omega^2$ with $DTSRT$ shows that the $K\omega^2$ strategy is a lot faster to reach a stable TSR then the $DTSRT$ but that it stabilize on a value a bit further away from the optimal TSR, λ_*. Adding the FF on $DTSRT$ makes it almost as fast as the $K\omega^2$ in TSR tracking but with some overshoot. Adding the FF for the $K\omega^2$ makes basically no difference when the wind increases but it takes it closer to the optimal TSR value when the wind decreases and that is why it has a smaller integrated TSR error.

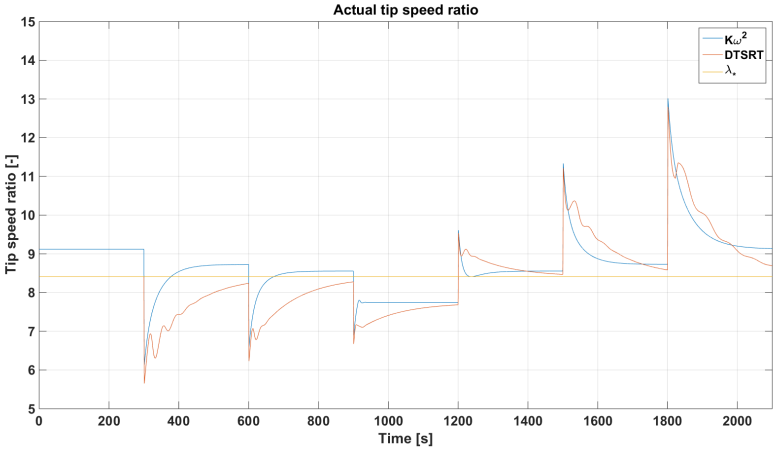

Figure 7.5: How the $K\omega^2$ and the $DTSRT$ control strategies manage to follow the optimal TSR.

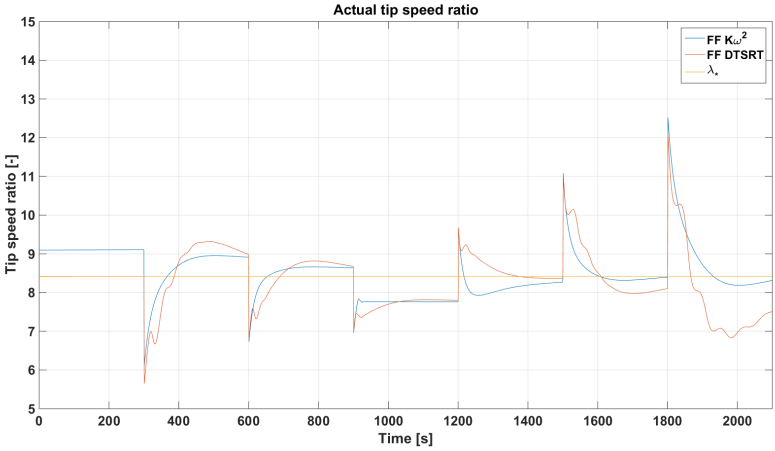

Figure 7.6: How the control strategies wiht FF follows the optimal TSR.

The power outputs from the system to the electric grid are shown in Figure 7.7. The value of the power output is at cut-in speed, 4 m/s, around 0.1 kW, at 6 m/s just over 0.5 kW, at 8 m/s around 15 kW and for the nominal wind speed, 10 m/s, it stabilizes somewhat higher than the rated power at a power of 28.9 kW. The power output curve for the strategies with FF looks similar and are presented in Appendix B.1.5.

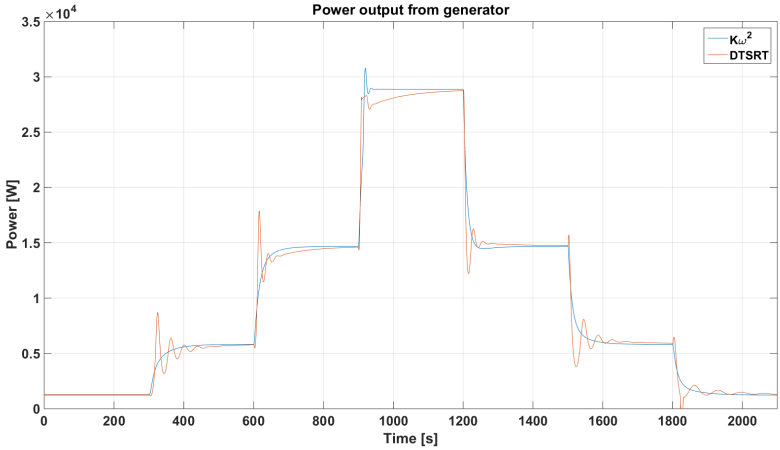

Figure 7.7: Delivered power to the grid for the $K\omega^2$ and the $DTSRT$ control strategies.

Figure 7.8 presents the total efficiency of the whole transmission, i.e. from the hydraulic pump shaft to the hydraulic motor shaft. These shows that the HST has a quite poor efficiency at cut-in speed of around 0.6, but from 6 m/s to 10 m/s it has a quite good overall efficiency from 0.8 to 0.86. For results from the simulations with the FF strategies see Appendix B.1.4.

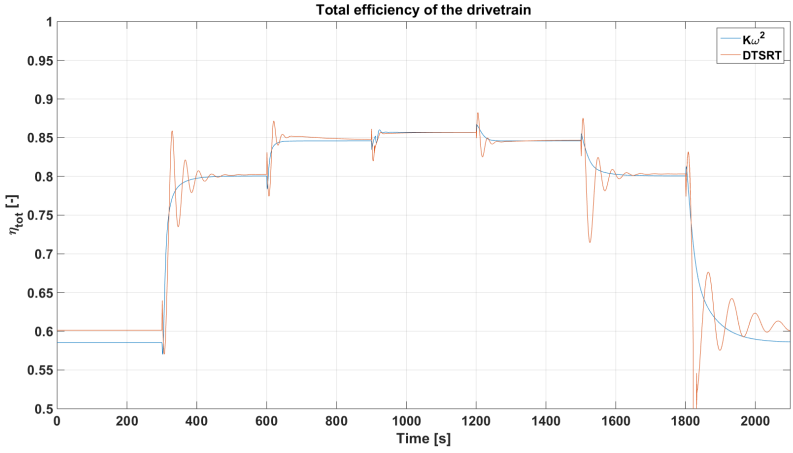

Figure 7.8: Total drivetrain efficiency for the two control strategies $K\omega^2$ and $DTSRT$.

The presented results of the control strategies is so far only based on steps in the wind speed. To compare them in a more realistic wind condition, wind data

from Earth Observing Laboratory [67] was used. The data is sampled once every second and the used wind profile is presented in Figure 7.9.

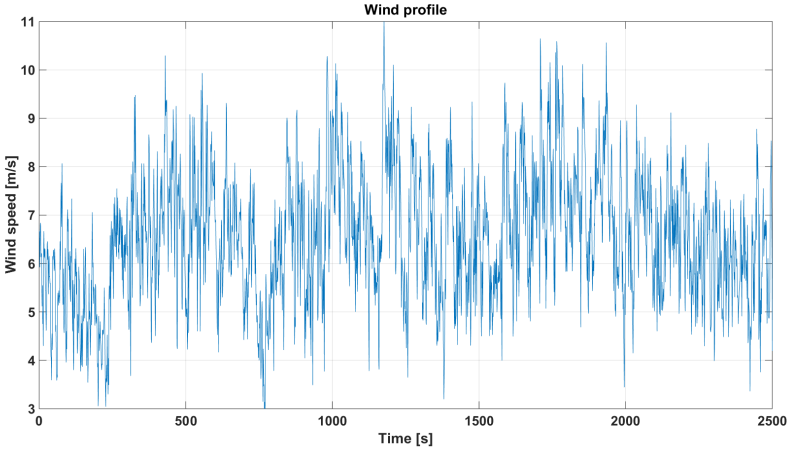

Figure 7.9: Real measured wind profile used to evaluate the performance of the control strategies with a sampling time of 1 second.

The results from the runs with the real wind profile is compiled and presented in Table 7.3.

Table 7.3: The performance result from the run with the real wind data.

	Mean P_{Out}	**Mean** $\eta_{HST,tot}$	$\int$ **ΔTSR**	$\int$ **ΔFreq**	**Max ΔFreq**	**Energy [kWh]**
$K\omega$	8549	0.8157	360	2310	0.07485	5.937
$DTSRT$	8484	0.7968	340.9	6998	0.6374	5.891
$FFK\omega$	8550	0.8161	358.4	2197	0.07289	5.937
$FFDTSRT$	8471	0.802	344.5	6707	0.5057	5.883

Also for the real wind profile the control strategy $K\omega^2$ with FF ranks the best but this time the pure $K\omega^2$ gives equally good results. The Integrated frequency error is more than 3 times bigger for the two control strategies using $DTSRT$ than the ones using the $K\omega^2$. Why can easily be seen in Figure 7.10 and 7.11, which shows that the $K\omega^2$ suppresses the wind oscillations much better than the $DTSR$. For the runs with the FF strategies the frequency deviation is, as in the results from the step wind profile, almost the same as their respective strategy without the FF. Noticeable from the result data is also that the control strategy with FF on the $DTSRT$ has a slightly larger Integrated TSR error than the strategy with pure $DTSRT$ so the improvement with FF shown in the result data from the step wind profile is not present here either.

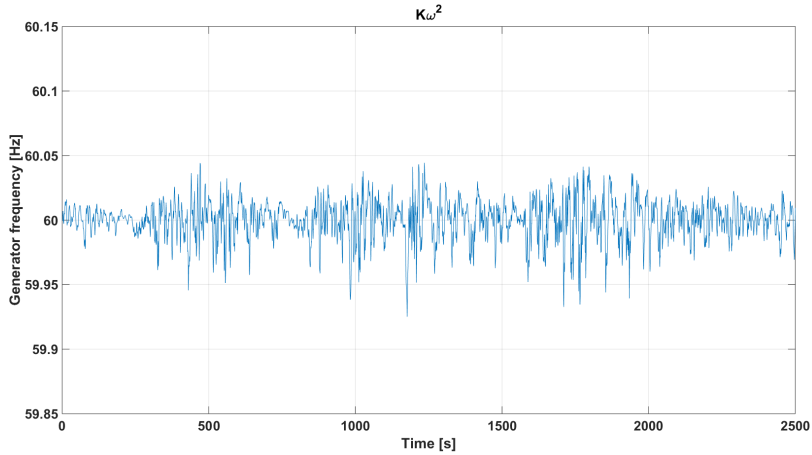

Figure 7.10: Generator frequency for the $K\omega^2$ control strategy.

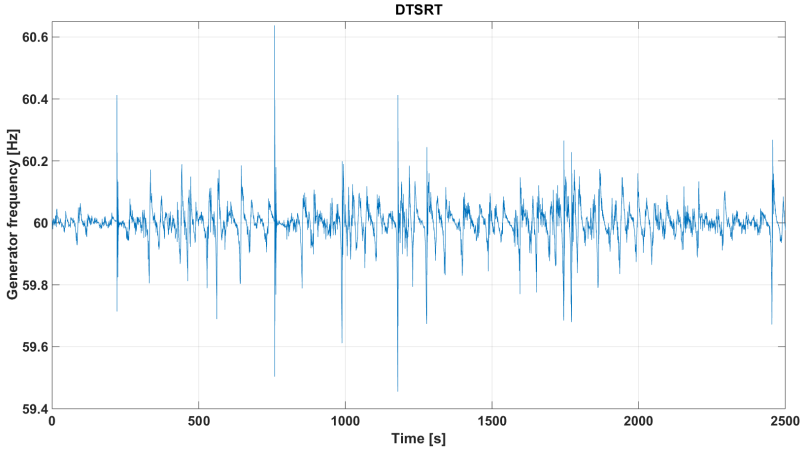

Figure 7.11: Generator frequency for the $DTSRT$ control strategy.

That the $K\omega^2$ filters the wind speed more than the $DTSRT$ is apparent when looking at the rotational speed of the wind turbine rotor, see Figure 7.12. For all the results from the FF strategies see Appendix B.2.

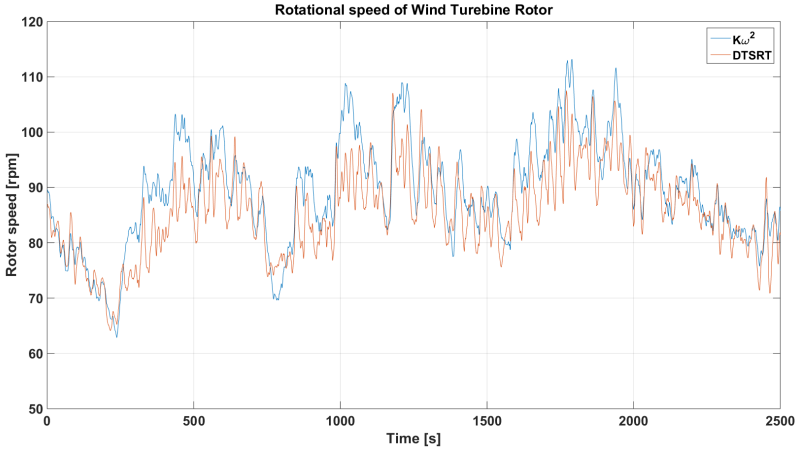

Figure 7.12: The rotational speed of the aerodynamic rotor for the $K\omega^2$ and the $DTSRT$ control strategies.

7.2 System dynamics

For a fixed pressure at the pump outlet of 100 *bar* and doing a step from 76.25 to 38.13 l/min at the motor inlet with the AMESim model presented in Figure 6.5 gave the pressure oscillations in the high pressure line presented in Figure 7.13. The pressure of 100 *bar* and flow of 76.25 corresponds to steady state values withheld from the AMESim model of the whole system at 7 m/s wind speed. The step down to 38.13 l/min corresponds to a 50% change in displacement.

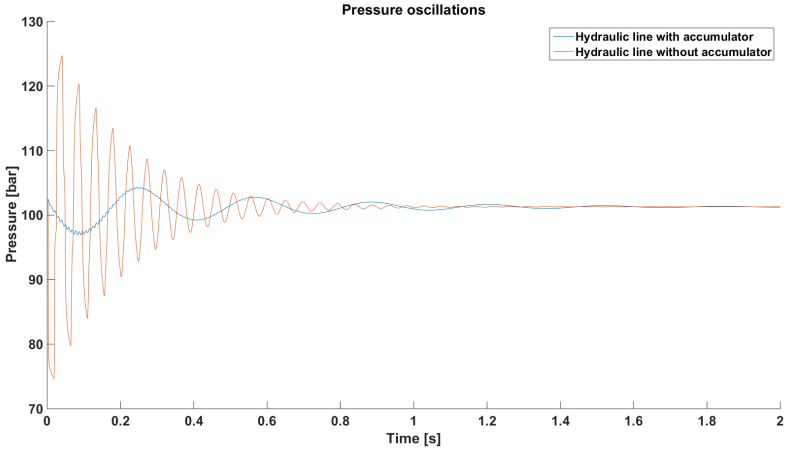

Figure 7.13: Pressure oscillation in the hydraulic lines that shows how the frequency response and damping differs between the hydraulic line with and without accumulator.

It is clear that the resonance frequencies are much higher for the line without an accumulator with a higher bulk modulus. The resonance frequencies were held from plotting the Fast Fourier Transform (FFT) of the pressure oscillations in the tube, see Figure 7.14.

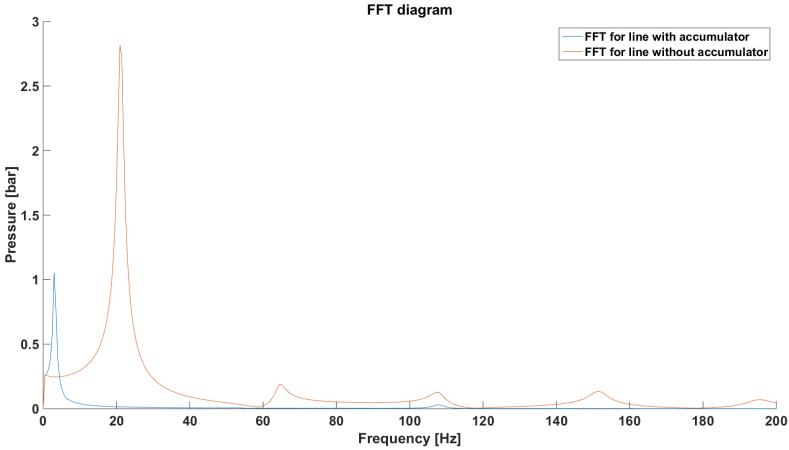

Figure 7.14: Fast Fourier transform plot of Figure 7.13 showing the resonance peaks of the two hydraulic lines.

The FFT diagram shows that for the line with high pressure accumulator only the first resonance frequency has a significant amplification, the higher tones are very well damped.

The four lowest resonance frequencies held from the FFT plot for a line without accumulator:

$$20.95,\ 64.83,\ 107.73,\ 151.61\ Hz$$

Resonance frequency from the FFT plot for a line with accumulator:

$$3.0\ Hz$$

The four lowest calculated analytical resonance frequencies for a pipe with open-closed ends were, for the line without accumulator:

$$21.88,\ 65.65,\ 109.42,\ 153.19\ Hz$$

and for the line with accumulator:

$$3.19,\ 9.58,\ 15.96,\ 22.34\ Hz$$

where $V_a = 1.9\ liters$ and system pressure of $p = 100\ bar$ was used when calculating the effective bulk modulus in Equation 6.3. Notice that the resonance frequency of the system with accumulator will be different for other system pressures. The lowest resonance frequency will, for a system pressure range of 30 to 200 bar, be in the range of 1.76 to 4.48 Hz.

Flow pulsations frequencies from the hydraulic pump and motor were calculated by multiplying the rotational speed with the number of pistons. The motor will run at a constant speed of 1800 rpm during operation and thus it only produce flow pulsations with only one frequency. The pump on the other hand runs

from approximately 600 to 1440 *rpm* giving a range of flow pulsation frequency. Figure 7.15 shows the hydraulic motor flow pulsation frequency compared to the calculated resonance frequencies of the two lines.

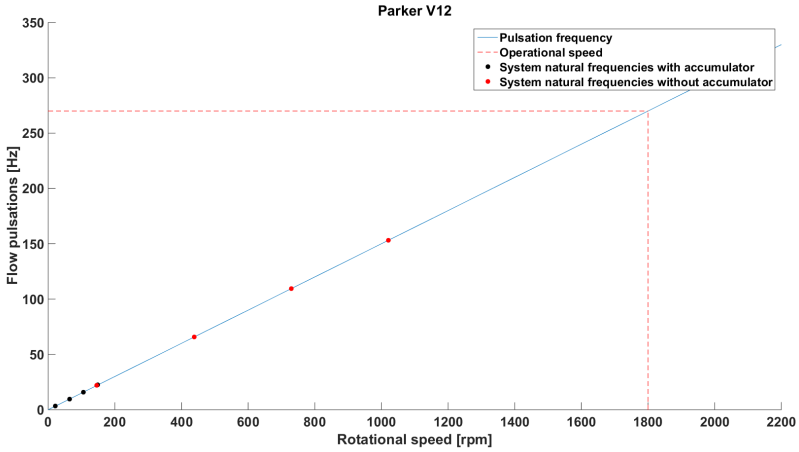

Figure 7.15: Flow pulsation frequency from the motor as a function of rotational speed. The calculated resonance frequencies for the lines are marked as well as the operating speed of the motor.

Figure 7.16 shows the frequency range of the flow pulsations from the pump, again compared to the calculated resonance frequencies.

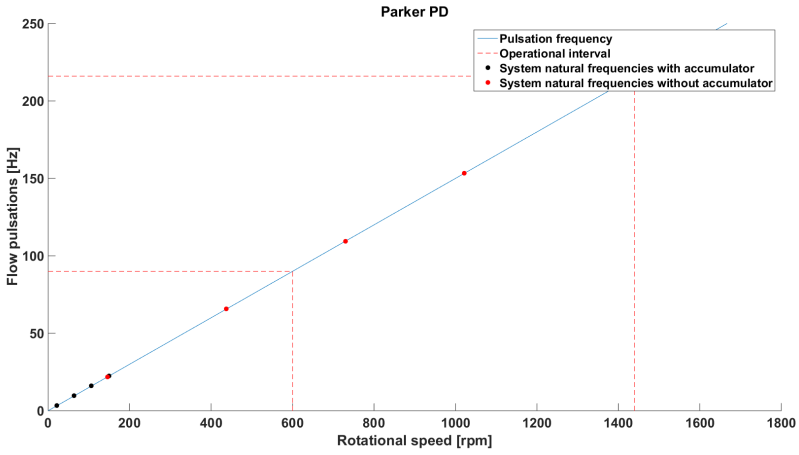

Figure 7.16: Flow pulsation frequency from the pump as a function of rotational speed. The calculated resonance frequencies for the lines are marked as well as the operating speed interval of the pump.

The wave propagation speed in the high pressure line was calculated according to Equation 6.2 resulting in a speed of 1313.3 m/s for the line with no accumulator connected and 191.5 m/s with accumulator. This gives, with a line length of 15 meters, a time delay of 0.011 seconds and 0.078 seconds, respectively.

The derived transfer function, Equation 6.12, was implemented in the AMESim model to evaluate how good they correlate. It was implemented by simply measuring the pressure difference over the pump Δp and subtract the linearization point pressure p_0 giving $\Delta p = p - p_0$. Similarly the wind speed change was calculated as $\Delta v = v - v_0$. Again the wind profile in Figure 7.9 was used for comparison. For the same linearization point as Equation 5.23 the resulting estimated pump speed compared to the system model pump speed is shown in Figure 7.17.

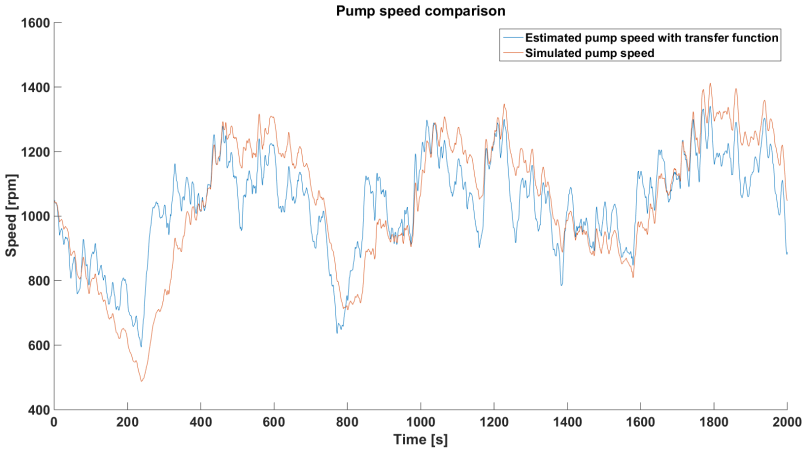

Figure 7.17: Simulated pump speed versus calculated pump speed from the linearized transfer function for the wind profile presented in Figure 7.9.

Comparing Figure 7.9 and Figure 7.17 it is easy to see how the rotor acts like a low pass filter on the wind speed changes.

Also an artificially constructed wind profile was simulated to compare the pump speeds for a more step like wind profile. Figure 7.18 shows the wind profile and Figure 7.19 shows the resulting pump speeds.

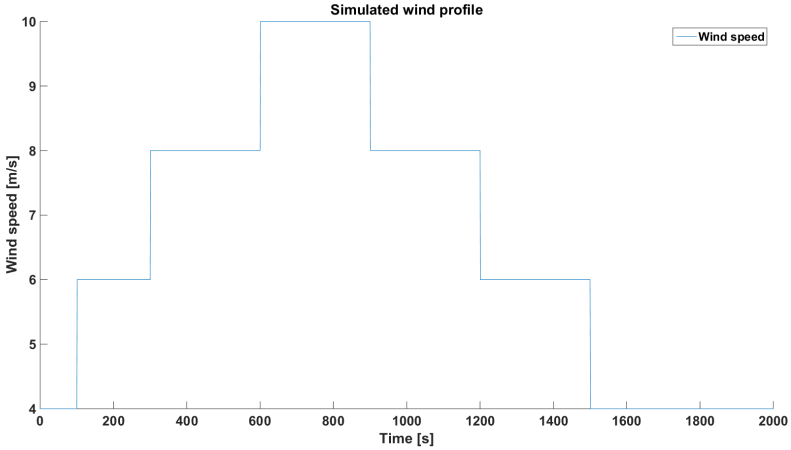

Figure 7.18: Constructed wind profile used for evaluating aerodynamic rotor dynamics.

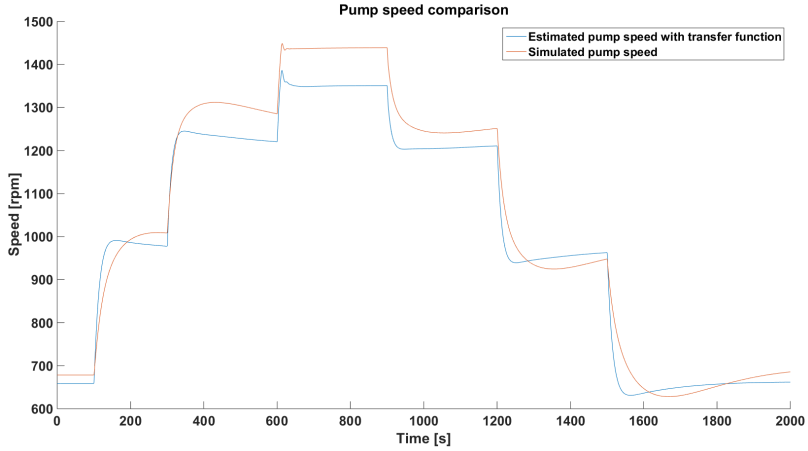

Figure 7.19: Simulated pump speed versus calculated pump speed from the linearized transfer function for the constructed wind profile.

The Bode diagram for the filter, Equation 6.13, is presented in Figure 7.20.

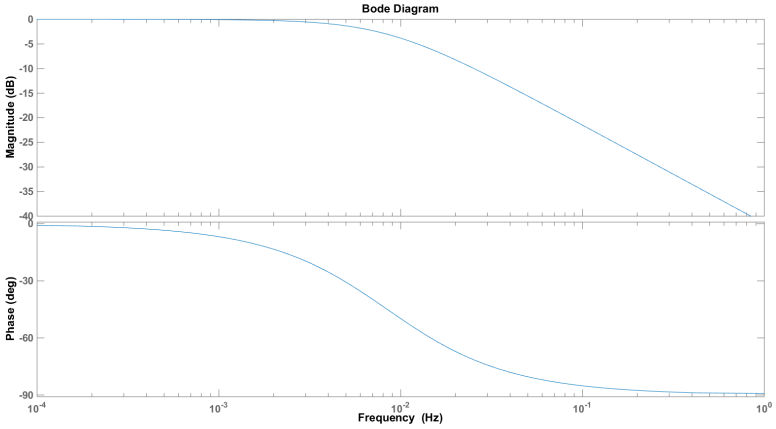

Figure 7.20: Bode diagram, for the derived first order low pass filter, showing how wind and pressure oscillations have a low pass filtered effect on the pump speed.

Studying the bode plot gives a break frequency of 0.0084 Hz which means that changes in wind speed and pressure faster than this frequency will be damped by more than half its amplitude when affecting the pump speed. The corresponding step response of the filter is presented in Figure 7.21.

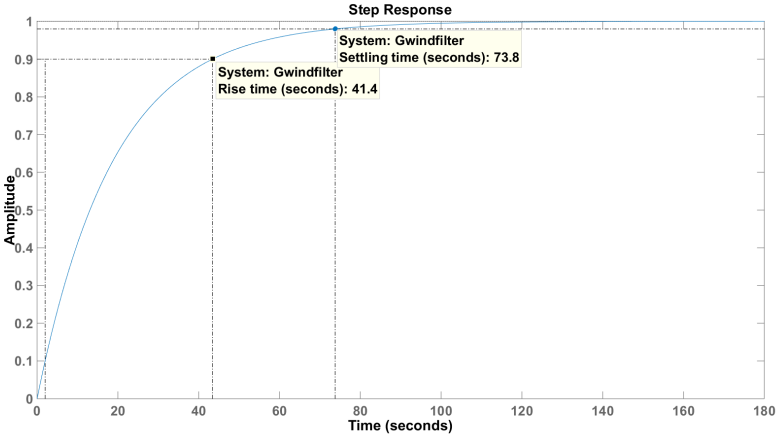

Figure 7.21: Step response of the derived filter showing rise time and settling time.

The step response shows a rise time of 41.4 seconds and a settling time of 73.8 seconds and gives an idea of how slow the rotor dynamics are.

Chapter 8

Discussion and conclusions

8.1 Methodology discussion

8.1.1 Selecting system components

Sizing the main components of the system by assuming efficiencies and deciding what power output the system should have, worked very good as an initial estimation. It served as a good base when determining components at the meeting with Parker. The estimation have also shown to give relatively good idea about the system quantities such as speeds, flows, torque and pressures.

A very important parameter that defines the system quantities is the number of poles for the synchronous generator. For the test platform one with four poles was chosen, setting the synchronous speed of 1800 rpm. If a two pole would have been chosen, the speed would have been 3600 rpm resulting in half the displacement of the motor for maintaining 200 bar nominal pressure. If a six pole or eight pole generator would have been chosen the motor speed would have been lower and thus, if the same motor would be used, the flow would be lower. This would imply higher system pressure to have the same output power but it would also enable either a smaller displacement or lower speed of the pump. When sizing the systems for higher power a smaller pump displacement could be more cost effective. The combination of having the ability to choose nominal speed of the motor by choosing poles of the generator and choosing nominal speed of the pump by using different gear ratios, leaves a great freedom for designing the system to have good balance between performance and cost.

The charge system was sized to compensate for the external volumetric losses. This will give an oversized charge system since all volumetric losses were modeled as external losses but also since the actual volumetric efficiencies of both the pump and the motor were higher than the estimated 95%. Considering rule of thumbs for charge system sizing it is recommended to have a flow capacity of 10% the maximum flow in the HST which would imply a flow of approximately 10 $liters/min$ for the system. And since the charge system is sized for 7.23 $liters/min$ it is not very far from this recommendation. For the test platform it is considered to be good having a little bit oversized system since it gives room for errors and will ensure that cavitation at the pump is avoided. Measurements can be done and suggestions for how to dimension the charge system to be more efficient can be made. Another option is to have a control of the electrical motor powering the charge pump. This could be made in a way to so that the overall efficiency of the drivetrain is improved.

When selecting the PRV for the charge circuit only the pressure setting range of the valve was considered. When a valve with the optional low pressure setting of 5 bar and that also could handle all charge pump flow was found, it was selected. Later when running the simulations and implementing the flow dependent pressure drop of the valves, it was seen that the pressure of the low pressure side was changing a lot depending on flow through the PRV. And because of the high efficiencies of the machines which gives a lower external leakage flow then initially estimated, the flow through the PRV is normally high. This gives an undesirable high pressure in the low pressure side of the HST.

A big change that was made to the system when adapting it to commercially available products from Parker was that a gearbox was added. This was initially seen as a big loss since not using a gearbox was one of the great advantages with the concept. Because it is one of the common components that cause downtime in wind turbines. Also that it will probably add some weigh since adding a gearbox should be heavier than increasing the displacement of the pump. But the advantages was shown to be many. It enabled to chose a standard pump that is very cost effective. The gear ratio enables a better speed range for the pump in terms of efficiency. Another benefit is that the mechanical break, needed for safety and locking the rotor when at low wind speeds, could be installed after the gearbox on the high speed shaft. This means that it would not have to generate such a high breaking torque as if it would be installed before the gearbox [68]. The low bulk modulus of the hydraulic system especially with an accumulator installed also reduce shock loading in the gearbox which increases the lifetime [39].

The decision finally fell on a system pressure of 200 bar. Initially the idea was to use 300 bar, since this would have enabled a smaller pump displacement for the same output power and it was also considered that most piston pumps and motors had higher efficiencies around this pressure. What limited the pressure was that the maximum pressure of the accumulators were 250 bar and that it was desired to keep the output power of the system as close as possible to the initial design of 20 kW. Considering the hydraulic machines chosen for the test platform, this was not a problem since their efficiencies does not change much between 200 and 300 bar. Another point of view is that if other accumulators and generator would be chosen it is possible to increase the rated power of the system by 50% just by allowing a higher maximum system pressure of 300 bar.

One interesting concept that was discussed during the project is to change to a open circuit HST where the reservoir must be placed in the nacelle. This would give some great benefits, the whole charging circuit could be removed giving lower overall losses, fewer components which reduce system complexity and it would ensure to always have pressure at the inlet of the pump. The negative part would be the addition of weight in the nacelle. The rule of thumb for sizing a reservoir for a HST is to have 3 times the mean flow rate of the pump [69]. For the test platform this means a reservoir size around 300 liters. This is for a 28 kW system, so if the power would increase to for example 280 kW having 200 bar maximum pressure, the reservoir would be about 10 times bigger. 3000 liters would mean roughly 3 tons of extra weight in the nacelle. But there exists methods for reducing the reservoir size up to 90% [70] and then the solution starts to get interesting again. This is nothing that has been researched about in this work but it could be an interesting concept to investigate for medium sized wind turbines.

8.1.2 Modeling the test platform

As always when modelling large complex systems, simplifications are necessary. When modelling the system in AMESim the intention has been to set every parameter to a reasonable value. But there is always room for improvements and there are a few changes that need to be made to have a good correlation with the

test platform.

One important thing that could not be set to the correct parameters are the hydraulic lines of the test platform, simply because they were not yet specified. When the CAD model of the platform is ready and all types and lengths of the hydraulic lines has been decided, they should be modeled to give a better estimation of pressure losses and dynamics in the model.

Another thing that can improve the model is to include the flow rate dependent pressure drop through the valve bodies. This would give a slightly higher pressure on the low pressure side because of the flow through the charge circuit pressure relief valve. Modeling these pressure drops is not considered to influence the results significantly.

The viscous friction losses in the aerodynamic rotor and gearbox is implemented to be one percent of the maximum torque. This is a very harsh estimation and more accurate data could be an improvement.

The information about that the motor had hydraulic proportional control did not come to knowledge in time to change this in the AMESim model. This type of control may have slightly different dynamics. Therefore these dynamics should be implemented in the model to make sure that the derived control strategies still works properly.

The efficiency models for the machines corresponds well for the pump but equally good for the motor. Since the available data of the pump is quite coarse, the model is sufficient for representing the pump efficiencies. The motor on the other hand, where more detailed data was obtained from the manufacturer, a lookup table or a more advanced model might be more suitable especially for the mechanical efficiency. Because this is where the model deviates most. But if only the operating range for the motor is regarded, which is 1800 rpm $\pm 1\%$, a pressure of 30 to 250 bar and displacement setting of 0.5 to 1.0 the model give a mechanical efficiency for the motor that deviates less than 1% from the given data, which is acceptable.

8.2 Result discussion

All in all, the selected components for the test platform is considered to be a good combination, that will be operating close to their optimal efficiencies when the system is running at nominal power.

8.2.1 Control strategy performance

The $K\omega^2$ control strategy gives, compared to the other strategies, a quite fast TSR tracking and are at the same time good at keeping the generator frequency close to 60 Hz. The $DTSRT$ on the other hand has a quite slow TSR tracking and gives large peaks and oscillations of the generator frequency. This strategy was on the forehand believed to give faster TSR tracking with the cost of some more oscillating generator frequency than the $K\omega^2$. This is since it actually controls directly on the TSR error and in that way is able to correspond directly to wind

speed change. But the results shows that this is not the case.

One reason for this is caused by what system quantity they use for control and the fact that the generator is coupled to an infinity bus. The infinity bus will prevent changes in frequency of the generator by increasing the torque. Since it is infinitely strong it can in theory apply any torque.

Why this matters so much is best described by what happens with the system during a change in wind speed. If the wind speed increases the control error for the $DTSRT$ will immediately increase due to lowered TSR. The P-part of the controller will then directly increase the displacement setting proportionally to the new control error, and increased displacement means lower system pressure. At he same time, when the wind speed increases, the torque from the wind will increase a lot since it is proportional to the wind speed in cubic. The torque will start to accelerate the rotor and thereby accelerate the pump. Since the pressure was reduced at the same time by increasing the displacement, the acceleration will be even bigger due to lower opposing torque from the pump.

When the pump speed increases the flow will increase and if the displacement setting of the motor is not adjusted accordingly this will increase the pressure and accelerate the generator. The generator will react on the change of speed by increasing its torque and thereby the pressure will increase even more.

Since the $DTSRT$ strategy do not have any pressure feedback it is "unaware" of the rising pressure and is not able compensate for it. The high pressure will start breaking the rotor which gives a lowered flow, that in turn reduces the pressure again. But it will be reduced to much, leading to the opposite behavior from the generator. This counteracting between the aerodynamic rotor and the generator will lead to low frequent oscillations which can be seen in the pressure, rotor speed and frequency.

The reason that the $K\omega^2$ can reduce/remove these oscillations is because it is regulating with respect to pressure. If the pressure increases it will adjust the displacement setting to counteract it. This way of controlling the system leads to that the displacement setting is adjusted accordingly when the rotor speed, hence the flow, increase or decrease. If the dynamics of the displacement control would be a lot slower then what was modeled the $K\omega^2$ strategy would not be able to suppress the oscillations fast enough which leads to a similar result as for the $DTSRT$.

One suggestion that could make the $DTSRT$ strategy better would be to add a derivative pressure feedback. This should reduce the oscillations as it does for the $K\omega^2$. It also gives a possibility to adjust how important TSR is versus keeping a stable pressure.

The safety controller in the $K\omega^2$ control strategy that prevent the rotational rotor speed to go above its rated speed does not consider the pressure it only considers the rotational speed like the $DTSRT$. It therefore acts like the $DTSRT$ and thus shows the same oscillating behavior. Therefore it would be good to derive the already present pressure feedback signal to help reduce the oscillations for the safety controller.

The two control strategies based on the $K\omega^2$ got an offset from the optimal

TSR at steady state. This comes from the fact that its control signal is the pressure on the high pressure side close to the motor and not the pressure difference over the pump. The reason for why it deviates more in TSR at low wind speeds is that the pressure on the low pressure side increases due to the characteristics of the charge circuit PRV.

The values used in all four control strategies of the optimal TSR is as mentioned in the Section 2.5 not an exact value since it is derived from a model and measured data of similar blade profiles. So the actual optimal TSR might vary from the one used in the controller. It might also change by time because of for example wear on the blades. A faulty value will lead to reduced power extraction for the wind turbine. It would therefore be good to observe the power output in relation to tip speed ratio and actively adjust the optimal TSR accordingly. This applies for all control strategies with maximum power tracking.

The FF takes into account the slow dynamics of the system but not the dynamics of the generator. That is why only using the FF will slowly get the system to its right position but with some oscillations on the way due to faster dynamics in the FF-links then in the actual system. When adding the FF to the $K\omega^2$ strategy and optimizing the parameters, the P-part gets bigger meanwhile the I-part gets a lot smaller. The later is caused by the effect of the static TSR error that $K\omega^2$ introduce, as just discussed, and because the FF itself controls the TSR closer to its optimal value.

The reason that a FF does not make the strategies $K\omega^2$ and $DTSR$ that much better for the real wind profile as for the step wind profile is probably because of it together with the generator and grid have slow dynamics and the fast changes of wind speed in the real profile.

If the wind has a profile similar to the one used here the conclusion is that adding the FF to the system might not give anything more than increased complexity to the control system. But if model prediction of the wind was added to the FF model it might give a better result. Adding the dynamics of the generator to the FF model will also give some improvement.

The $DTSRT$ was tested with three different controllers. The results shows that first tuning a PI- controller and then adding a D-part afterwards only made the controller worse for this system, so it is not considered to be a good approach. Comparing the results from using a PI-controller or a PID-controller shows similar results. One thing to consider is that there is no noise modeled on the measured signals. With noise on the signal, which will be the case on a real system, the D-part will let some of it through even though much of the noise is suppressed by the filter on the D-part. This will reduce the performance of the PID-controller. With this in mind the conclusion is that it is better to not use a D-part and only use a PI-controller. The control system will then have a bit less complexity and fewer parameters to tune but with basically the same performance.

The output power at nominal speed is 28.9 kW which is a bit higher than the nominal power which the system was sized for. This relates to the fact that the efficiency of the motor is a bit higher than the one used for the dimensioning of the system, with a total efficiency of 94.3% instead of 90%. The total efficiency of the pump is also higher than the 90% that was assumed during dimensioning, but

just a little with its 90.6%. This is why the model delivers more power.

The results in this study are dependent on the generator and grid connection model which were taken from the previous study made by Flesch [2]. If this model turns out to not be that accurate many of the result presented in this study might also be inaccurate and wrong. Therefore verifications that the generator and grid connection model is accurate has to be conducted when the test platform is built.

Studying on the results from all the four control strategies they show good overall characteristics in frequency of the delivered electrical energy. Keeping the error from 60 Hz in within 1% (0.6 Hz) all the time. Which is well inside the limits for a power source in the power range of mid-sized wind turbines according to the Swedish regulations. They state that the frequency should be kept within 2% most of the time [71]. Therefore the results makes the concept look promising to be able to replace the need of a frequency converter.

The results showed that the drivetrain had a poor efficiency of only 60% at 4 m/s. But here only 1 kW is produced so the loss in kW of extracted power is not so large. The results also show that already at 6 m/s, the efficiency have increased a lot and reaches 80%. In this region the available energy in the wind is still quite low and the extracted power is 5 kW. The more the wind speed increases the more the efficiency increases so at 8 m/s and an extracted power of 15 kW the efficiency is almost 85%. Finally at nominal wind speed of 10 m/s and an extracted power of 28.9 kW the efficiency reaches its maximum of 86% which can be regarded as a good value. So an HST drivetrain have regions of poor efficiency but these are at low wind speeds where the available power in the wind is also very low. For the regions with a lot of available power where every percentage of increased efficiency will give a lot more produced energy, the HST drivetrain have a high efficiency.

8.2.2 System dynamics

It is important to have in mind that the resulting frequencies only gives a hint of frequency range for the test platform. When all hydraulic lines, type of hydraulic fluid and other parameters that affects the result are specified, a new frequency analysis is needed to be able to compare model and real system.

Considering the derived transfer function for the rotor dynamics as a low pass filter, it has a break frequency of 0.0084 Hz. The derived function seem to have faster dynamics than what the AMESim model gives which should imply that the break frequency is even lower than this value. The pump and motor pulsations were in the range of 90-270 Hz. Frequency analysis showed that the significant resonance frequency (natural frequency) for the transmission line, with a high pressure accumulator connected, will be somewhere in the range of 1-10 Hz. This means that the frequencies are well separated and the risk of noise emissions from these components in the system are reduced. The line without high pressure accumulator had higher resonance frequencies in the range of 20-160 Hz. This is well within the range of the pump pulsations, but the natural frequency, which have the highest amplification, is around 20 Hz. Considering this the noise emissions should not be significant without an accumulator either. But some higher resonance frequencies will match a couple of different pump speeds, thus the system

without an accumulator should have more noise emissions from pump pulsations than the system with accumulator.

The wave propagation delay time in the high pressure line calculated to 0.011 seconds for the system without accumulator and 0.078 seconds for the system with accumulator. This is nothing that is significant for the system dynamics since the dynamics that the rotor inertia introduce to the system is of much slower characteristics. Though, what it may affect is the stability of the closed loop system. The time delays in a system should be considered when designing a controller and choosing proper sampling time [54].

What sets the main characteristics of the system is the aerodynamic rotor that with its big inertia low pass filters the wind and makes the dynamics of the whole system slow. A unit step in wind gives a rise time of 41.2 seconds for the derived transfer function of rotor dynamics. This gives an idea of why the system is acting the way it does and why it is hard to have a fast TSR tracking. But that the system is slow does not necessarily mean that it is a disadvantage. It is unfavorable in one way, since it is not possible to ideally follow the wind speed and get the maximum power output. But it is the slow dynamics that enables to have a stable speed of the motor and thus a stable frequency output from the generator.

As explained in Section 4.2.5, the dynamics of the hydraulic proportional control of the motor was not modeled. The dynamic difference that it will cause, probably a bit slower response time, is not believed to make any significant difference to the system. But before testing the derived controllers on the test platform it is recommended that the motor control dynamics are evaluated in the AMESim model.

8.3 Conclusions

This study has shown promising results towards the conclusion that a wind turbine using a HST can deliver electric energy well within the electric grid standard without the need of a power converter. However this has to be validated on the test bench.

The choosing and sizing of components and results from the model of them shows that it is possible to realize a drivetrain using existing standard hydraulic components for a wind turbine with nominal power of 28 kW. Reaching a nominal power of 100 kW with existing standard components should not be a problem either but to reach 1 MW in nominal power there might be some challenges regarding the huge displacement of the pump or pumps, due to limited product range.

The model shows that the HST have a good overall efficiency, between 80 - 86%, for most of its working range. The only part where it has a low efficiency is at low wind speeds. This should however not give a significant impact on the total energy production over time, since in the low speed region the available power in the wind is really low.

Studying the different line models in AMESim have given a good idea of how this system should be modeled to study the influence of wave propagation. The line

model that is recommended to be used is the $CFD\ 1D\ Lax - Wendroff$ model which gave the best result to simulation time ratio. An effective bulk modulus should be calculated which considers fluid, entrapped air, accumulator and wall compliance. The relative roughness of the pipes and hoses should be put into the model to have a good estimation of pressure losses. Number of states in the CFD model for frequency dependent friction should be decided upon weighting simulation time versus accuracy.

To control a wind turbine using a HST in a good way the control strategy has to consider the slow dynamics the big inertia of the rotor gives the system. It also has to consider the fact that the generator is directly coupled to the grid so it needs something to counteract the torque changes and oscillations this gives together with the rotor. Therefore a pressure feedback should be used to get a good performance.

For a mid-size wind turbine using a HST it should be possible to reduce the weight in the nacelle and obtain easier maintenance by placing most of the drive-train components on the ground. Simulations results shows that the losses in the hydraulic lines are quite small and the dynamic analysis shown that the lines are not long enough to give controllability problems since the dynamics of the turbine is so slow.

Considering if the concept is suitable to become a commercial product, it can be concluded that the studied areas made in this thesis work, have shown promising results. The hydrostatic transmission is able to replace a frequency converter, it can be built from existing standard hydraulic components and it has a good overall efficiency at nominal power.

8.4 Proposal for future studies

- When all parameters of the hydraulic lines are set for the test platform, implement them in the AMESim model and perform a new dynamic analyze with the proposed method.
- Model the proportional hydraulic control dynamics of the motor and evaluate the derived controllers.
- Find the best way to simulate the rotor inertia so that the torque on the pump shaft has a corresponding dynamic behavior.
- Evaluate the AMESim model and adjust its parameters from measurements on the test platform.
- Investigate how synchronization of generator and grid will be performed, both on the test platform and in a real wind turbine.
- Investigate the open loop HST concept discussed in Section 8.1.2.
- The cost of the drivetrain should be evaluated and compared to other concepts.

- Evaluate system performance in control region 3. Possibly by implementing pitch control in the AMESim model.
- Perform a lifetime analyze of the drivetrain.

Another interesting idea that can be implemented in a control strategy is to, when at low wind speeds, allow for increased rotational velocity of the pump by lowering the pressure. This will give a higher flow and thus a higher displacement setting of the motor which increases its efficiency. A point can be found where it is more efficient to have a slightly worse C_p and thus a lower power input from the rotor but higher efficiency of the HST and thus a higher overall efficiency generating a higher power output. This can be especially interesting for wind turbine design with two blade design since their C_p versus λ curve, see Figure 2.19, is a little bit more flat and a change in tip speed ratio does not affect the C_p value that much.

Bibliography

[1] Hydraulic Pump Devision. *Hydraulic Pump Devision, Product Range*. Parker Hannifin Corporation, Marysville, OH, USA, hy28-2673-01/hpd/us edition, 2012.

[2] Eduardo Augusto Flesch. Hydrostatic transmission project for horizontal axis wind turbines. master thesis, Federal Univeristy of Santa Catarina, UFSC, November 2012.

[3] Hydraulic Cartridge Systems Devision. *Hydraulic Cartridge Systems, Threaded Cartridge Valves and Integrated Hydraulic Products*. Parker Hannifin Corporation, Lincolnshire, IL, USA, hy15-3502/us edition, September 2010.

[4] Accumulator and Cooler Division. *Oil Coolers For Temperature Optimization In Hydraulic Systems*. Parker Hannifin Corporation, Rockford, IL, USA, hy10-1700/americas edition, 2013.

[5] History of wind energy, u.s department of energy. `http://energy.gov/eere/wind/history-wind-energy`, 2015.

[6] Installed wind power capacity is expected to grow 62% in 2015. `http://www.portalabeeolica.org.br/index.php/noticias/3134-capacidade-instalada-de-energia-e%C3%B3lica-deve-crescer-62-em-2015.html`, March 2015.

[7] Associaçã Brasileira de Energia Eólica. Boletim de dados mar.2015. `http://www.abeeolica.org.br/pdf/Boletim-de-Dados-ABEEolica-Marco-2015-%20Publico.pdf`, March 2015.

[8] Wind energy scenarios for 2020. `http://www.ewea.org/fileadmin/files/library/publications/reports/EWEA-Wind-energy-scenarios-2020.pdf`, July 2014.

[9] Wind in power 2014 european statistics. `http://www.ewea.org/fileadmin/files/library/publications/statistics/EWEA-Annual-Statistics-2014.pdf`, February 2015.

[10] Offshore wind research and development, u.s department of energy. http://energy.gov/eere/wind/offshore-wind-research-and-development.

[11] Vestas Wind Systems. Vestas and mitsubishi heavy industries form a joint venture dedicated to offshore wind energy, company announcement no. 41/2013. http://vestas.com/en/media/~/media/c25bb62b1a6d4d0d8a8873a36597fb46.ashx, September 2013.

[12] David Weston. Mitsubishi drops seaangel brand name. http://www.windpoweroffshore.com/article/1332901/mitsubishi-drops-seaangel-brand-name, February 2015.

[13] Hydraulics and Pneumatics. Hydrostatic transmissions. http://hydraulicspneumatics.com/200/TechZone/HydraulicPumpsM/Article/False/6450/TechZone-HydraulicPumpsM, January 2012.

[14] Institutionen för konstruktions & produktionsteknik. *Formelsamling i Hydraulik och pneumatik*. Linköpings Tekniska Högskola, 1995.

[15] Karl-Erik Rydberg. Efficiencies for variable hydraulic pumps and motors-mathematical models and operation conditions. Technical report, IEI/FluMeS, 2009.

[16] C.R. Burrows and K.A. Edge. *Power Transmission and Motion Control: PTMC 2002*. John Wiley & Sons, 2002.

[17] Andreas Johansson. *Design Principles for Noise Reduction in Hydraulic Piston Pumps*. PhD thesis, Linköpings universitet, 2005.

[18] Liselott Ericson. *On Fluid Power Pump and Motor Design - Tools for Noise Reduction*. PhD thesis, Linköpings universitet, 2011.

[19] Bonnie Trowbridge. Accumulators increase efficiency and provide smooth operation in hydraulic systems. http://hydraulicspneumatics.com/200/TechZone/Accumulators/Article/False/87472/TechZone-Accumulators, June 2011.

[20] Josh Cosford. Accumulators add functionality to hydraulic circuits. http://hydraulicspneumatics.com/accumulators/accumulators-add-functionality-hydraulic-circuits, February 2014.

[21] A. Parr. *Hydraulics and Pneumatics*. Elsevier Science, 1999.

[22] F. Yeaple. *Fluid Power Design Handbook, Second Edition*. Fluid Power and Control. Marcel Dekker, Inc, 1990.

[23] R.C. Dorf. *The Electrical Engineering Handbook,Second Edition*. Electrical Engineering Handbook. Taylor & Francis, 1997.

[24] A. E. Fitzgerald, Charles Kingsley, and Stephen D. Umans. *Electric machinery*. McGraw-Hill, Boston, Mass., 6th edition, 2003.

[25] W. Shepherd and L. Zhang. *Electricity Generation Using Wind Power*. World Scientific Publishing Company, 2011.

[26] G. Klempner and I. Kerszenbaum. *Operation and Maintenance of Large Turbo-Generators*. IEEE Press Series on Power Engineering. Wiley, 2004.

[27] E. Hau. *Wind Turbines: Fundamentals, Technologies, Application, Economics*. Springer, 2006.

[28] Danfoss. *Facts Worth Knowing about Frequency Converters*. Danfoss, 2014.

[29] Tsuneo Kume Mahesh M. Swamy and Noriyuki Takada. Evaluation of an alternate soft-charge circuit for diode front-end variable-frequency drives. *IEEE Transactions on industry applications*, 46(5):1999 – 2007, 2010.

[30] Variable-frequency drive. `http://en.wikipedia.org/wiki/Variable-frequency_drive`, December 2014.

[31] Power Electronics A to Z. Comparison of inverters: Vsi vs csi. `http://www.completepowerelectronics.com/vsi-vs-csi-comparison-inverters/`, January 2014.

[32] T. Burton, N. Jenkins, D. Sharpe, and E. Bossanyi. *Wind Energy Handbook*. Wiley, 2011.

[33] T. Ackermann. *Wind Power in Power Systems*. Wiley, 2005.

[34] Emrah Kulunk. Aerodynamics of wind turbines, fundamental and advanced topics in wind power, dr.rupp carriveau (ed.). `http://www.intechopen.com/books/fundamental-and-advanced-topics-in-wind-power/aerodynamics-of-windturbines`, June 2011.

[35] M.H. Ali. *Wind Energy Systems: Solutions for Power Quality and Stabilization*. Electrical engineering. Taylor & Francis, 2012.

[36] Feng Wang and Kim A. Stelson. Model predictive control for power optimization in a hydrostatic wind turbine. In *Proceedings of The 13th Scandinavian International Conference on Fluid Power, Linköping, Sweden*, pages 155–160, June 2013.

[37] K.E. Johnson, Lucy Y. Pao, M.J. Balas, and L.J. Fingersh. Control of variable-speed wind turbines: standard and adaptive techniques for maximizing energy capture. *Control Systems, IEEE*, 26(3):70–81, June 2006.

[38] Johannes Schmitz, Nils Vatheuer, and Hubertus Murrenhoff. Hydrostatic drive train in wind energy plants. In *Proceedings of 52nd National Conference on Fluid Power, Las Vegas, NV*, pages 1017–1022, 2011.

[39] Brenen Thul, Rahul Dutta, and Kim A Stelson. Hydrostatic transmission for mid-size wind turbines. In *Proceedings of 52nd National Conference on Fluid Power, Las Vegas, NV*, pages 443–458, 2011.

[40] Martin Foster. Worlds largest floating wind turbine installed at fukushima. `http://www.windpoweroffshore.com/article/1358221/worlds-largest-floating-turbine-installed-fukushima`, July 2015.

[41] offshoreWIND staff. Exclusive: Mhi denies ditching seaangel. `http://www.offshorewind.biz/2015/02/19/exclusive-mhi-denies-ditching-seaangel/`, February 2015.

[42] Win Rampen et al. Gearless transmissions of large wind turbines-the history and future of hydraulic drives. *Artemis IP Ltd., Midlothian, UK*, 2006.

[43] Parker Hannifin Manufacturing Sweden AB. *Installation and start-up information Hydraulic Motors Series V12, V14 and T12*. Pump and Motor Division, Trollhättan, Sweden, hy30-8223-inst/eu edition, March 2014.

[44] Hydraulic Pump Devision. *P1/PD Series Medium Pressure Axial Piston Pumps*. Parker Hannifin Corporation, Lincolnshire, IL, USA, hy28-2665-01/p1/uk edition, January 2014.

[45] REIVAX Automation and Control. *SNX100 User's manual*. Reivax, Rodovia Jose Carlos Daux, Florianopolis, SC, pr-02-02-02-02-rev 008.i01 edition, 2014.

[46] Charles R Cornell. Dynamic simulation of a hydrostatically propelled vehicle. Technical report, SAE Technical Paper, 1981.

[47] Absolute roughness of pipe material. `https://neutrium.net/fluid_flow/absolute-roughness/`, May 19 2012.

[48] R.C. Binder. *Fluid Mechanics*, volume 3rd Edition. Prentice-Hall, Inc, Englewood Cliffs, NJ, 1956.

[49] Hose Products Division. *Hose, Fittings and Equipment*. Parker Hannifin Corporation, Wickliffe, OH, USA, catalog 4400 edition, February 2015.

[50] S.M. Muyeen, J. Tamura, and T. Murata. *Stability Augmentation of a Grid-connected Wind Farm*. Green Energy and Technology. Springer London, 2008.

[51] Angel Gaspar Gonzalez Rodriguez. Improvement of a fixed-speed wind turbine soft-starter based on a sliding-mode controller. doctoral thesis, University of Seville, Department of Electrical Engineering, March 2006.

[52] Anders Grauers. Efficiency of three energy wind energy generator systems. *IEEE Transactions on Energy Conversion*, 11(3):650–657, September 1996.

[53] D.I Guta N. Vasiliu G.C Vasiliu, D. Vasiliu. Tuning the electro-hydraulic servomotors by numerical simulation. *UPB Scientific Bulletin*, 74(3):229–240, 2012.

[54] S.Gunnarsson P.Lindskog L.Ljung J.Löfberg T.McKelvey A.Stenman J-E.Strömberg M.Engqvist, T.Glad. *Industriell reglerteknik Kurskompendium*. ISY, Linköping universitet, 2014.

[55] A. Jarquin Laguna N.F.B. Diepeveen. Dynamic modeling of fluid power transmissions for wind turbines. In *EWEA OFFSHORE 2011*. Offshore Wind Group, TU Delft, Netherlands, 2011.

[56] Finding the elastic constants g and k. `http://www.efunda.com/formulae/solid_mechanics/mat_mechanics/elastic_constants_g_k.cfm`, 2015.

[57] David Beasley. An overview of genetic algorithms: Part 1. fundamentals. *University computing*, 15(2):58–69, 1993.

[58] David Beasley, David R Bull, Ralph R Martin, et al. An overview of genetic algorithms: Part 2, research topics. *University computing*, 15(4):170–181, 1993.

[59] Karl J Astrom and T Hägglund. Pid controllers: Theory, design and tuning. *Research Triangle Park: 2nd Ed. Instrumentation, Systems and Automatic Society*, 1995.

[60] Introduction: Frequency domain methods for controller design. `http://ctms.engin.umich.edu/CTMS/index.php?example=Introduction&section=ControlFrequency`, March 2007.

[61] Nigel Johnston. The transmission line method for modelling laminar flow of liquid in pipelines. *IMechE, Part I: J Systems and Control Engineering*, (226(5):):586–597, 2012.

[62] Product documentation: segmented pipeline. `http://www.mathworks.com/help/physmod/hydro/ref/segmentedpipeline.html`, 2015.

[63] Lms imagine, contents of the hydraulic lines library: Hlg0020d-hydraulic line cfd 1d lax-wendroff (c-ir-***-c-ir), 2013.

[64] D K Longmore D N Johnston K Sanada, C W Richards. A finite element model of hydraulic pipelines using an iptimized interlacing grid system. *Part 1: Journal of Systems and Control Engineering*, pages –222, IMechE 1993.

[65] Standing sound waves (longitudinal standing waves). `http://www.acs.psu.edu/drussell/Demos/StandingWaves/StandingWaves.html`, May 2012.

[66] G.K. Costa and N. Sepehri. *Hydrostatic Transmissions and Actuators: Operation, Modelling and Applications*. Wiley, 2015.

[67] Earth Observing Laboratory. One second dataset. `https://www.eol.ucar.edu/field_projects/pcaps/one-second-dataset`, 2011.

[68] Brakes 101. `http://www.windpowerengineering.com/design/mechanical/brakes/brakes-101/`, January 2012.

[69] Hydraulics and Pneumatics. Fundamentals of hydraulic reservoirs. http://hydraulicspneumatics.com/200/TechZone/ReservoirsAcces/Article/False/6448/TechZone-ReservoirsAcces, Jan 2012.

[70] PMC Group. Pmc cyklontank. http://www.pmcgroup.se/Global/Subsidiaries/PMC-Hydraulics/Documents/cyklontank_pmc_hydraulics_swe.pdf?epslanguage=sv, 2012.

[71] Gojart Neziri and Hans Svensson. Teknisk utredning för anslutning av vindkraftverk till elektriskt nät. 2009.

Appendix A

Model parameters

A.1 Hydraulic components

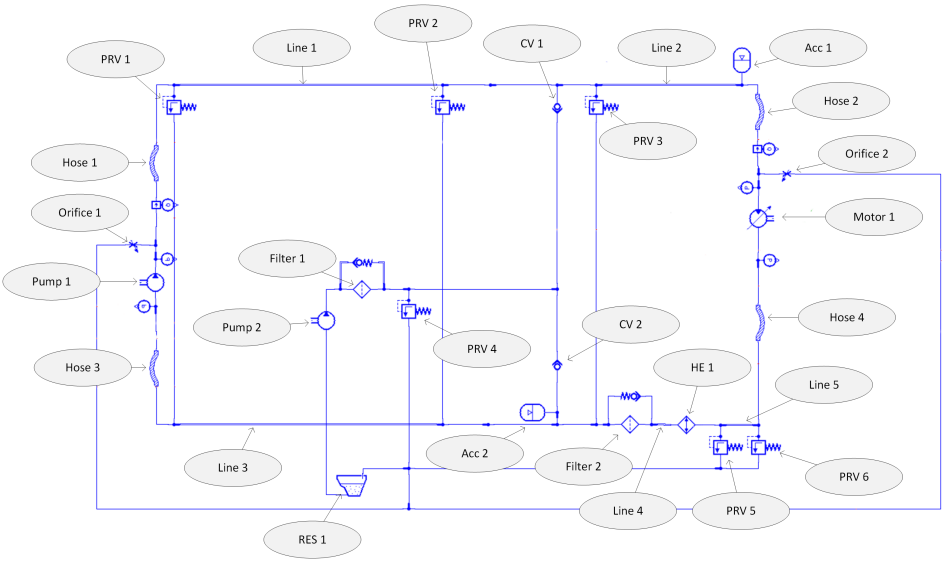

Figure A.1: Indexing for Table A.1 of hydraulic components in the AMESim model.

Table A.1: Parameters and submodels used in the AMESim model for the hydraulic components. Index refers to Figure A.1.

Index: — (fluid properties)	**Submodel: FP04**	
Parameter	**Value**	**Unit**
type of fluid properties	elemtary	
index of hydraulic fluid	0	
temperature	40	degC
density	870	kg/m**3
bulk modulus	1500	MPa
absolute viscosity	0.02748	Pas
absolute viscosity of air/gas	0.02	cP
saturation pressure (for dissolved air/gas)	1000	bar
air/gas content	0.1	%
polytropic index for air/gas/vapor content	1.4	

Index: Pump 1	**Submodel: PU001**	
Parameter	**Value**	**Unit**
index of hydraulic fluid	0	
pump displacement	71.7	cc/rev
typical speed of pump	1440	rev/min

Index: Pump 2	**Submodel: PU001**	
Parameter	**Value**	**Unit**
index of hydraulic fluid	0	
pump displacement	8	cc/rev
typical speed of pump	1330	rev/min

Index: Motor 1	**Submodel: MO002**	
Parameter	**Value**	**Unit**
index of hydraulic fluid	0	
pump displacement	60	cc/rev
typical speed of pump	1800	rev/min

Index: Acc 1	**Submodel: HA000**	
Parameter	**Value**	**Unit**
index of hydraulic fluid	0	
isothermal initialization	1	
gas precharge pressure	30	bar
accumulator volume	1.9	L
polytropic index	1.4	
accumulator orifice diameter	19	mm
critical flow number	1000	
flow coefficient for orifice	1	

Index: Acc 2	**Submodel: HA000**	
Parameter	**Value**	**Unit**
index of hydraulic fluid	0	
isothermal initialization	1	
gas precharge pressure	2	bar
accumulator volume	9.47	L
polytropic index	1.4	
accumulator orifice diameter	25	mm
critical flow number	1000	
flow coefficient for orifice	1	

Index: PRV 1, PRV 2, PRV 3	Submodel: RV000	
Parameter	**Value**	**Unit**
index of hydraulic fluid	0	
relief valve cracking pressure	220	bar
relief valve flow rate pressure gradient	3.9478	L/min/bar
valve hysteresis	0	bar
dynamics	no (static)	

Index: PRV 4	Submodel: RV000	
Parameter	**Value**	**Unit**
index of hydraulic fluid	0	
relief valve cracking pressure	2	bar
relief valve flow rate pressure gradient	1.2	L/min/bar
valve hysteresis	0	bar
dynamics	no (static)	

Index: PRV 5, PRV 6	Submodel: RV000	
Parameter	**Value**	**Unit**
index of hydraulic fluid	0	
relief valve cracking pressure	25	bar
relief valve flow rate pressure gradient	3.9478	L/min/bar
valve hysteresis	0	bar
dynamics	no (static)	

Index: CV 1, CV 2	Submodel: CV000	
Parameter	**Value**	**Unit**
index of hydraulic fluid	0	
check valve cracking pressure	0.3	bar
check valve flow rate pressure gradient	20.6364	L/min/bar
hysteresis for opening/closing	0	bar

Index: Orifice 1, Orifice 2	Submodel: VOR000	
Parameter	**Value**	**Unit**
index of hydraulic fluid	0	
parameter set for pressure drop	pressure drop/flow rate	
minimum signal value	0	
maximum signal value	1	
characteristic flow rate at maximum opening	110	L/min
corresponding pressure drop	200	bar
critical flow number (laminar ->turbulent)	1.00E-12	

Index: Filter 1	Submodel: OR0000	
Parameter	**Value**	**Unit**
index of hydraulic fluid	0	
parameter set for pressure drop	pressure drop/flow rate	
characteristic flow rate	7	L/min
corresponding pressure drop	0.7	bar
critical flow number (laminar ->turbulent)	1000	

Index: Filter 2	Submodel: OR0000	
Parameter	**Value**	**Unit**
index of hydraulic fluid	0	
parameter set for pressure drop	pressure drop/flow rate	
characteristic flow rate	200	L/min
corresponding pressure drop	0.7	bar
critical flow number (laminar ->turbulent)	1000	

Index: Res 1	Submodel: TK1	
Parameter	**Value**	**Unit**
index of hydraulic fluid	0	
#height of liquid in tank	0.9	m
tank area	0.25	m**2
minimum height alarm level	0.1	m
maximum height alarm level	1	m

Index: HE 1	Submodel: OR0000	
Parameter	**Value**	**Unit**
index of hydraulic fluid	0	
parameter set for pressure drop	pressure drop/flow rate	
characteristic flow rate	200	L/min
corresponding pressure drop	0.7	bar
critical flow number (laminar ->turbulent)	1000	

Index: Line 1	Submodel: HL001	
Parameter	**Value**	**Unit**
index of hydraulic fluid	0	
diameter of pipe	19	mm
pipe length	8	m
relative roughness	0.0043	
angle line makes with horizontal	-90	degree
evaluation of Bulk modulus	calculated bulk modulus	
wall thickness	3	mm
Young's modulus for material	2.06E+06	bar

Index: Line 2	Submodel: HL000	
Parameter	**Value**	**Unit**
index of hydraulic fluid	0	
bulk modulus calculated=1 user specified=2	1	
diameter of pipe	19	mm
pipe length	0.001	m
wall thickness	3	mm
Young's modulus for material	2.06E+06	bar
user specified effective bulk modulus	8000	bar

Index: Line 3	Submodel: HL001	
Parameter	**Value**	**Unit**
index of hydraulic fluid	0	
diameter of pipe	25	mm
pipe length	8	m
relative roughness	0.0033	
angle line makes with horizontal	90	degree
evaluation of Bulk modulus	calculated bulk modulus	
wall thickness	3	mm
Young's modulus for material	2.06E+06	bar

Index: Line 4, Line 5	Submodel: HL000	
Parameter	**Value**	**Unit**
index of hydraulic fluid	0	
bulk modulus calculated=1 user specified=2	1	
diameter of pipe	25	mm
pipe length	0.001	m
wall thickness	3	mm
Young's modulus for material	2.06E+06	bar
user specified effective bulk modulus	8000	bar

Index: Hose 1, Hose 2	Submodel: HH01	
Parameter	**Value**	**Unit**
index of hydraulic fluid	0	
pipe bulk modulus	calculated bulk modulus	
diameter of pipe	19	mm
pipe length	3	m
relative roughness	0.0097	
angle line makes with horizontal	0	degree
wall thickness	5.2	mm
Young's modulus for material	5250	MPa

Index: Hose 3, Hose 4	Submodel: HH01R	
Parameter	**Value**	**Unit**
index of hydraulic fluid	0	
pipe bulk modulus	calculated bulk modulus	
diameter of pipe	25	mm
pipe length	3	m
relative roughness	0.0097	
angle line makes with horizontal	0	degree
wall thickness	5.2	mm
Young's modulus for material	5250	MPa

A.2 Motor displacement setting dynamics

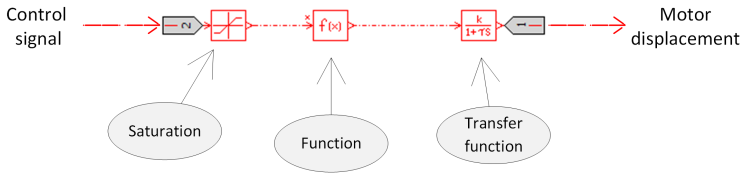

Figure A.2: Motor displacement setting model with indexing of submodels for Table A.2.

Table A.2: The parameters used in the motor displacement setting model.

Index: Saturation	**Submodel: SAT0**	
Parameter	**Value**	**Unit**
minimum permitted value	2	
maximum permitted value	10	

Index: Function	**Submodel: FX00**	
Parameter	**Value**	**Unit**
position/position_max	x/10	

Index: Transfer function	**Submodel: LAG1**	
Parameter	**Value**	**Unit**
time constant	25	ms
value of gain	1	

A.3 Inertia and gearbox

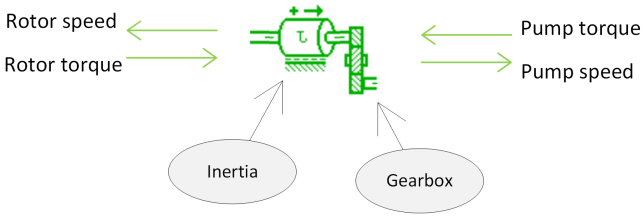

Figure A.3: Inertia and gearbox model in AMESim. For submodel parameters see Table A.3.

Table A.3: Parameters used in the inertia and gearbox submodels.

Index: Inertia	**Submodel: RL01**	
Parameter	**Value**	**Unit**
moment of inertia	8070	kgm**2
coefficient of viscous friction	0.25	Nm/(rev/min)
Coulomb friction torque	0	Nm
stiction torque	0	Nm

Index: Gearbox	**Submodel: RN000**	
Parameter	**Value**	**Unit**
gear ratio	12	

A.4 Electric motor powering the charge pump

A simple constant speed prime mover submodel was used to model the electric motor that will power the charge pump. The submodel used is called $PM000$ and only has one parameter to set, shaft speed. The shaft speed was set to 1130 *rpm* corresponding to a six pole induction motor running at rated power with a slip of 6%.

Appendix B

Control performance simulation results

B.1 Stepping wind profile

This section presents all graphs for the evaluated control strategies when simulating a wind profile with steps of 2 m/s.

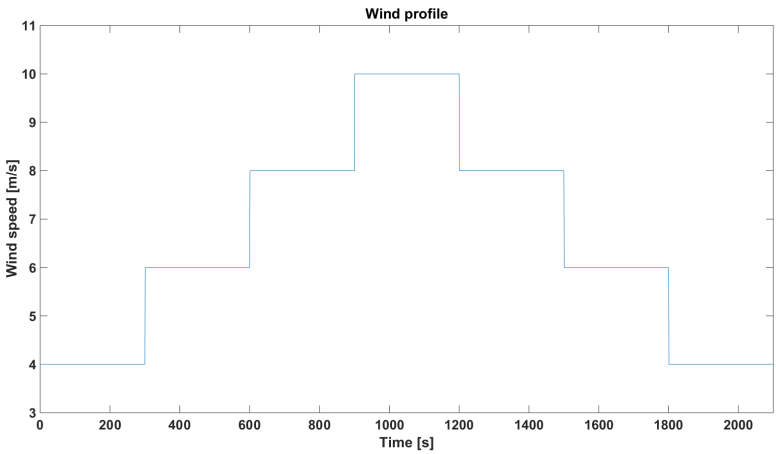

Figure B.1: Wind profile used for comparing control strategies.

B.1.1 Generator frequency

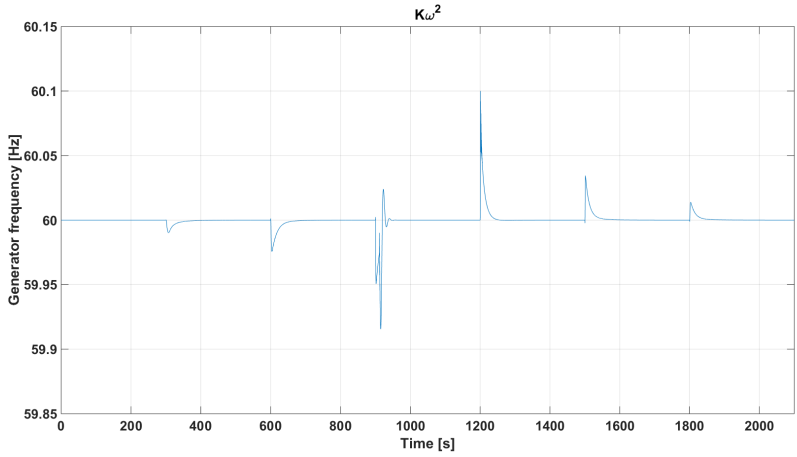

Figure B.2: Generator frequency for the $K\omega^2$ control strategy.

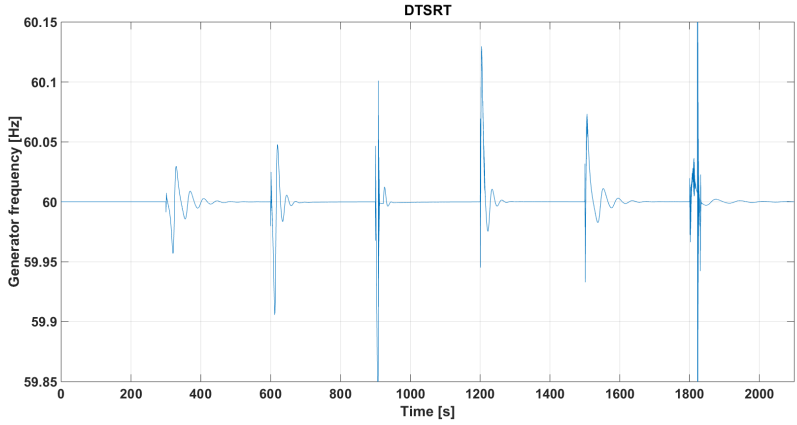

Figure B.3: Generator frequency for the Direct Tip Speed Ratio Tracking (DTSRT) control strategy.

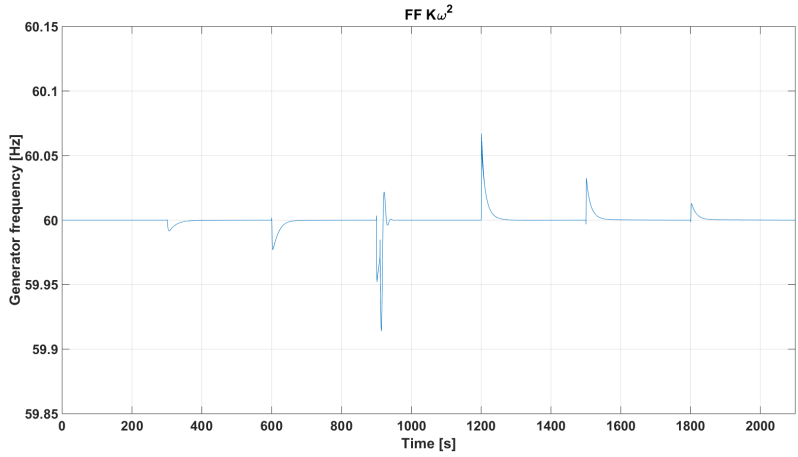

Figure B.4: Generator frequency for the $K\omega^2$ with feedforward control strategy.

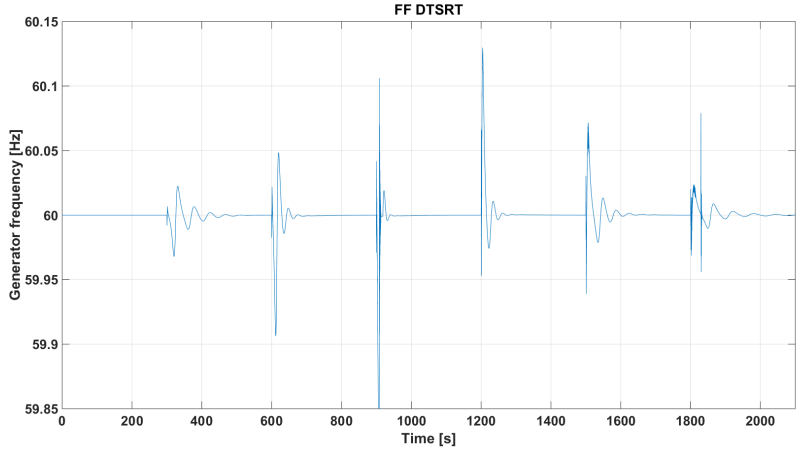

Figure B.5: Generator frequency for the DTSRT with feedforward control strategy.

B.1.2 Motor inlet pressure

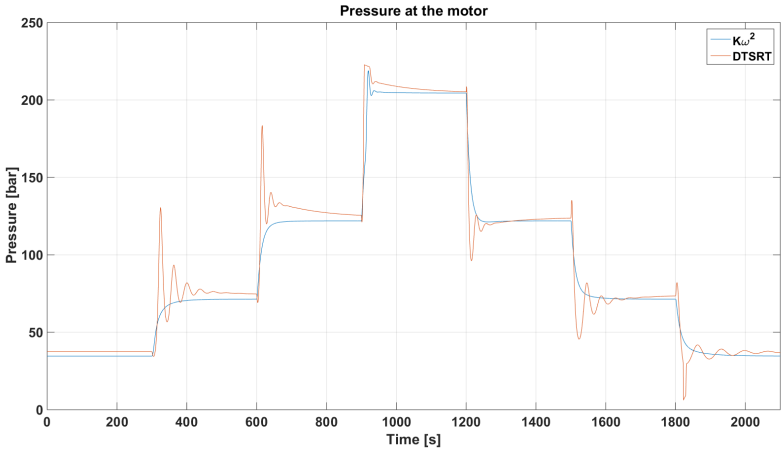

Figure B.6: Motor inlet pressure for the $K\omega^2$ and DTSRT control strategies.

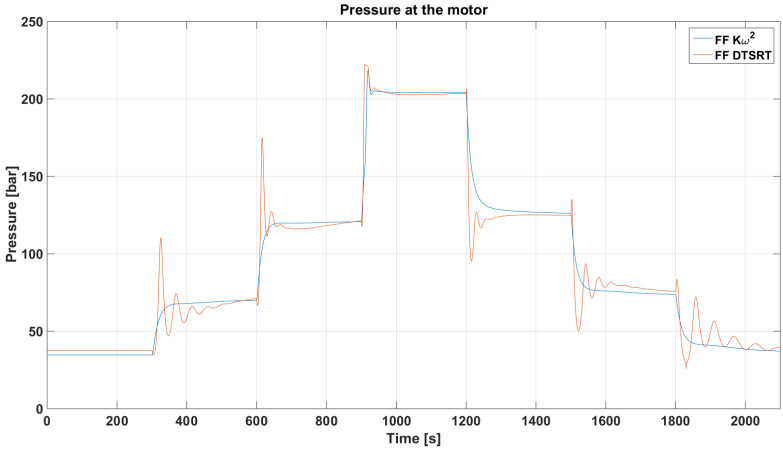

Figure B.7: Motor inlet pressure for the $K\omega^2$ and DTSRT, both with feedforward, control strategies.

B.1.3 Tip speed ratio

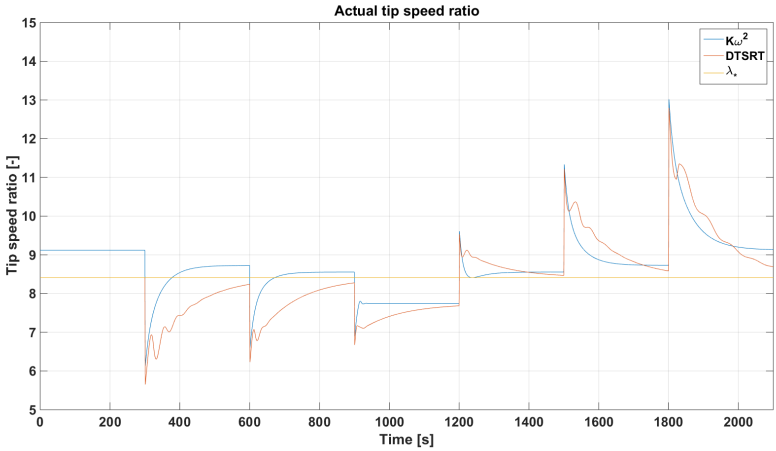

Figure B.8: Tip speed ratio for the $K\omega^2$ and DTSRT control strategies.

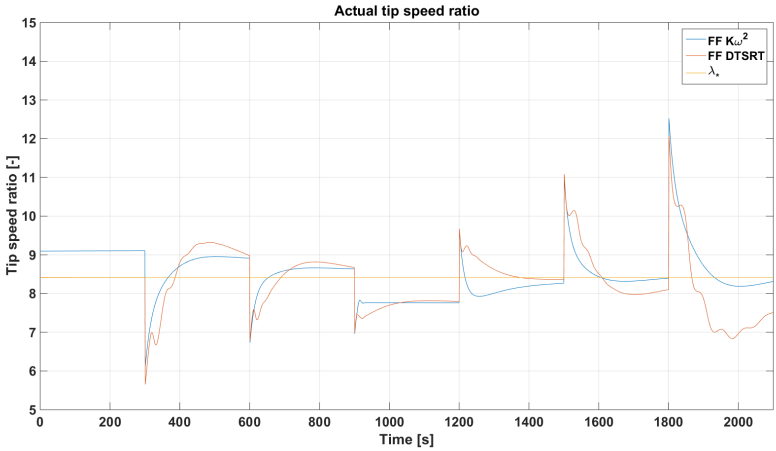

Figure B.9: Tip speed ratio for the $K\omega^2$ and DTSRT, both with feedforward, control strategies.

B.1.4 Drivetrain overall efficiency

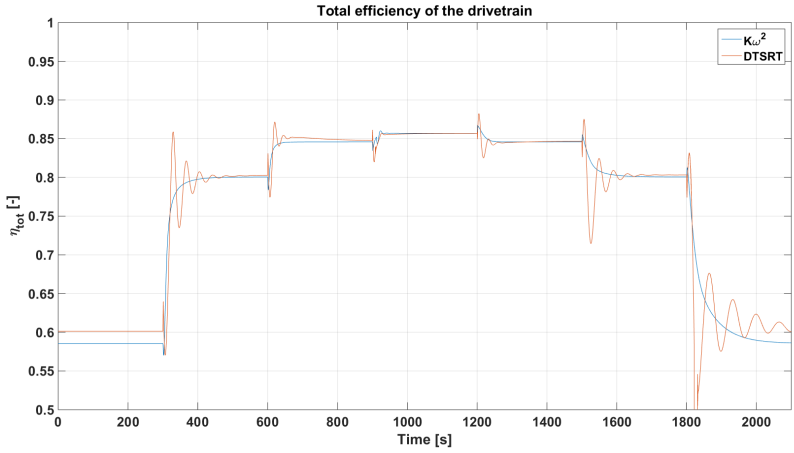

Figure B.10: Overall efficiency for the $K\omega^2$ and DTSRT control strategies.

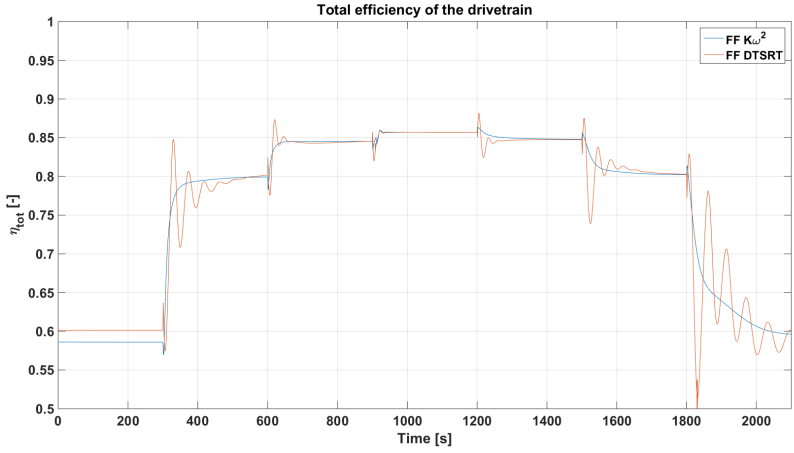

Figure B.11: Overall efficiency for the $K\omega^2$ and DTSRT, both with feedforward, control strategies.

B.1.5 Power delivered to the grid

Figure B.12: Power delivered to the grid for the $K\omega^2$ and DTSRT control strategies.

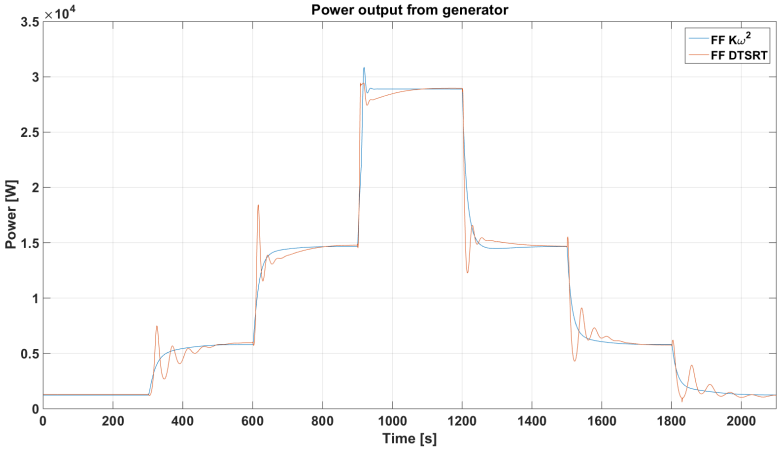

Figure B.13: Power delivered for the $K\omega^2$ and DTSRT, both with feedforward, control strategies.

B.2 Real wind profile

This section presents all graphs for the evaluated control strategies when simulating a real wind profile from data extracted by Earth Observing Laboratory [67].

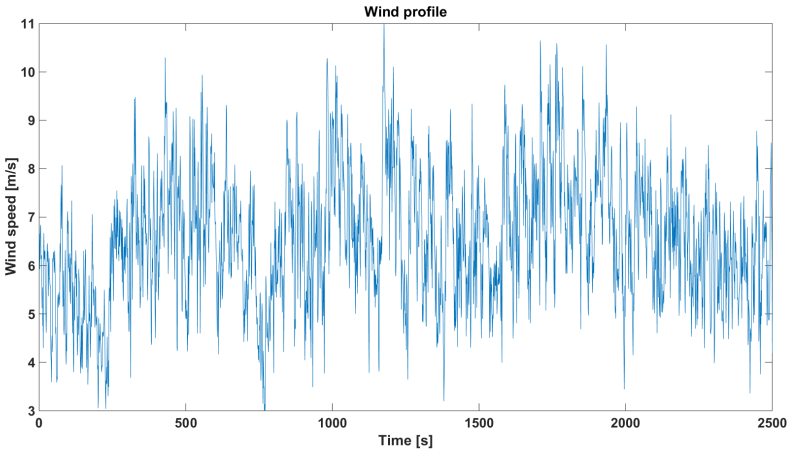

Figure B.14: Wind profile used for comparing control strategies.

B.2.1 Generator frequency

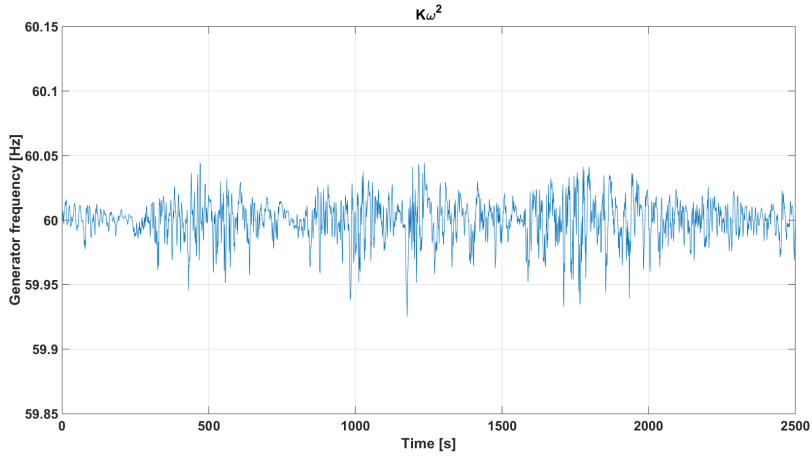

Figure B.15: Generator frequency for the $K\omega^2$ control strategy.

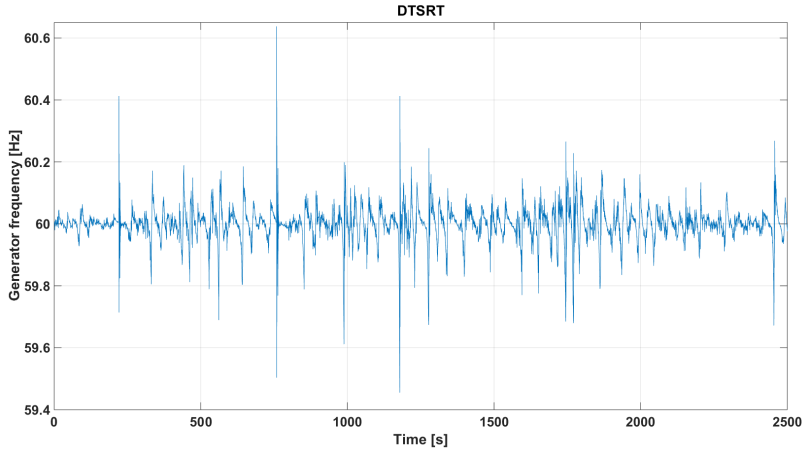

Figure B.16: Generator frequency for the Direct Tip Speed Ratio Tracking (DTSRT) control strategy.

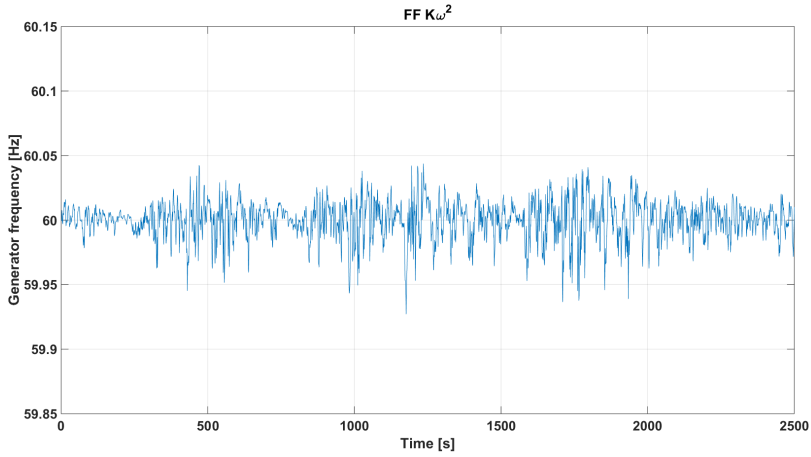

Figure B.17: Generator frequency for the $K\omega^2$ with feedforward control strategy.

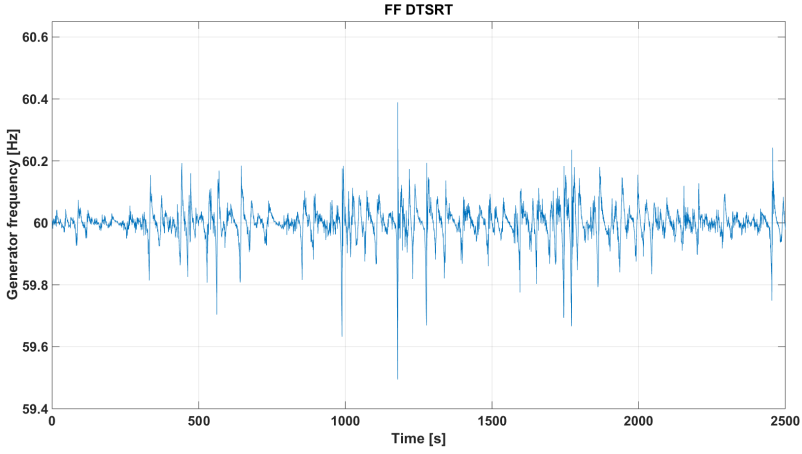

Figure B.18: Generator frequency for the DTSRT with feedforward control strategy.

B.2.2 Motor inlet pressure

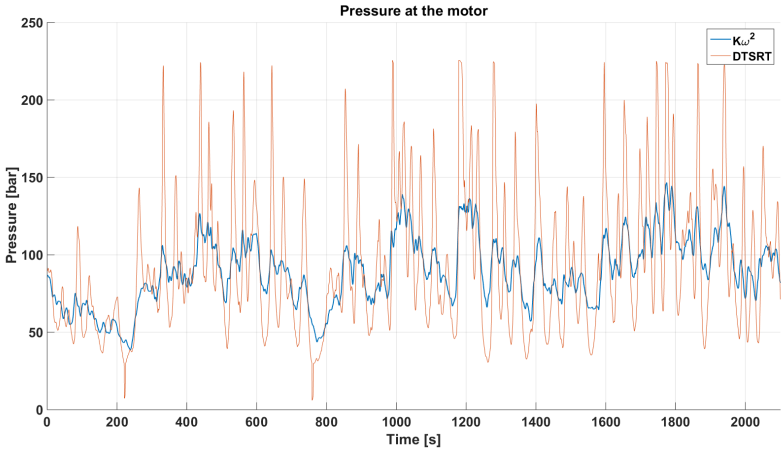

Figure B.19: Motor inlet pressure for the $K\omega^2$ and DTSRT control strategies.

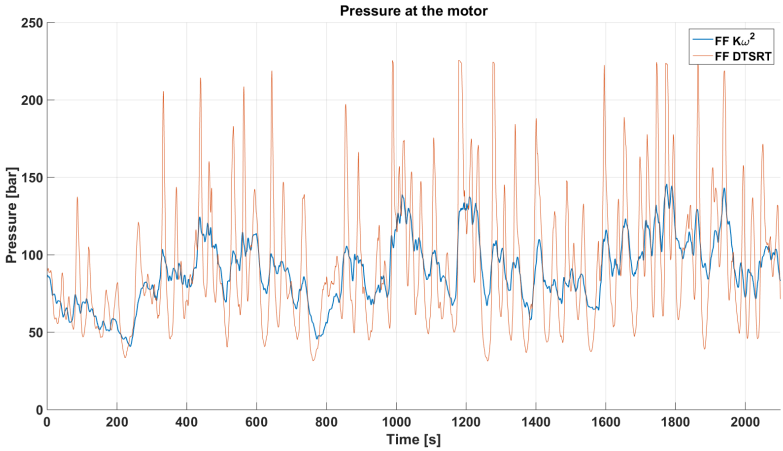

Figure B.20: Motor inlet pressure for the $K\omega^2$ and DTSRT, both with feedforward, control strategies.

B.2.3 Tip speed ratio

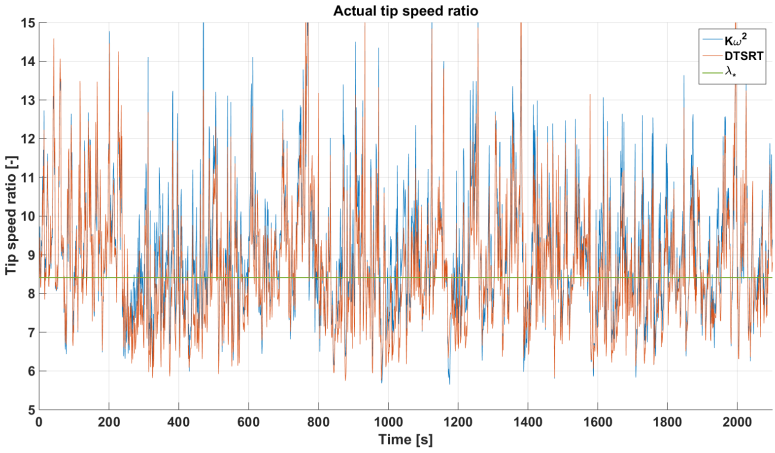

Figure B.21: Tip speed ratio for the $K\omega^2$ and DTSRT control strategies.

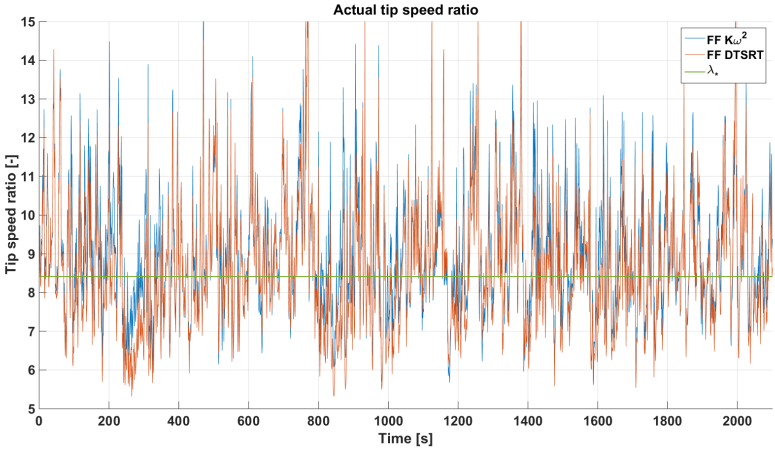

Figure B.22: Tip speed ratio for the $K\omega^2$ and DTSRT, both with feedforward, control strategies.

B.2.4 Rotational speed of the aerodynamic rotor

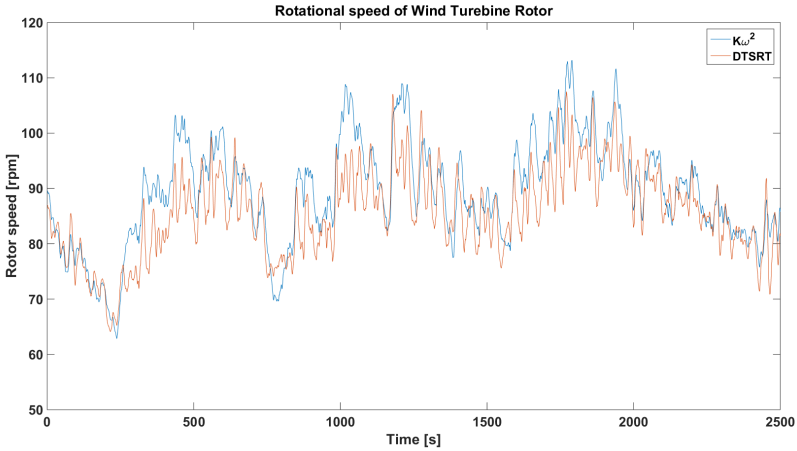

Figure B.23: Aerodynamic rotor speed for the $K\omega^2$ and DTSRT control strategies.

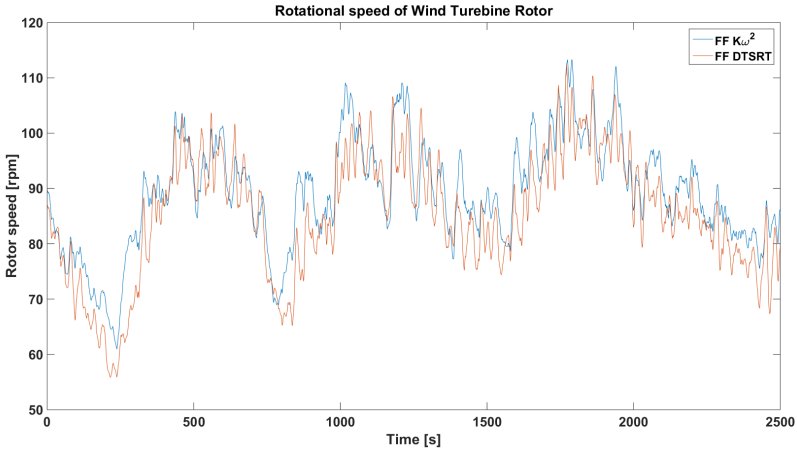

Figure B.24: Aerodynamic rotor speed for the $K\omega^2$ and DTSRT, both with feed-forward, control strategies.

B.2.5 Drivetrain overall efficiency

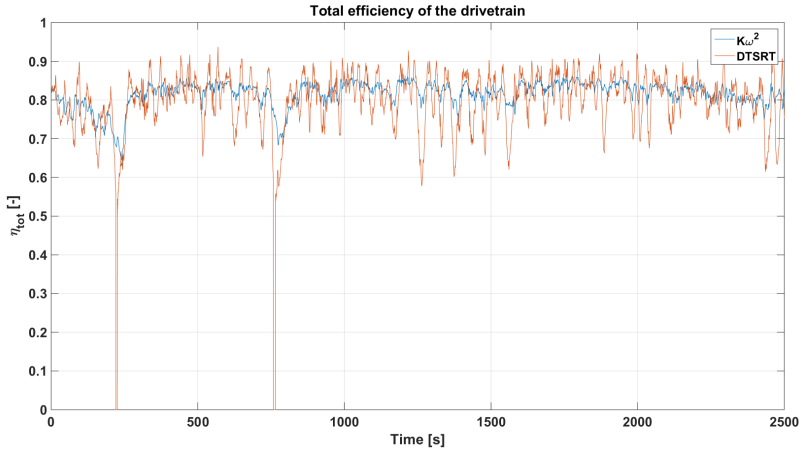

Figure B.25: Overall efficiency for the $K\omega^2$ and DTSRT control strategies.

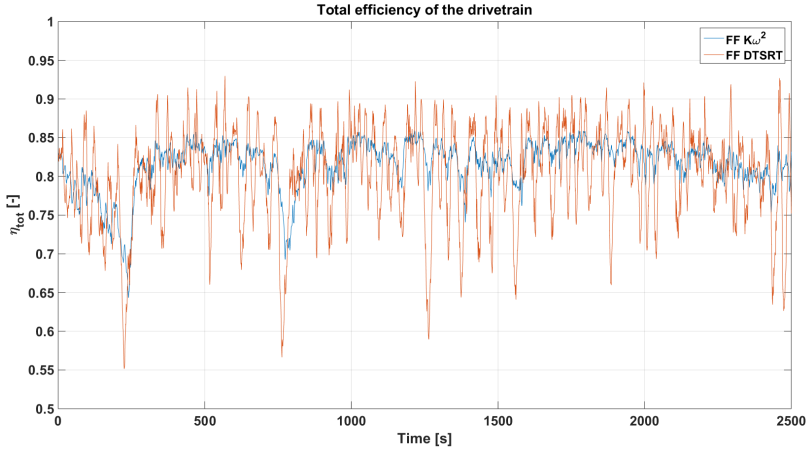

Figure B.26: Overall efficiency for the $K\omega^2$ and DTSRT, both with feedforward, control strategies.

B.2.6 Power delivered to the grid

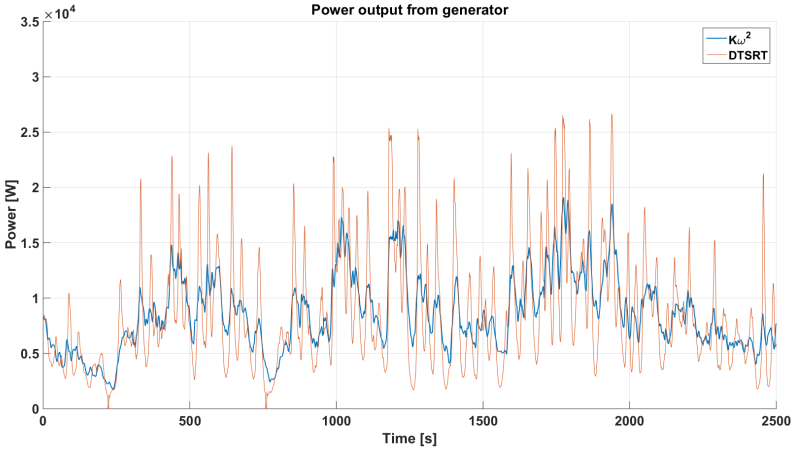

Figure B.27: Power delivered to the grid for the $K\omega^2$ and DTSRT control strategies.

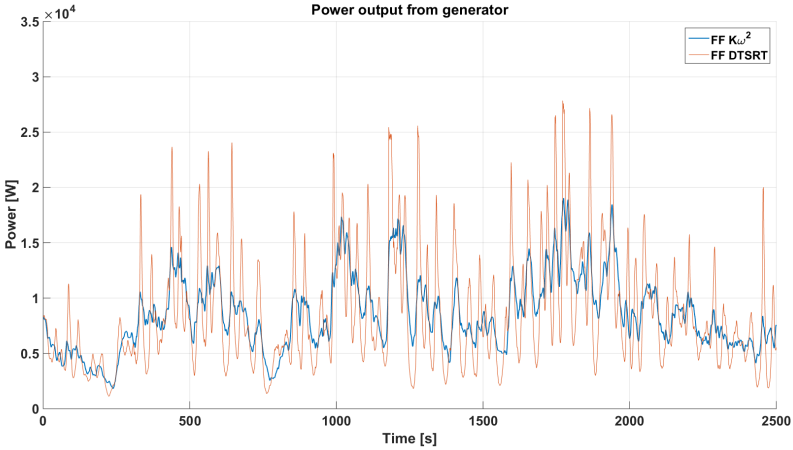

Figure B.28: Power delivered for the $K\omega^2$ and DTSRT, both with feedforward, control strategies.